



# รายงานวิจัยฉบับสมบูรณ์

## โครงการ

"จีโนมของไวรัสไข้เลือดออกสามารถอยู่รอดในเซลล์มนุษย์ได้อย่างไร: การทำแผนที่ทั่วทั้งจีโนมของโปรตีน เกาะติดบนอาร์เอ็นเอไวรัสโดยใช้เทคนิค PAR-CLIP"

"How can dengue genomic RNA survive in human cells?: Genome-wide mapping of protein-binding on viral RNA using PAR-CLIP"

โดย ผู้ช่วยศาสตราจารย์ ดร. ศรินทร์ ฉิมณรงค์ สถาบันชีววิทยาศาสตร์โมเลกุล มหาวิทยาลัยมหิดล

# รายงานวิจัยฉบับสมบูรณ์

## โครงการ

"จีโนมของไวรัสไข้เลือดออกสามารถอยู่รอดในเซลล์มนุษย์ได้อย่างไร: การทำแผนที่ทั่วทั้งจีโนมของโปรตีน เกาะติดบนอาร์เอ็นเอไวรัสโดยใช้เทคนิค PAR-CLIP"

"How can dengue genomic RNA survive in human cells?: Genome-wide mapping of protein-binding on viral RNA using PAR-CLIP"

ผศ.ดร. ศรินทร์ ฉิมณรงค์ สถาบันชีววิทยาศาสตร์โมเลกุล มหาวิทยาลัยมหิดล

# สนับสนุนโดยสำนักงานกองทุนสนับสนุนการวิจัย และมหาวิทยาลัยมหิดล

(ความเห็นในรายงานนี้เป็นของผู้วิจัย สกว. และมหาวิทยาลัยมหิดลไม่จำเป็นต้องเห็นด้วยเสมอไป)

## Table of contents

	Page
1. Abstract	3
2. Introduction	5
3. Literature review	6
4. References	9
5. Objective	10
6. Materials and Methods	10
7. Results and Discussion	17
8. Output	29
9. ภาคผนวก	31
List of tables	
1. GO terms showing enrichment of particular interest	23
2. DENV RNA-interacting proteins are prominent in the viral literature	23
3. DENV proteins identified by NS5 IP	27
4. NS5 interactors identified in this study and other earlier reports	27
5. Correlation between vRNA interactors from this study and other databases	28
List of figures	
Existing model of viral RNA replication in infected cells	7
2. Y3H β-galactosidase expression assay of DENV NS5 with genomic RNA fragments	8
3. The TAP-tag (His–FLAG) insertion into DENV NS5	11
4. SPR RNA-binding activity of DENV-2 RdRp with 5´-UTR RNA	17
5. <i>In vitro</i> Alpha binding assay of RdRp with truncated 3´SL RNA	18
6. Schematic diagram of modified PAR-CLIP in this study	18
7. In vitro synthesis of DENV genomic RNAs using run-off transcription	19
8. Flow cytometry analysis of infection efficiency of etDENV	20
9. Validation of stability of etDENV	21
10. TAP isolation of tagged DENV NS5 from infected Huh7 cells	22
11. The first Interactome map of DENV RNA in Huh7 cells via PAR-CLIP	23
12. NS5 interactome in Huh-7 cells	26
13. Inhibition of NS5 phosphorylation by PKC promotes viral replication	29

#### **Abstract**

Dengue virus (DENV), an ~10.7-kb positive-sense RNA virus, is the most common arthropodcommunicated pathogen in the world. Despite dengue's clear epidemiological importance, mechanisms for its replication remain elusive. Recently, we have identified a consensus RNA promoter sequence in the SL element in the 3´-UTR of viral genome. This RNA element is specifically recognized by the viral non-structural protein 5 (NS5), which is an exclusive viral RNA-dependent RNA polymerase or RdRp, in viral replication cycle in infected cells. We utilized this robust interaction to establish a new experimental method for analyzing in vivo global interaction of host-pathogen, so-called PAR-CLIP (Photoactivatable-Ribonucleoside-Enhanced Crosslinking and Immunoprecipitation). In the first stage, we developed a novel recombinant DENV that contains a TAP (tandemaffinity purification) -tag epitope including an octahistidine (8×His) tag followed by a FLAG tag inside the methyltransferase (MTase) domain of the NS5 protein. We showed that this engineered, tagged (et) DENV was infective in several human cell lines and the tags were stable over multiple viral passages, suggesting negligible structural and functional disturbance of NS5. This is so far the first report of stable, infectious tagged DENV. In the mid stage of the project, we performed a large-scale production of etDENV, and further provided proof-ofconcept for the use of rationally tagged virus by revealing a high confidence NS5 interaction network in human hepatic cells. Our analysis uncovered previously unrecognized hnRNP complexes and several low-abundance fatty acid metabolism genes, which have been implicated in viral life cycle. Our study has set a new standard for investigation of host-flavivirus interaction. In the last term of the study, we have completed the PAR-CLIP procedure and explored the global interactome of DENV RNA genome with the human factors for the first time. The results revealed uncharacterized complexes involved in interaction with viral RNA such as RNA processing, MCM complex, and chaperones. Although essential roles played by these human complexes in DENV replication definitely require further study to complete the full picture, this work, for the first time, provided mean of investigation and two interactome layers of DENV RNA and NS5 with human proteome. Our results suggest hostpathogen interaction is more prevalent but shaped than earlier believed.

#### (ภาษาไทย)

ไวรัสไข้เลือดออกเป็นอาร์เอนเอไวรัสที่มีสารพันธุกรรรมเป็นอาร์เอนเอสายบวกขนาดประมาณ 10.7 กิโลเบส (kb) โดยเชื้อไวรัส ดังกล่าวอาศัยสัตว์จำพวกแมลงในการแพร่กระจาย ทั้งๆที่ความสำคัญทางระบาดวิทยาของไวรัสเป็นที่ทราบแน่ชัด แต่กระบวนการ เพิ่มจำนวนของไวรัสในเซลล์ยังไม่สามารถอธิบายได้อย่างชัดเจน เมื่อเร็วๆนี้ คณะผู้วิจัยได้ค้นพบลำดับของนิวคลีโอไทด์ที่เป็น RNA promoter อยู่บนโครงสร้างของอาร์เอนเอนที่เรียกว่า SL บริเวณด้าน 3´-UTR ของจีโนมไวรัส โดยโครงสร้างของอาร์เอนเอดังกล่าว เป็นบริเวณที่เกาะจำเพาะของโปรตีน NS5 (viral non-structural protein 5) ซึ่งเป็นอาร์เอนเอพอลิเมอเรส (RNA-dependent RNA polymerase หรือ RdRp) ของไวรัสที่ทำหน้าที่ในการเพิ่มจำนวนสารพันธุกรรมในเซลล์ที่ติดเชื้อ คณะผู้วิจัยมีความคิดใหม่ อาศัยปฏิสัมพันธ์จำเพาะของอาร์เอนเอโปรโมเตอร์ที่ค้นพบนี้สร้างวิธีการใหม่ที่เรียกว่า PAR-CLIP ซึ่งย่อมาจาก Photoactivatable-Ribonucleoside-Enhanced Crosslinking and Immunoprecipitation ในการศึกษาวิเคราะห์ปฏิสัมพันธ์ ทั้งหมดภายในเซลล์เจ้าบ้านที่สัมพันธ์กับเชื้อไวรัส ในระยะแรกของโครงการวิจัยคณะผู้วิจัยได้พัฒนาไวรัสไข้เลือดออกลูกผสมชนิด ใหม่ โดยทำการติดฉลากหรือ tag epitope ( 8xHis tag ตามด้วย FLAG tag) ภายในบริเวณ methyltransferase domain (MTase) ของโปรตีน NS5 ซึ่งผลการสร้างไวรัสลูกผสมที่มีการติดฉลากดังกล่าว สามารถทำให้ human cell line หลายชนิดติดเชื้อ

ได้ และฉลากที่ติดในไวรัสสามารถคงอยู่ตลอดการเพาะเลี้ยงไวรัสหลายๆ รอบ นั้นแสดงให้เห็นว่าบริเวณที่ติดฉลากไม่มีผลกระทบ ต่อโครงสร้างและหน้าที่ของโปรตีน NS5 และนี่เป็นผลการรายงานครั้งแรกที่มีการติดฉลากไวรัสไข้เลือดออกโดยไม่ส่งผลเสียต่อ ไวรัสได้ ในระยะกลางของโครงการนี้ คณะผู้วิจัยได้เพิ่มจำนวนไวรัสลูกผสม (etDENV) และนำไปใช้ทดสอบความเป็นไปได้ของไวรัส ลูกผสมต่อการศึกษาเครือข่ายปฏิสัมพันธ์ของโปรตีน NS5 ในเซลล์ตับของมนุษย์ (human hepatic cells) จากผลการวิเคราะห์ เรา พบ heterogeneous nuclear ribonucleoprotein (hnRNP) complexes ที่ยังไม่มีการค้นพบมาก่อน รวมถึงหลายๆยืนใน กระบวนการเมตาบอลิซึมของกรดไขมันที่เกี่ยวพันกับวงจรชีวิตของไวรัส ซึ่งการศึกษาของเราได้สร้างมาตราฐานใหม่ ในการ ตรวจสอบปฏิสัมพันธ์ระหว่าง flavivirus และเซลล์เจ้าบ้าน ในระยะสุดท้ายของการศึกษา คณะผู้วิจัยได้ดำเนินการกระบวนการ PAR-CLIP และสำรวจ global interactome ของสารพันธุกรรมอาร์เอนเอของไวรัสไข้เลือดออกกับโปรตีนภายในเซลล์มนุษย์ (human factors) เป็นครั้งแรก ผลการศึกษาได้เผยถึง complexes ใหม่ที่เกี่ยวข้องกับปฏิสัมพันธ์กับสายอาร์เอนเอของไวรัส ตัวอย่างเช่น RNA processing, MCM complex และ chaperones แม้ว่าบทบาทสำคัญของ human complexes ที่ค้นพบนั้น ต่อกระบวนการเพิ่มจำนวนไวรัสไข้เลือดออกยังต้องอาศัยการศึกษาเพิ่มเติมเพื่อทำให้ภาพรวมของการศึกษาสมบูรณ์แบบ แต่ โครงการวิจัยนี้ได้สร้างวิธีการศึกษาปฏิสัมพันธ์ของไวรัสภายในเซลล์ รวมถึงแสดง interactome layers ของ DENV RNA และ โปรตีน NS5 กับ human proteome เป็นครั้งแรก จากผลการศึกษาทั้งหมดแสดงให้เห็นว่าลักษณะโครงสร้างปฏิสัมพันธ์ระหว่าง เชื้อโรคและเซลล์เจ้าบ้าน (host-pathogen interaction) นั้นมีความหลากหลายแต่เป็นรูปร่างที่จำเพาะมากกว่าที่คยเชื่อกันมา

## **Executive Summary**

## ความสำคัญและที่มาของปัญหา (Introduction)

Dengue fever is an infectious tropical disease caused by the dengue virus (DENV), which is transmitted via several species of mosquito within the genus Aedes, principally A. aegypti. Symptoms range from a mild fever, to incapacitating high fever, with severe headache, pain behind the eyes, muscle and joint pain, and rash. However, complex infection with different circulating serotypes (DENV1-4) may lead to the life-threatening dengue hemorrhagic fever (DHF), resulting in bleeding, low levels of blood platelets and blood plasma leakage, or to dengue shock syndrome (DSS), where dangerously low blood pressure occurs [1]. Today about 2.5 billion people, or 40% of the world's population, live in areas where there is a risk of dengue transmission according to the World Health Organization (WHO). Dengue is endemic in at least 100 countries in Asia, the Pacific, the Americas, Africa, and the Caribbean. It is estimates that 50 to 100 million infections occur yearly, including 500,000 DHF cases and 22,000 deaths, mostly among children [2]. In 2010, the incidence of dengue marked 2fold increase to 112,992 cases over the previous year in Thailand (http://dhf.ddc.moph.go.th/). About 0.1% (139 cases) of those infected died. Neither a vaccine nor an antiviral therapy is currently available for prevention and treatment of DENV infection [3]. Current treatments are mostly symptomatic, and they make use of analgesics for the containment of fever and fluid replacement to address the vascular leakage in DHF and DSS patients. Hence, at present, the only method to control or prevent the transmission of DENV is to combat vector mosquitoes. Moreover, development of a vaccine for DENV has been challenging, principally because of the need to immunize and induce long-lasting protection against all 4 serotypes of DENV simultaneously; an incompletely immunized individual may be sensitized to DHF or DSS. These complications have underscored the importance for development of an effective therapy for DENV and other flavivirus infections.

Towards discovery of therapeutic compounds against DENV, deep understanding of the whole viral life cycle in infected cells is indispensable. To date, a vast majority of DENV studies in the country and overseas have mainly focused on mechanisms for receptor-mediated cell entry or endocytosis, and broad cellular effects in the late phase of infection such as cell stress, immune response, and cell death or apoptosis. The studies usually investigated a limited number of proteins or a single pathway, and were mostly performed via *in vitro* experiments with mammalian cell lines. Only few *in vivo* evidence have been clearly revealed. Since DENV likely utilizes multiple receptors on different cell targets' surfaces, a single block of DENV receptor using small molecule and antibody has unknown consequences. On the other hand, complex cellular responses to massive viral particles in the late infection state should be a part of general actions to defense against viral attack, and possibly diverge in human body. Therefore, it is obvious that the global study of host–pathogen interactions at an earlier stage upon infection is necessary for successful neutralization of DENV.

In contrast, there is a knowledge gap in viral life cycle concerning the replication process of viral RNA (vRNA) in host cells. The currently-believed model is drawn in Fig. 1. However, without the breakthrough in the field, this model is deficient in unbiased evidence, and remains unconvincing. Very recently, <u>our group has discovered the consensus promoter sequence, where the viral polymerase specifically recognizes, in DENV</u>

genomic RNA for the first time by utilizing a modified yeast three-hybrid (Y3H) system (Fig. 2; in press). Our finding reveals the genuine DENV promoter residing in the 3´-end of the genome, but not in the 5´-end as previously thought, casting doubt onto the current model of DENV replication. In order to extend results from our previous works to provide more comprehensive understanding of DENV life cycle in human cells, we propose here a deep analysis of global interactions between vRNA and proteins occurring inside infected cells using a newly-developed technique called PAR-CLIP. This proposal is based on our hypothesis that DENV RNA requires extensive interactions with proteins to survive in infected cells in the absence of a poly(A) tail. The knowledge gained from the project will renew the model of DENV replication, and provide a new avenue for the development of antiviral therapy by inhibiting essential interactions with vRNA at the first stage following cell entry.

#### Literature review

Flaviviruses comprise one of the three genera within the Flaviviridae family. The Flavivirus genus is divided into three groups based on their ecological characteristics, mosquito-borne, tick-borne, and no-known vector flaviviruses. Among the mosquito-borne flaviviruses, there are important human pathogens such as dengue virus (DENV), yellow fever virus (YFV), West Nile virus (WNV), Saint Luis encephalitis virus (SLEV), and Japanese encephalitis virus (JEV). Like all flaviviruses, DENV is an enveloped virus possessing an ~10.7-kb, positive-sense, single-stranded RNA genome that is translated as one long polyprotein and cleaved into 10 viral proteins: three structural (capsid; C, premembrane, prM; and envelope, E) and seven nonstructural (NS1, NS2A, NS2B, NS3, NS4A, NS4B, and NS5) proteins [4]. DENV circulates as a complex of four antigenically distinct serotypes, DEN1–4. DENV RNA genome contains a type 1 cap (m7GpppAmp) structure at the 5´-end but lack 3´ poly(A) tail [5], and its single coding region is flanked by highly structured 5´-untranslated region (UTR) which is about 100 nucleotides (nt) in length, and an ~450-nt 3´-UTR [6].

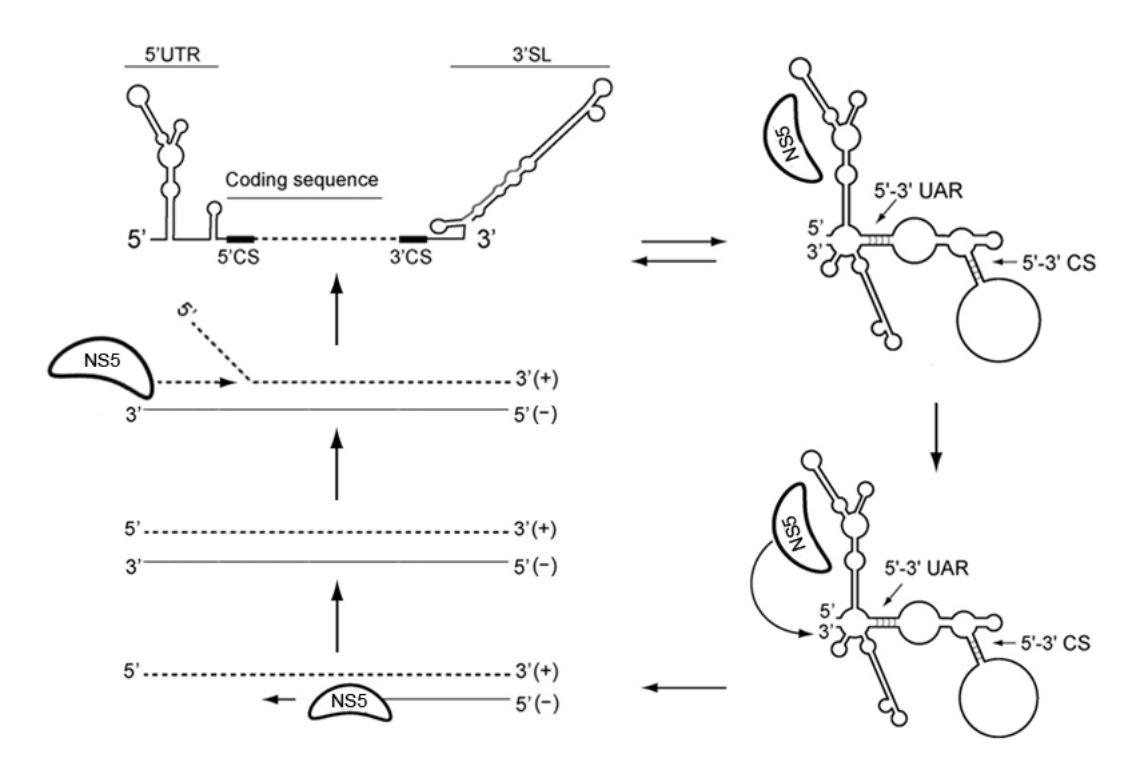


Figure 1. Existing model of viral RNA replication in infected cells.

DENV RNA replication takes place in the cytoplasm following the endocytosis [7], whereby several viral NS and host proteins are believed to constitute the replication complex, the proposed replication machinery of flaviviruses [8]. Two key enzymes in replication, NS3 and NS5, the RNA helicase and RNA-dependent RNA polymerase (RdRp), respectively, interact within the cytoplasm of infected cells. An only existing model of DENV replication is shown in **Fig. 1**. The synthesis of DENV RNA minus strand is likely initiated by the DENV genome cyclization in the absence of proteins, which is mediated by hybridization between UAR (Upstream AUG Region) and CS (Cyclization Sequence) in both 5´- and 3´-termini. The viral RdRp then binds to a 5´ stem-loop (SLA) in 5´-UTR, and by long-range RNA-RNA interactions the polymerase is transferred to the site of initiation at the 3´- end of the genome [9]. The newly synthesized minus strand servers as template for production of the genomic strand [10] (**Fig. 1**). Very recently, our research group has discovered a strong interaction with RdRp occurring at the stem loop (SL) element nearby the 3´-end of DENV genome, casting doubt onto the current model of DENV replication (**Fig. 2**; in press).

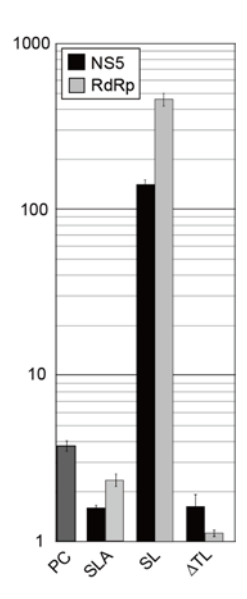




Figure 2. (Left panel) Y3H β-galactosidase expression assay showing the interaction strength of DENV genomic RNA fragments with the full-length NS5 (black) or RdRp subunit (gray). Vertical axis shows "Miller Units." Error bars display standard deviation of the mean. PC, the positive control IRE–IRP interacting pair; SLA, DENV  $5^{'}$  SLA; SL, DENV  $3^{'}$  SL; and  $\Delta$ TL, SL with the deletion of putative promoter sequence. It is noted that RdRp strongly interacted with  $3^{'}$  SL (over 2 orders of magnitude compared to  $5^{'}$  SLA), and simple removal of the top loop of  $3^{'}$  SL completely killed this interaction. (Right panel) The predicted secondary structure of dengue SL element in the  $3^{'}$ -UTR. The conserved RdRp-interacting sequences (CACAG) are indicated in bold.

Our *in vivo* analysis of the yeast three-hybrid (Y3H) system revealed >100 times stronger binding affinity to 3´ SL than 5´SLA by DENV RdRp. We also discovered a short consensus promoter sequence in 3´ SL, where its deletion extinguished the RdRp interaction (**Fig. 2**). <u>Our results indicate that the current model of DENV replication remains controversial</u>, and there is requirement for deeper studies to understand the accurate replication model. Moreover, the current model assumes that the DENV genome exists in cells as a naked RNA, which is highly unlikely. Several lines of evidence recently proved that flaviviral vRNAs interact with cellular proteins to stabilize and promote the replication such as eukaryotic initiation factor 1A (eIF1A) [11,12], human La autoantigen (La) [13], poly-pyrimidine tract binding protein (PTB) [14], Y-box binding protein 1 (YB-1) [15], and heterogenous nuclear ribonucleoproteins (hnRNP A1, hnRNP A2/B1 and hnRNP Q) [16]. It has also been reported that the RNA degradation pathway may play an important role in the quantity control of the vRNA turnover [17]. Hence, the accurate mechanism for DENV RNA replication in cells seems to be much more complex than previously thought.

The search for inhibitors against vRNA replication is a key research in virology field. The idea was corroborated by a success in HIV drug by interrupting viral RNA polymerase to block viral replication in an early state. However, the real mechanism of DENV replication in human cells still remains enigmatic as mentioned above, and the global genome-wide interaction with vRNA inside the infected cell remains mostly elusive. To address these issues, we propose to adapt a new technological platform called PAR-CLIP (Photoactivatable-Ribonucleoside-Enhanced Crosslinking and Immunoprecipitation) [18] to viral RNA for the first time (Fig. 4). We

wish to find missing pieces of the jigsaw puzzle of DENV replication, and open new avenues for development of therapeutic agents in the future.

#### Reference

- 1. Gubler, D.J. (1998) Dengue and Dengue Hemorrhagic Fever. Clin Microbiol Rev. 11(3), 480-96.
- 2. WHO. (2010) Dengue: Guidelines for diagnosis treatment prevention and control, World Health Organization (Geneva).
- 3. Whitehead, S.S., Blaney, J.E., Durbin, A.P., Murphy, B.R. (2007) Prospects for a dengue virus vaccine. *Nat Rev Microbiol.* **5**(7), 518-28.
- 4. Kuno, G., Chang, G.J., Tsuchiya, K.R., Karabatsos, N., Cropp, C.B. (1998) Phylogeny of the genus Flavivirus. *J Virol.* **72**(1), 73-83.
- 5. Lodeiro, M.F., Filomatori, C.V., Gamarnik, A.V. (2009) Structural and functional studies of the promoter element for dengue virus RNA replication. *J Virol.* **83**(2), 993-1008.
- 6. Markoff, L. (2003) 5´- and 3´-noncoding regions in flavivirus RNA. Adv Virus Res. **59**, 177-228.
- 7. Modis, Y., Ogata, S., Clements, D., Harrison, S.C. (2004) Structure of the dengue virus envelope protein after membrane fusion. *Nature.* **427**(6972), 313-9.
- 8. Paranjape, S.M., Harris, E. (2010) Control of dengue virus translation and replication. *Curr Top Microbiol Immunol.* **338**, 15-34.
- 9. Alvarez, D.E., Lodeiro, M.F., Ludueña, S.J., Pietrasanta, L.I., Gamarnik, A.V. (2005) Long-range RNA-RNA interactions circularize the dengue virus genome. *J Virol.* **79**(11), 6631-43.
- 10. Villordo, S.M., Gamarnik, A.V. (2009) Genome cyclization as strategy for flavivirus RNA replication. *Virus Res.* **139**(2), 230-9.
- 11. Davis, W.G., Blackwell, J.L., Shi, P.Y., Brinton, M.A. (2007) Interaction between the cellular protein eEF1A and the 3´-terminal stem-loop of West Nile virus genomic RNA facilitates viral minus-strand RNA synthesis. *Virology*. **81**(18), 10172-87.
- 12. De Nova-Ocampo, M., Villegas-Sepúlveda, N., del Angel, R.M. (2002) Translation elongation factor-1alpha, La, and PTB interact with the 3´ untranslated region of dengue 4 virus RNA. *Virology.* **295**(2), 337-47.
- 13. Vashist, S., Anantpadma, M., Sharma, H., Vrati, S. (2009) La protein binds the predicted loop structures in the 39 non-coding region of Japanese encephalitis virus genome: role in virus replication. *J Gen Virol.* **90**(6), 1343-52.
- 14. Anwar, A., Leong, K.M., Ng, M.L., Chu, J.J., Garcia-Blanco, M.A. (2009) The polypyrimidine tract-binding protein is required for efficient dengue virus propagation and associates with the viral replication machinery. *J Biol Chem.* **284**(25), 17021-9.
- 15. Paranjape, S.M., Harris, E. (2007) Y Box-binding protein-1 binds to the dengue virus 3<sup>´</sup>-untranslated region and mediates antiviral effects. *J Biol Chem.* **282**(42), 30497-508.
- 16. Noisakran, S., Sengsai, S., Thongboonkerd, V., Kanlaya, R., Sinchaikul, S., Chen, S.T., et al. (2008) Identification of human hnRNP C1/C2 as a dengue virus NS1-interacting protein. *Biochem Biophys Res Commun.* **372**(1), 67-72.

- 17. Pijlman, G.P., Funk, A., Kondratieva, N., Leung, J., Torres, S., van der Aa, L., Liu, W.J., Palmenberg, A.C., Shi, P.Y., Hall, R.A., Khromykh, A.A. (2008) A highly structured, nuclease-resistant, noncoding RNA produced by flaviviruses is required for pathogenicity. *Cell Host & Microbe* **4**(6), 579-591.
- 18. Hafner, M., Landthaler, M., Burger, L., Khorshid, M., Hausser, J., Berninger, P., Rothballer, A., Ascano, M. Jr., Jungkamp, A.C., Munschauer, M., Ulrich, A., Wardle, G.S., Dewell, S., Zavolan, M., Tuschl, T. (2010). Transcriptome-wide identification of RNA-binding protein and microRNA target sites by PAR-CLIP. *Cell* **141**(1), 129–141.

### วัตถุประสงค์ (Objective)

- 1. To expand our previous research outcome and apply a new technological platform to address an important question concerning the stabilization and replication of DENV RNA in human cells.
- 2. To genome-wide explore the global interaction between DENV RNA and proteins in infected cells.
- 3. To provide comprehensive understanding about the viral life cycle in human cells and provide fundamental knowledge for development of therapeutic treatment in the future.
- 4. To produce high-motivated, world-class young researchers including Ph.D. and M.Sc. students, and also, publications on high-impacted international scientific journals.

## เนื้อหางานวิจัย

#### Materials and Methods

#### Construction of DENV cDNA with a TAP-tag

We first cloned the whole cDNA from DENV serotype 2 strain 16681 into a pBR322 vector fused with an upstream T7 promoter sequence. Thereafter, we used the standard QuikChange procedure with pairs of long primers to insert a TAP tag (amino acid sequence: GGGHHHHHHHHHGGGDYKDDDDKGGG) into 4 different regions in viral NS5 (**Fig. 3**). Specific criteria for tag-insertion were 1) regions are less conserved among flaviviral NS5; 2) regions are in a loop distant from the active sites (methylase and polymerase sites) of NS5; and 3) regions are exposed to the solvent in the crystal structure (PDB ID: 2J7W). All clones were thoroughly validated via sequencing of the complete genome (10723 nts).

#### In vitro run-off transcription

Viral RNA was generated via the in vitro run-off transcription with linearized DNA template. In our experience, kit-generated RNA (RiboMAX, Promega) is produced at higher concentrations and purity than RNA synthesized from individually purchased components. In brief, a 50 µl transcription reaction consisted of ATP at 2 mM, other NTPs at 7.5 mM, "A-cap" analog (to reproduce DENV's 5 cap structure) at 3 mM, 5 µg template, 5× buffer, and 5 µl proprietary enzyme mix. The reaction was incubated at 37°C for 3-4 hours, followed by DNA removal with 5 U RQ1 RNase-free DNase at 37°C for 15 minutes. RNA is then purified with the RNeasy kit (Qiagen), and visualized via 1% TBE-agarose gel electrophoresis. Typically, our protocol gave the final yield of 50 µg vRNAs.

#### Transfection of vRNA

Delivery of RNA via electroporation was found to be more efficient than by liposome-based transfection. BHK cells grown to near-confluency were incubated with trypsin at 37°C for 4 minutes, followed by addition of media to inhibit trypsin. Cells were transferred into a 50 ml tube and the suspension was brought to 50 ml by addition of RNase-free PBS. Cell counting was then performed. Centrifugation (1500 rpm, 7 min) followed by PBS washing was performed twice. Optimem media was added to bring cells to  $10^6$  cells/ml. 5  $\mu$ g RNA per million cells was added. In general,  $2 \times 10^6$  cells were used. Electroporation proceeded at 1500 mV, 25  $\mu$ F, two times. Cells were then incubated at room temperature for twenty minutes, followed by transfer into a culture flask and addition of the standard culture media.

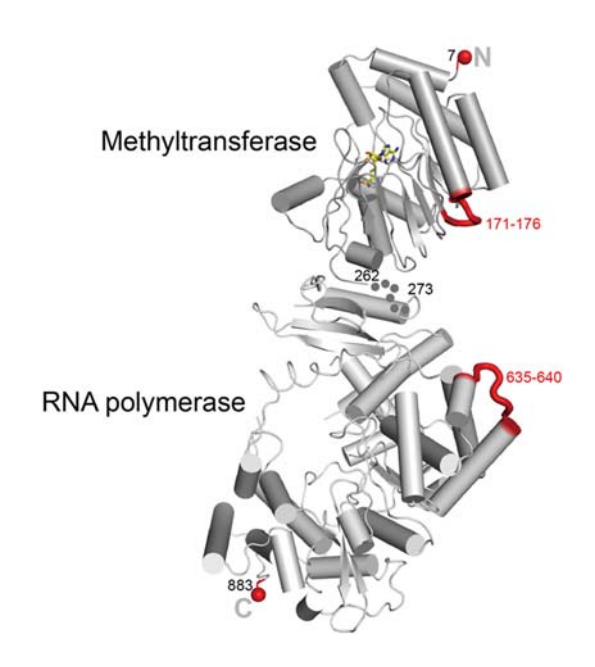


**Figure 3.** The TAP-tag (His–FLAG) was inserted into four different regions (colored in red) of DENV NS5 in the viral genome: the N terminus, the methyltransferase domain (residues 171-176), the RNA polymerase domain (residues 635-640), and the C terminus.

#### Cell culture and viral Infection

C6/36 cells line was use for viral propagation, cultured in 10% FBS, 10% tryptose phosphate broth at 27°C. BHK-21, HepG2, and HEK293 were cultured with 10% FBS,  $1\times$  Pen-Step DMEM at 37°C at 5% CO<sub>2</sub>. Cells of 75-90% confluence were incubated with virus at 37°C for 90 min. Cells were then washed with PBS, and supplied with 2% FBS and  $1\times$  Pen-Step DMEM. Infected cells were culture at 37°C, with 5% CO<sub>2</sub>.

### Focus-Forming Unit (FFU) Assay

The FFU assay is a relatively convenient and accurate method for establishing viral titers so that further experiments may be performed at known multiplicities of infection (MOI). Infected cells are fixed and permeabilized, treated with primary and secondary antibodies, with microscopy allowing quantification of infected cell clusters (focus-forming units). Each unit is assumed to represent a single infected cell, as spread of virus throughout the supernatant is strongly limited by the addition of agar or a gum to the culture media. In our own work, the antibody of interest is DENV anti-envelope (Millipore, 4G2). In brief,  $2 \times 10^4$  BHK cells were

plated in each well of a 96 well plate and allowed to grow overnight under standard conditions. Viral 10x dilutions ( $10^{-1}$ – $10^{-8}$ ) were performed in triplicates, with culture media used as the diluent. Media was then removed from the plated cells, replaced with viral dilutions and allowed to incubate for 2 hours.  $100 \, \mu l$  of standard media supplemented with 1.5% gum tragacanth was then added to the cells, which were allowed to incubate for three days. Media was then discarded and the cells washed with PBS. Cells were fixed with  $100 \, \mu l$  of 3.7% paraformaldehyde, with gentle shaking over 10 minutes. Fixative was removed, and cells permeabilized with  $100 \, \mu l$  of 1% Triton X-100 in PBS. Permeabilization solution was removed and cells were washed with PBS three times (3x).  $50 \, \mu l$  primary antibody ( $1:20000 \, dilution$ ) was applied to cells followed by  $30 \, minutes$  of incubation at 30%C. Cells were again washed with PBS 3x, followed by treatment with  $50 \, \mu l$  secondary HRP-conjugated antibody ( $1:20000 \, dilution$ ) and  $30 \, minutes$  of incubation. Cells were again washed with PBS 3x.  $1:2000 \, dilution$ 0 was added. Foci were visible within  $1:2000 \, dilution$ 1 minutes via microscopy. FFU quantification was performed according to the various dilutions.

#### Validation of viral stability

In order to verify that the clone containing a TAP-tag inside the methyltransferase domain was stable, BHK cells were grown to 80% confluence and infected with the tagged virus at an MOI of 0.5. Upon observation of CPE (cell detachment, cell rounding, and plaque formation), 200 µl of supernatant was collected. vRNA was isolated via a standard TRIzol extraction procedure. Reverse transcription (SuperScript III, Invitrogen) was performed using a primer complementary to the final 25 nucleotides of the DENV-2 3´ terminus. PCR was then conducted using a forward primer complementary to the NS4B coding regions and a reverse primer complementary to the beginning of RdRp coding region. The PCR product was purified (QIAGEN PCR purification) and sequenced to confirmed stability of the mutant virus with certainty.

#### <u>Immunofluorescence</u>

Cells were seeded onto coverslips, washed with PBS, and fixed with 3% paraformaldehyde and 2% sucrose. After 3 PBS washes, cells were incubated with Triton X-100 solution (0.5% Triton X-100, 20 mM Hepes pH 7.8, 50 mM NaCl, 3 mM MgCl<sub>2</sub>, and 300 mM Sucrose) for 5 min on ice. Subsequently, cells were 3-4 times washed by PBS, and stained with primary and secondary antibodies.

#### Flow Cytometry

Cells were treated with cold PBS and centrifuged at 3,000 rpm. The cell pellets were fixed with 3.7% formaldehyde in PBS for 10-15 min. Then, washing with PBS were performed and permeabilization with 0.5% Saponin in FACs wash (2% FBS, 2 mM EDTA, 0.05% AB human serum in PBS) for 20 min. Next, the anti E protein and anti-FLAG antibody in FACs wash with 0.5% Saponin were stain for 60 min at 4°C. The cells were washed with FACs wash with 0.5% Saponin before stain with secondary antibody. The diluted goat anti mouse FITC and goat anti rabbit APC in FACs were stain the cells for 60 min at 4°C in dark. The cells were washed with FACs wash with 0.5% Saponin 2 times. Finally, the cells were fixed with 1% formaldehyde in PBS before analyze by FACSCalibur.

#### <u>Small-scale test of nickel-affinity pull-down of vRNA complexes</u>

HepG2 cells were grown in in DMEM media supplemented with 10% FBS and 1% penicillin-streptomycin in two T75 flasks to 80% confluence. In one flask (the infection condition), media was then withdrawn and replaced with infected supernatant at an MOI of 0.5, with additional media added to a final volume of 12 ml an hour later. The other flask (uninfected) was treated similarly, but without virus. Both flasks received 4thiouridine (S<sup>4</sup>U) at a final concentration of 100 µM at this time. After 48 hours, media was removed from both flasks and cells were treated with PBS. Cells were removed with a sterile rubber policeman and placed on standard petri dishes. UV crosslinking was performed at 0.15 J/cm<sup>2</sup> for 15 minutes. Cells were pelleted at a low speed. Lysis was then achieved for 30 minutes at 4°C using a standard NP40 lysis buffer (50 mM HEPES pH 7.5, 150 mM KCl, 2 mM EDTA, 0.5% NP40, 1% Triton X-100, 0.5 mM DTT, protease inhibitor, and RNase inhibitor at recommended levels) at roughly 3 volumes buffer per pellet volume. The samples were cleared by centrifuging at 13,000 rpm at 4°C for 15 min. Cleared supernatant was then applied to pre-washed Ni-NTA resin (QIAGEN) at a ratio of 2:1 supernatant/beads, and rotated overnight at 4°C. Washing was performed 3 times with 3 volumes wash buffer (25 mM Tris-HCl/NaPO<sub>4</sub>, 0.3 M NaCl, 20 mM β-mercaptoethanol, 25 mM imidazole, pH 7.4) with 2 volumes buffer per volume of resin, with centrifugation at 3,000 RCF for 5 min at 4°C, separating resin and buffer. Resin was then incubated at 22°C for 15 min in wash buffer supplemented with RNase T1 (0.1 U/μl), followed by 3 more washes. Resin-bound proteins were eluted with 250 mM imidazole. Fractions were collected at all steps, and concentrated by TCA prior to SDS-PAGE analysis.

#### PAR-CLIP

Cells were lysed with 3 volumes cell lysis buffer per pellet for 30 minutes on ice with occasional gentle agitation, and its completion was checked under microscopy. The lysate was extracted via centrifugation at 13,000 rpm for 15 min at 4°C. Cleared lysate was directly applied to pre-equilibrated Ni-NTA beads. Best results were obtained with small bed volumes of beads. Currently, lysate corresponding to  $10^7$  cells (approximately 1.5 mg lysate protein) was applied to a 10  $\mu$ l bed volume. The binding was performed for 1 h at 4°C, and then unbound fraction, designated "flow through" was removed by centrifugation at 2500 rpm. At least 5 cycles of washing with 100  $\mu$ l washing buffer for 10 min at 4°C were performed. Elution from Ni-NTA was accomplished with 20  $\mu$ l elution buffer and repeated at least 4 times. It is important to save appropriate volumes of fractions for possible Western blotting or Bradford assays.

Ni-elution fractions were combined with pre-equilibrated anti-FLAG M2 affinity beads (Sigma-Aldrich). The volumes of bedded beads per estimated protein content were the same as the Ni-NTA step above (10  $\mu$ l / 1.5mg protein). The beads were rotated at 4°C for 1 h before collection of the flow through fraction. Washing with 500  $\mu$ l TBS buffer (10 mM Tris pH 7.5, 150 mM NaCl) is performed 3 times. Then, we treated the FLAG resin with 100 U/ $\mu$ l RNase T1 (NEB) for 20 minutes at 22°C to release proteins that interacted with DENV RNAs. The supernatant was collected for SDS-PAGE and LC/MS/MS analyses. The FLAG resin was further washed twice with TBS to remove RNase T1. Protein–RNA complexes including NS5 that remained on the beads was also subjected to SDS-PAGE and LC/MS/MS analyses.

Solutions used in PAR-CLIP are described as below.

Nickel basic solution": 50 mM HEPES pH 7.2, 150 mM KCl, 1% Triton X-100, 25 mM imidazole, 10% Glycerol,
 50 mM NaCl, 2% RNasin (NEB), 1× protease inhibitor, 1× phosphatase inhibitor

- Lysis buffer: 77.5% basic solution, 5 mM β-mercaptoethanol, 0.3% RNase-free DNase I, 1% NP-40
- Ni wash buffer: 77.5% basic solution, 1% NP-40, 5 mM β-mercaptoethanol
- Ni elution buffer: 77.5% basic solution, 22.5% 1 M imidazole

#### NS5 pulldown for detection of protein-protein interactions

The His-tag-affinity pulldown step was omitted to avoid high salt condition. Instead, a protein–protein crosslinking step was added to increase the yield of the complexes. Specifically, infected cells were carefully washed with PBS, and cell pellets were incubated with 2 mM dimethyl pimelimidate (DMP) at room temperature for 20 minutes to crosslink protein–protein complexes. Cells were lysed with CLB buffer) 50 mM Tris-HCl pH 7.4, 250 mM NaCl, 0.5% NP-40, 1 mM glycerophosphate, 1 mM sodium orthovanadate, and 5 mM EDTA(. The total cell lysates were pre-cleared with the protein G agarose (Roche) to reduce non-specific binding for 60 minutes at 4°C, and subsequently gently mixed with EZview<sup>TM</sup> Red Anti-FLAG M2 affinity gels (Sigma) for 4 hours at 4°C. After washing 3 times with 50 mM Tris-HCl pH 7.4 and 150 mM NaCl, bound proteins were eluted with 30 μl of 1 M glycine pH 2.5 three times. The samples were neutralized by adding 10 μl 1 M Tris-HCl pH 8.0, and concentrated using 10-kDa-cutoff Amicon® Ultra filters (Millipore).

#### Sample preparation for the mass spectrometry

Co-IP samples were separated by SDS-PAGE, and the gel was stained with colloidal Coomassie dye, and destained with  $ddH_2O$  overnight. Strongly staining bands of interest (e.g. those at the expected NS5 size of 103 kDa) were specifically excised, diced into approximate 1 mm² fragments, and placed in Eppendorf tubes, with non-staining regions being stored in separate tubes. 200  $\mu$ l of a solution composed of 25 mM ammonium bicarbonate (Ambic) and 50% acetonitrile (ACN) was applied to each sample, vortexed, briefly centrifuged, and allowed to stand for 10 min. Supernatant was then discarded via aspiration. Application and removal of Ambic/ACN was repeated, followed by SpeedVac treatment at medium heat for about 30min.A reduction step followed with application of 100  $\mu$ l DTT in 25 mM AmBic. The reaction proceeded for 1 hour at 56°C. Alkylation (specifically, blocking of cysteine residues to prevent reformation of disulfide bridges) was conducted by adding 100  $\mu$ l of 55 mM iodoacetamide (IAA) in 25 mM AmBic to each sample. The reaction occurred in the dark for 45 min at room temperature. The solution was then removed and the samples were dehydrated with 200  $\mu$ l of 25 mM Ambic in 50% ACN, vortexed, and allowed to stand for 10 min. This step was repeated once more and then samples were dried via SpeedVac.

Trypsinization was performed with "Trypsin Gold" suspended in 25 mM Ambic. Each sample tube received about 2  $\mu$ g of trypsin. 75  $\mu$ l of this solution was applied to each sample for 30 min at 4°C. The solution was then removed and samples rehydrated with 200  $\mu$ l of 25 mM Ambic, followed by overnight incubation at 37°C. Peptide extraction and desalting were achieved as follows. 200  $\mu$ l of 50% ACN and 0.5% formic acid were added to the samples, vortexed, and allowed to stand for 20 min. The supernatant was then transferred to new sample tubes. This extraction process was repeated two more times. The samples were placed in a SpeedVac and dried at moderate heat. "ZipTips" (200  $\mu$ l tips containing "solid phase extraction" paper) were treated with wetting and equilibration solution. The ZipTips were inserted into eppendorf tubes with a small hole in the cover and centrifuged at low speed, followed by treatment with washing solution samples are

treated with washing solution and centrifugation. Elution solution was then added, followed by centrifugation to isolate the peptides of interest. The desalted peptides were transferred to new tubes and dried in a SpeedVac.

For dimethyl labeling, a distinct peptide preparation method was used. Here, we sought to compare protein levels of infected cells at various time points. For such an effort, a peptide-preparation method that eliminates the imprecision associated with removal of two or more parallel gel slices (e.g. control vs. mutant or 24 hpi vs. 48 hpi) and separate injection into a mass spectrometer would be preferred. Dimethyl labeling was chosen for this purpose, allowing mixing of up to three differentially-labeled peptide samples followed by a single injection. The approach offers many of the advantages of the popular SILAC method, but at a fraction of the cost. In brief, a TCA-prepared sample was dissolved in 25 mM TEAB buffer (pH 8.0) supplemented with 5% deoxycholate to a final volume of 100 μl. Centrifugation in Amicon filter columns may be performed three times to remove low-molecular weight contaminants, using the above buffer components. A final 100 µl product is desirable. The protein mix was then incubated with a final 10 mM concentration of DTT at room temperature for 30 min. Iodoacetamide (IAA) was added to a final 15 mM and incubated 30 min at room temperature, in the dark. IAA was then inhibited by addition of 40 mM DTT and room-temperature incubation for 15 min. TEAB was added to produce a final 25 mM concentration in 1000 µl. Standard trypsin digestion was then performed 14-16 hr at 37°C. Formic acid (FA) was added to a final 0.5% concentration, with incubation at room temperature for 15 min. Centrifugation was then performed at high speed, 4°C for 15 min, followed by collection of supernatant. "Speed Vac" at moderate temperature (not high) was performed to until dry. 100 µl of 100mM TEAB was added, followed by addition of 15 µl of 4% formaldehyde isotope (the choice of three isotopes was determined by experimental design) and incubation for one hour. The reaction was quenched by addition of 1% ammonia on ice. Keeping the mix on ice, 15  $\mu$ l 100% FA was added. The samples may then be mixed as desired. The standard desalting step involving the use of "Zip tips" (see above) follows.

#### Mass spectrometry (MS) analysis

Mass spectrometry was performed in Dr. Trairak Pisitkun's group at Chulalongkorn University on a Thermo-Scientific "Q Exactive plus" platform. Mass spectrometry results were initially analyzed according to the GPM database (future work will include at least one other database, e.g. "Skyline"). Parent mass errors between -10 to 10 ppm were used. The matching proteome was *H. sapiens* male and female. The database was winnowed by excluding common contaminants (e.g. keratin) and, most significantly, by excluding all proteins that were found in both mutant (TAP-tagged virus) and control (wild-type virus). That is, only proteins found exclusively in the mutant samples were considered as potential DENV RNA interactors. Proteins could be ranked by several means. Most simply, unique peptide fragments could be counted. Bias for high-molecular weight proteins could be eliminated or reduced by dividing the unique peptide count by the putative protein's mass. GPM also generates a number of confidence measures based on the probability of false positives.

The presumed DENV-RNA interaction network was generated via the STRING 10.0 database (http://www.string-db.org) at a confidence mode of 0.4. Gene ontology (GO) groupings were gotten from DAVID (http://david.abcc.ncifcrf.gov/). A lab database of known flaviviralinteractors was constructed by extensive literature survey; this database could be used, for example, for determining overlap between our results and other results, for selecting promising protein candidates for future study, and more.

#### Purification of DENV-2 RdRp

We cloned the RdRp domain, residues 277-900, of NS5 from DENV serotype 2 cDNA into between *Nhel* and *Xhol* sites in the pET-28b vector. The construct was fused with the His tag and the thrombin cleavage site at the N-terminus. Expression of RdRp were induced in *E. coli* Rosetta (DE3) with 200  $\mu$ M IPTG at OD<sub>600</sub> = 0.6-0.7 at 18°C, and proceeded for 16 hours. Cells were harvested by centrifugation at 6,000 g for 10 min at 4°C. Soluble proteins were extracted and fractionated by ultracentrifugation at 100,000 g for 1 h at 4°C prior to subjected to a three-step chromatography including the nickel-affinity, the anion exchange, and the gel filtration. In some cases, the His-tag was completely removed from the recombinant RdRp by addition of 2 units thrombin per 1 mg protein and dialysis against the lysis buffer for 2 days at 4°C. The purified RdRp were flash frozen by liquid nitrogen in 50 mM Tris-HCl pH 7.6, 100 mM KCl, 2 mM DTT and 10% glycerol, and stored at -80°C until use.

#### SPR RNA-binding assay

The 5´-UTR (nucleotides 1-159) containing the SLA element was amplified from DENV-2 cDNA with a forward primer carring the T7 class II promoter. PCR products were subjected to the *in vitro* run-off transcription with T7 RNA polymerase. Transcribed products were separated on long denaturing acrylamide gels, and visualized by staining with 0.1% toluidine blue O. Desired RNA bands were excised, and extracted from gels with a solution containing 0.3 M NaOAc pH 6.0, 0.5 mM EDTA, 5 mM Mg(OAc)<sub>2</sub>, and 0.1% SDS overnight at 4°C with shaking. 5´-UTR RNA pellets were collected via ethanol precipitation, washed several times with 70% ethanol, and stored at -30°C.

The RNA-binding ability of the recombinant RdRp was determined by surface plasmon resonance (SPR) analysis using the Biacore X100 biosensor (GE Healthcare). N-terminal His-tagged RdRp was immobilized on a CM5 sensor chip by the amine coupling method according to manufacturer's instructions. In brief, 1.8  $\mu$ g RdRp was diluted in 70  $\mu$ l of the solution containing 10 mM sodium acetate pH 6.5, 150 mM NaCl, 0.5 mM MgCl<sub>2</sub>, and 0.05% surfactant P20, and injected with a flow rate of 5  $\mu$ l/min for 360 s. The total immobilization level was adjusted to about 3,000 RU. Binding analyses were determined at 25°C at a flow rate of 40  $\mu$ l/min in solution containing 10 mM HEPES pH 7.5, 150 mM NaCl, 0.5 mM MgCl<sub>2</sub>, and 0.05% surfactant P20. The association phase was followed for 60 s, while dissociation phase was followed for 180 s. SLA RNA was injected with increasing concentrations (6.25, 12.5, 25, 50 and 75 nM) in a single analysis cycle without regeneration. The experiments were repeated in triplicate for each protein concentration. The tRNA<sup>mix</sup> from baker's yeast was used as a negative control for non-specfic RNA-binding activity of RdRp. Dissociation constants ( $K_d$ ) were estimated by Scatchard plot analysis using Biacore X100 evaluation software.

#### *In vitro* Alpha binding assay

AlphaScreen Histidine (nickel chelate) Detection Kit (PerkinElmer) was exploited in this study. 5′-Biotinylated RNAs were purchased from Integrated DNA Technologies (Coralville, IA), including truncated SL (Bi-miniSL: 5′-biotin-ACAGCAUCAUUCCAGGCACAGAACGCCAGAAAAUGGAAUGGUGCUG), truncated SL with deletion in the top loop (Bi-miniSLΔTL: 5′-biotin-ACAGCAUCAUUCCAGGCACGCCAGAAAAUGGAAUGGUGCUG), and truncated SLA (Bi-miniSLA: 5′-biotin-ACUACGUGGACCGACAAAGACAGAUUCUUUGAGGGAGCUAAGCUCAACGU AG). All RNAs were pre-heated at 70°C for 3 min, and then slowly cooled down to room temperature in a folding buffer (20 mM HEPES pH 7.4, 50 mM NaCl, 2 mM EDTA) before use. All assays were performed in 384-well white-gray

AlphaPlates (PerkinElmer; 6005350) in 25  $\mu$ l reactions at room temperature. Initially, assay conditions were extensively optimized by cross-titration between protein and RNA concentrations to yield the maximum Alpha signal, and to determine the "hooking zone", where quenching of the signal is observed due to an excess of the binding partner. 200 nM RdRp and RNA (total 12  $\mu$ l) were incubated in the reaction mixture containing 25 mM HEPES pH 7.4, 100 mM NaCl, 2 mM MgCl<sub>2</sub>, and 0.1% BSA for 30 min. Then the nickel chelated acceptor beads (30  $\mu$ g/ml final concentration) were added and incubated in the dark for 30 min, following by addition of the streptavidin donor beads (20  $\mu$ g/ml final concentration) and a 30 min incubation in the dark before the assay was conducted on an EnSpire<sup>TM</sup> 2300 Multilabel Plate Reader (PerkinElmer). Equilibrium dissociation constants ( $K_0$ ) between SL and RdRp were quantified from the saturation binding experiments. The data was then fitted on a nonlinear regression curve by using the one-site binding mode in GraphPad Prism software (San Diego, CA).

#### Results and Discussion

We have discovered a robust, specific interaction between DENV RdRp or NS5 and the SL RNA element in the 3´-UTR of the viral positive genome (**Fig. 2**, in press). The interaction is governed by the conserved sequence of CACAG in the top loop (TL) of 3´ SL. In Y3H context, 3´SL has higher affinity with RdRp than 5´SLA by beyond 2 orders of magnitude. To investigate the binding kinetics of DENV RdRp *in vitro*, we cloned, overexpressed, and purified the DENV-2 RdRp protein from *E. coli*, and initially characterized the interaction with 5´ SLA using surface plasmon resonance (SPR) (**Fig. 4**). RdRp interacted with 5´ DENV RNA with  $K_d \approx 53$  nM. This result was already published [Kamkaew M and Chimnaronk S. (2015) *Protein Expr. Purif.* **112**, 43-9]. The obtained  $K_d$  was comparable to previously reported value of 11 nM using EMSA.

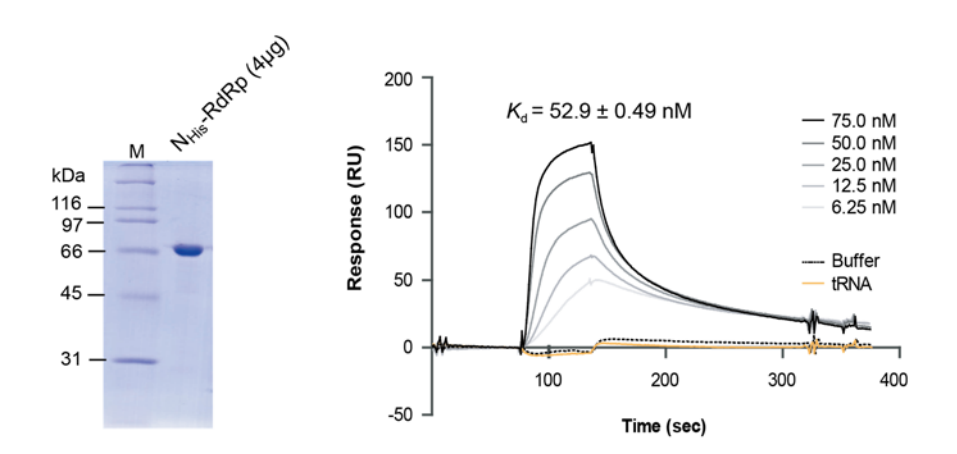
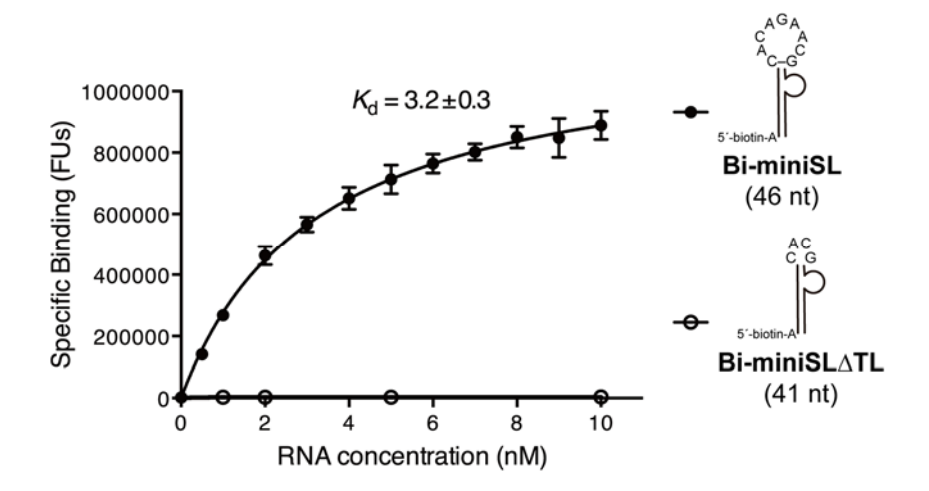


Figure 4. RNA-binding activity of DENV-2 RdRp was measured via SPR analysis with 5'-UTR RNA. The left panel shows the purified RdRp and the right panel shows SPR sensorgrams. Equilibrium dissociation constant ( $K_d$ ) was determined from the binding curves at various concentrations of RNA from 6.25 nM to 75 nM. tRNA was used as a negative control.

Next, we investigated the binding affinity of RdRp with 3´SL. This time, we developed an *in vitro* binding assay called Alpha assay. This assay possesses multiple advantages beyond EMSA or SPR: 1) the assay is completely performed in solution in the concentration range of the  $K_d$ ; 2) The signal-to-noise level is extremely

high; 3) The assay is highly reproducible and can be performed in a high-throughput manner. SL binds to RdRp with  $K_d \sim 3$  nM, whereas the deletion of the top loop completely abolished the binding signal (**Fig. 5**). Our results clearly revealed that the top loop (TL) of 3<sup>'</sup> SL is an exclusive binding site of RdRp in the viral genome. This is the first time that this interaction is characterized [Hodge K, Tunghirun C, Kamkaew M, Limjindaporn T, Yenchitsomanus PT, Chimnaronk S. (2016) *J Biol Chem.* In press].



**Figure 5.** *In vitro* Alpha binding assay. Saturation binding experiment of RdRp with truncated 3´SL. The alpha binding signal is shown in fluorescence unit (FU). Mean and standard deviation values derive from three independent experiments. We note that SLA did not show a binding signal in both saturation binding and competition assay.

We took advantage of strong affinity of RdRp against the viral genome to explore viral RNA interactions in human cells via modified PAR-CLIP procedure (Fig. 6).

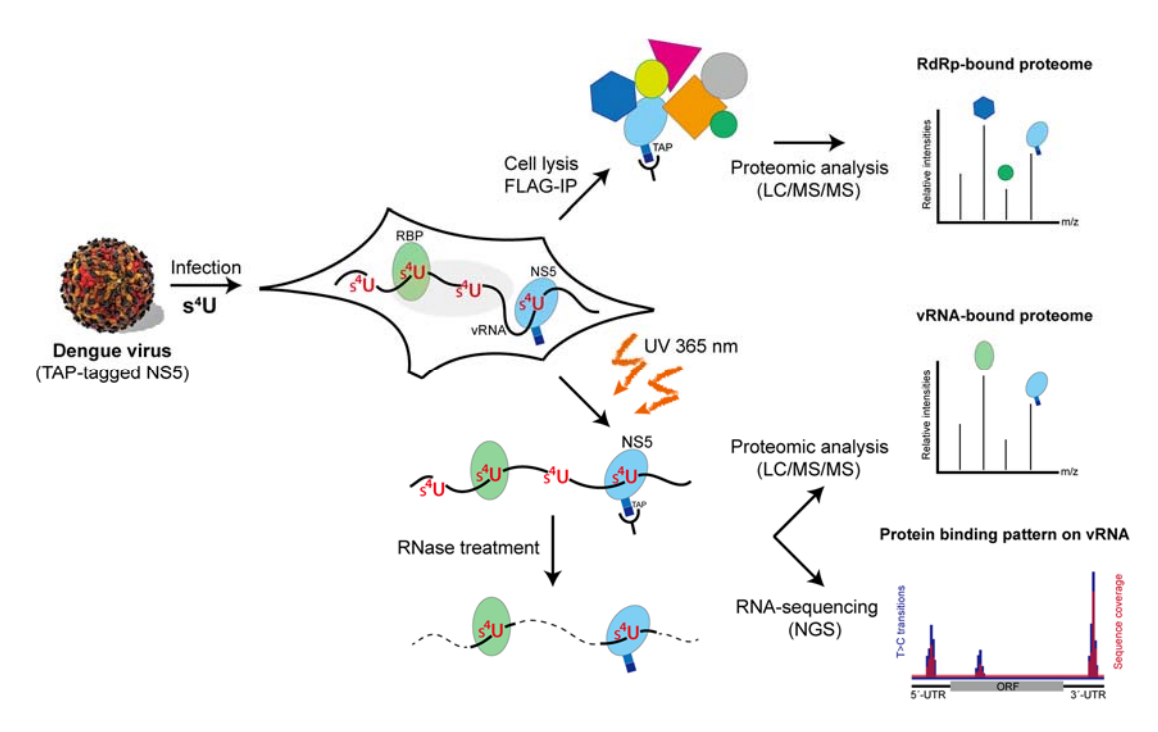
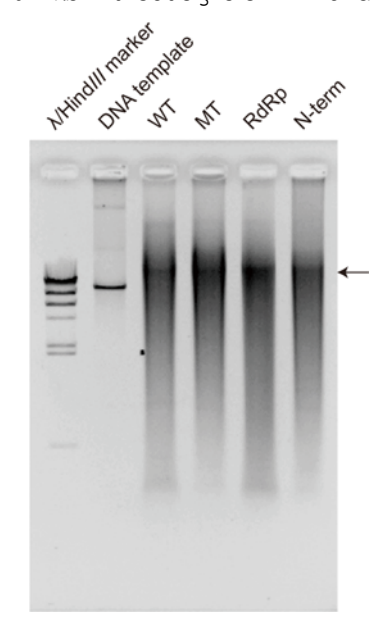


Figure 6. Schematic diagram of modified PAR-CLIP in this study.

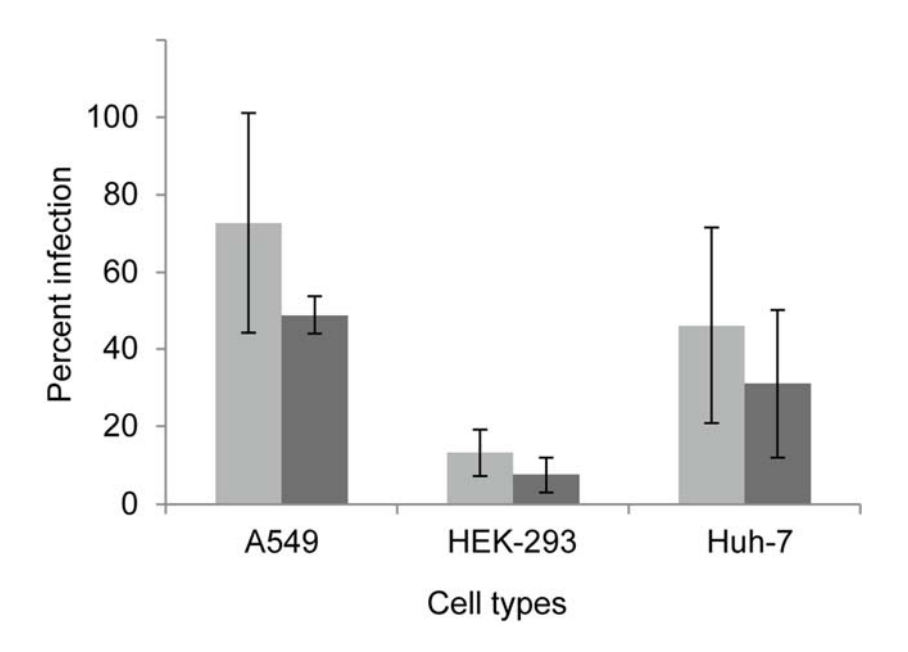
Our idea is to crosslink NS5 with the viral genome *in vivo*, and perform co-immunoprecipitation (co-IP) of NS5 to isolate all human factors that interacts with the viral RNA. To perform co-IP efficiently, we have cloned the full-length 10.7-kb DENV-2 cDNA, and performed QuikChange to insert the TAP-tag including hexahistidine and FLAG tags into the NS5 protein at the earlier stage of this study. Four different regions in NS5, which are the N- and C-termini, two loops in the methyltransferase domain (MT, residues 171-176) and the polymerase domain (RdRp, residues 635-640), were selected by a severe criteria described above in Methods to minimize deleterious effects to the viral replication (Fig. 3). vRNAs were synthesized by the *in vitro* run-off transcription, and thoroughly purified to eliminate any contaminations of the DNA template (Fig. 7). *In vitro* transcribed vRNAs showed a single population of about 10.7 kb without signs of DNA and RNase contaminations.



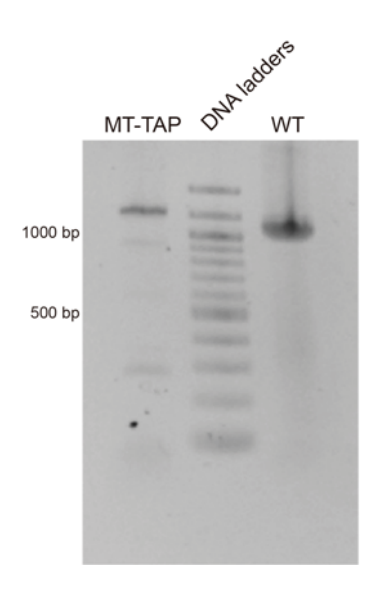
**Figure 7.** *In vitro* synthesis of DENV genomic RNAs using run-off transcription with T7 RNA polymerase. Purified 10.7-kb vRNAs were visualized on a denaturing agarose gel, revealing pure transcripts without DNA template contaminations.

All vRNAs including non-tagged construct (WT) as the control were transfected into BHK-21 cells using electroporation. Cells were maintained until days 7, and then the presence of DENV E protein in cells were detected by immunofluorescence. In addition, at day 6<sup>th</sup>, the media were subjected to the FFU assay to investigate the formation of infectious virus. Interestingly, only the DENV construct with the TAP-tag in the methyltransferase domain (MT) showed the production of the E protein in cells, and produced the infectious virus, comparable to the wild-type (WT). At this point, we have no clear explanation why a short TAP-tag epitope destroyed the ability of viral replication or production in cells. It is most likely that the tag disrupted the structure and function of NS5. Nonetheless, we focused on only this infectious clone and others were not pursued. Hereafter, the MT viral clone that contains a TAP tag inside the methyltransferase domain of NS5 is designated etDENV (engineered, tagged DENV). We further characterized etDENV and showed that our etDENV possesses infectability comparable to that of the wild-type virus with different human cell lines (Fig. 8).

Next, we questioned if this engineered DENV would be stable during several cell passages. After 3 passages in BHK cells, we extracted vRNA and performed RT-PCR of cDNA fragment containing regions of the TAP-tag in NS5. The results evidently showed the TAP tag in NS5 after cell passaging (**Fig. 9**). We further confirmed the whole sequence of DENV clone at the 7<sup>th</sup> passage, showing the intact TAP-tag in the viral genome. Our results showed one of significant breakthroughs in the field. Our etDENV was infectious and stable during several passages. We also noted that this is the first report to insert the tag epitope into the infectious DENV. The development of etDENV was recently published [Poyomtip T, Hodge K, Matangkasombut P, Sakuntabhai A, Pisitkun T, Jirawatnotai S, Chimnaronk S. (2016) *J Gen Virol.* **97**(3), 646-58].



**Figure 8.** Flow cytometry analysis with anti-E antibody revealed that etDENV could infect several human cell lines. Light and dark grey bars represent DENV-2 16681 and etDENV, respectively.



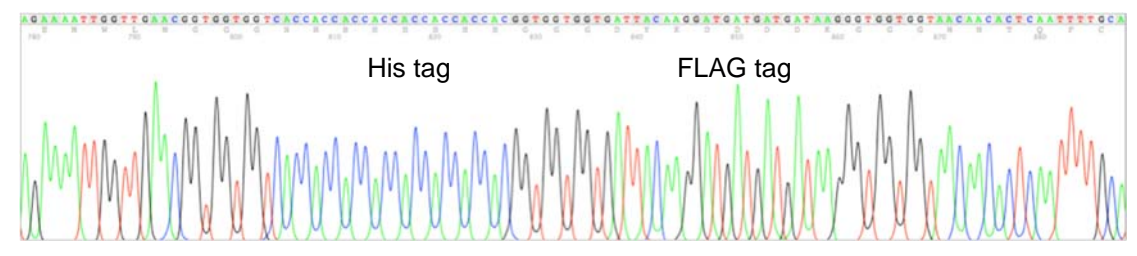


**Figure 9.** Validation of stability of etDENV. After 3 passages in BHK-21 cells, the tagged DENV (MT-TAP) shows larger RT-PCR product than the wild-type (WT) according the TAP-tag in the methyltransferase domain (top panel). The virus was also sequenced after the 7<sup>th</sup> passage (bottom panel). The profile around the TAP-tag region is shown.

Our results revealed that etDENV is suitable for our modified PAR-CLIP. Next, we performed a large-scale production of etDENV in the Vero cell line. This process was performed with the collaboration with Dr. Sutee Yoksan at the Institute of Molecular Biosciences, Mahidol University. Finally, we obtained 1 liter of the virus stock possessing approximately  $3 \times 10^7$  PFU/ml. We spent a few months for this process to obtain high yield and quality of the virus, which were crucial for PAR-CLIP. While our etDENV genome was stable during the viral passage, we decided to use only the secondary passage for the stock to guarantee intact tag inside viral genome. To test PAR-CLIP, approximately  $4 \times 10^7$  Huh7 cells was infected with etDENV at MOI 1 in the presence of 100  $\mu$ M s<sup>4</sup>U in the media. At 48 h after infection, cells were exposed to UVA to cross-link protein and RNA inside the cell prior to PAR-CLIP via two steps of nickel and FLAG affinity resins (Fig. 10). The results showed significant breakthrough in isolation of NS5 from DENV-infected cells with high yield and purity for the first time. We estimated a minimum of 500 ng NS5 could be isolated from  $10^7$  Huh7 cells, which was sufficient for further proteomics analysis with mass spectrometry.

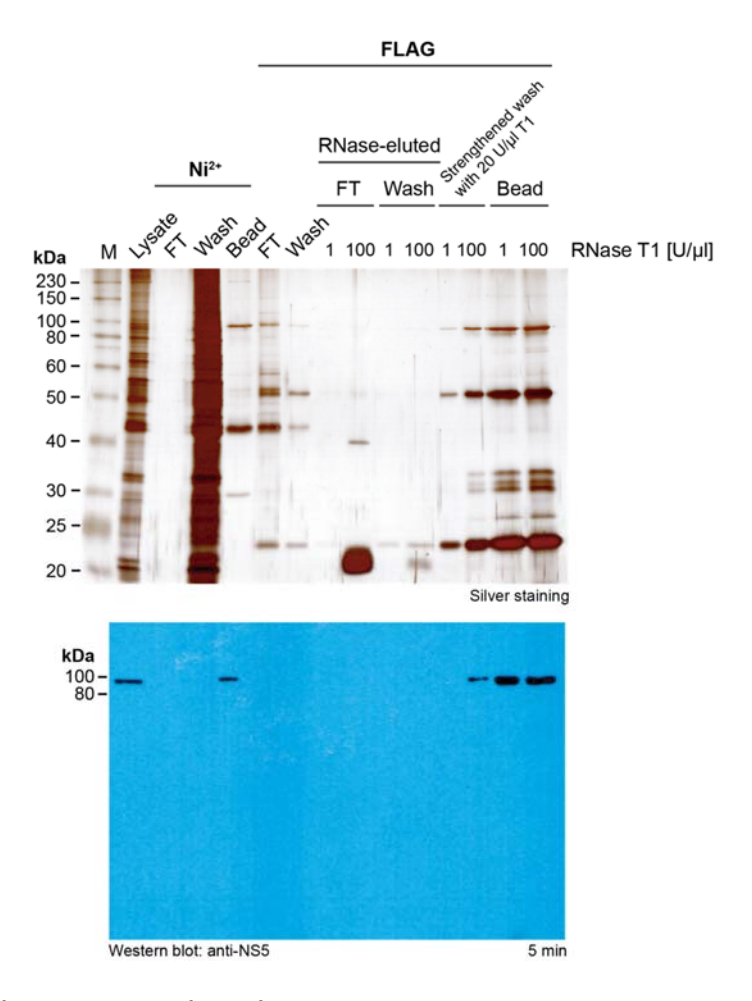


Figure 10. TAP isolation of tagged DENV NS5 from infected Huh7 cells. Fractions including cell lysate, resin-run-throughs, washes, and elutions were loaded onto a SDS-PAGE, and blotted with anti-DENV NS5 antibody. NS5 bands are seen at the correct molecular size of 106 kDa. Intense bands of 50 and ~23 kDa seen in the silver staining correspond to heavy and light chains of the anti-FLAG antibody, respectively.

To this end, we performed PAR-CLIP by infected the human Huh7 cells with etDENV at MOI 5 in the presence of 100  $\mu$ M s<sup>4</sup>U in the media. At 48 h after infection, cells were exposed to UVA to cross-link protein and RNA inside the cell prior to PAR-CLIP via two steps of nickel and FLAG affinity resins. Proteins interacting with vRNA were eluted from FLAG beads with acidic condition, and subjected to MS analysis. The resulting GPM-based list of 122 proteins found only in tagged NS5 elutions was judged to be highly satisfactory based on several criteria. First, nucleotide and RNA-binding proteins were highly enriched ( $p = 6 \times 10^{-16}$ , **Table 1**). Secondly, the STRING network showed clear clustering of proteins (**Fig. 11**), suggesting well-defined viral or host strategies. Finally, comparing our protein list against our database of host proteins known to be relevant in flaviviral infections showed that 60% of our proteins were also seen in the database (**Table 2**). While our protein list and network conformed well to general expectations, there were a number of surprises. For example, minichromosome maintenance (MCM) proteins were prominent in our results, though flaviviral associations with this complex are absent in the literature. Also, proteins associated with mitochondrial lumen were enriched in our results, again with little mention in the literature. We are currently planning to validate these vRNA interactors using distinct approaches such as Y3H and siRNA.

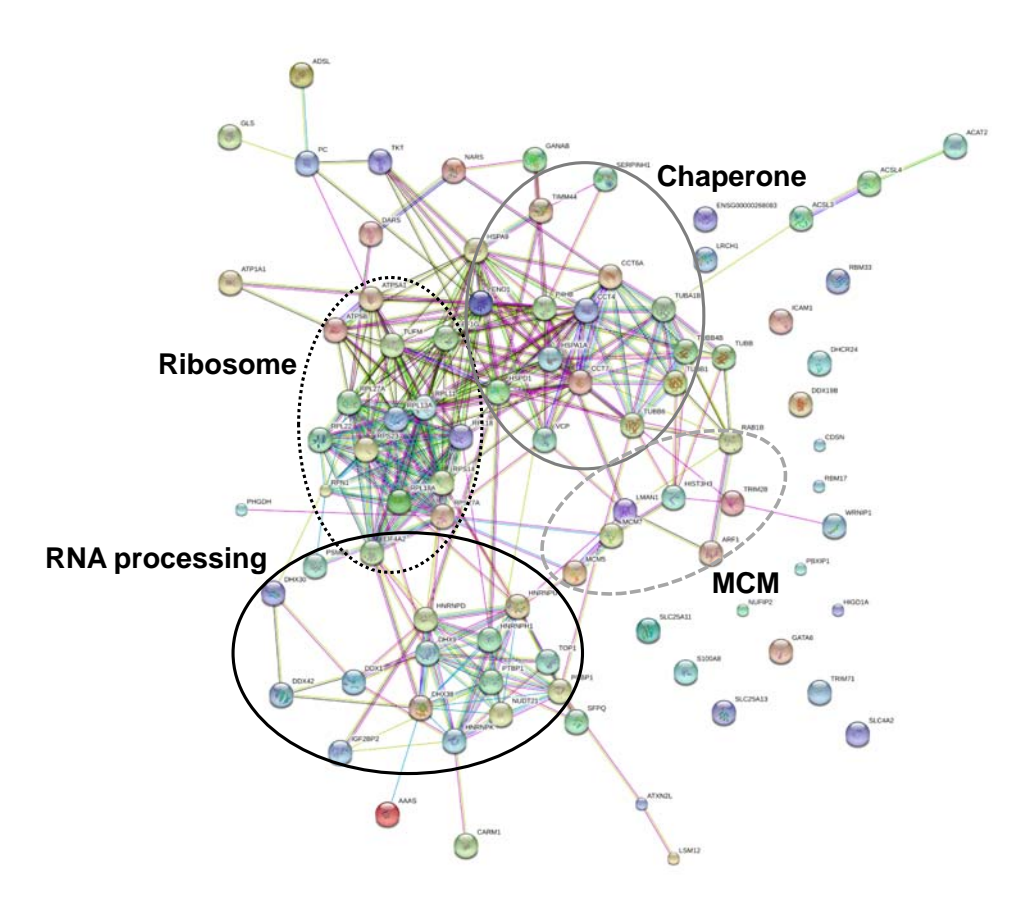


Figure 11. The first Interactome map of DENV RNA in Huh7 cells via PAR-CLIP. Note that interacting proteins show strong clustering into functional groups, with few outliers.

**Table 1.** GO terms showing enrichment of particular interest.

	<u> </u>
Group	<i>P</i> -value (Benjamini-correction)
RNA-binding	$6 \times 10^{-16}$
Chaperones	$4.4 \times 10^{-7}$
Helicases	$5.5 \times 10^{-5}$
Organelle Lumen	$5.7 \times 10^{-6}$
Tubulin	$6.6 \times 10^{-4}$
Mitochondrial matrix	9.5 × 10 <sup>-4</sup>

**Table 2.** DENV RNA-interacting proteins obtained from our PAR-CLIP are prominent in the viral literature. Note that functions of these interactors may or may not relate to RNA-binding.

Mentions in the viral literature			
At least 4	3	2	1
GRP78	ACTB	CMC2	PTBP1

ENOA	ATPB	HS90B	PKP2
ATPA	TBA1B	GRP75	KPYM
HNRPU	CKAP4	RL22	SYIM
RS14	HNRPD	TCPA	GANAB
	RS27A	TBA1B	SERA
	HNRPK	TIF1B	DESP
	ENPL	DSG1	HNRPL
	AT2A2	DHX9	TIM44
		HNRPD	RL18A
		ARF1	NUFP2
		CH60	M2OM
		TCPQ	DDX5
		AT1A1	DHX15
		RPN1	PDE4D
		RL27A	FINC
		H31T	TCPD
		PCBP1	SYDC
		FAS	SFPQ
		AT2A2	COPA
		PSMD2	WRIP1
		EFTU	TIF1B
		PDIA1	TCPH
		RS23	RL13A
		TBB4B	RL11
		TBB5	U520
		HSP71	DD19B
		LIN41	PBIP1
			AT1A1
			TKT
			TERA
			HNRH1
			TBB6
			HIG1A
			DDX42
			LIN41
			EF1G

At the same time, we also decided to analyze the interactome of NS5 in parallel to investigate differences in the two interaction layers. We performed IP of NS5 via a single FLAG affinity step, and MS analysis. only DENV NS5 interactors that were found in etDENV IP samples, but not in the control, were considered in our analysis. Moreover, we utilized two distinct algorithms for peptide identification, and only 97 proteins overlapping between 554 X! Tandem and 199 SEQUEST candidates were considered, and mapped by STRING 10.0 software. To reveal a high-confidence interactome, this network was reconstructed to include two forms of information (Fig. 12). First, STRING's protein-protein interaction confidence levels were shown as edge widths. Secondly, relative peptide abundances from mass spectrometry were indicated by node sizes. In addition to the host proteins, the NS3 helicase was identified, confirming its role as the major viral protein interacting with NS5 (Table 3). Our NS5 interaction network contained only 4 proteins that were also reported as NS5 interactors in recent genome-wide studies (Table 4). Intriguingly, the heterogeneous nuclear ribonucleoproteins (hnRNPs) were identified as the main NS5 complex for the first time. Several NS5 interactors related to the protein-folding pathway have already been shown to be up-regulated upon DENV infection. The NS5 interactome was recently published [Poyomtip T, Hodge K, Matangkasombut P, Sakuntabhai A, Pisitkun T, Jirawatnotai S, Chimnaronk S. (2016) *J Gen Virol.* 97(3), 646-58].

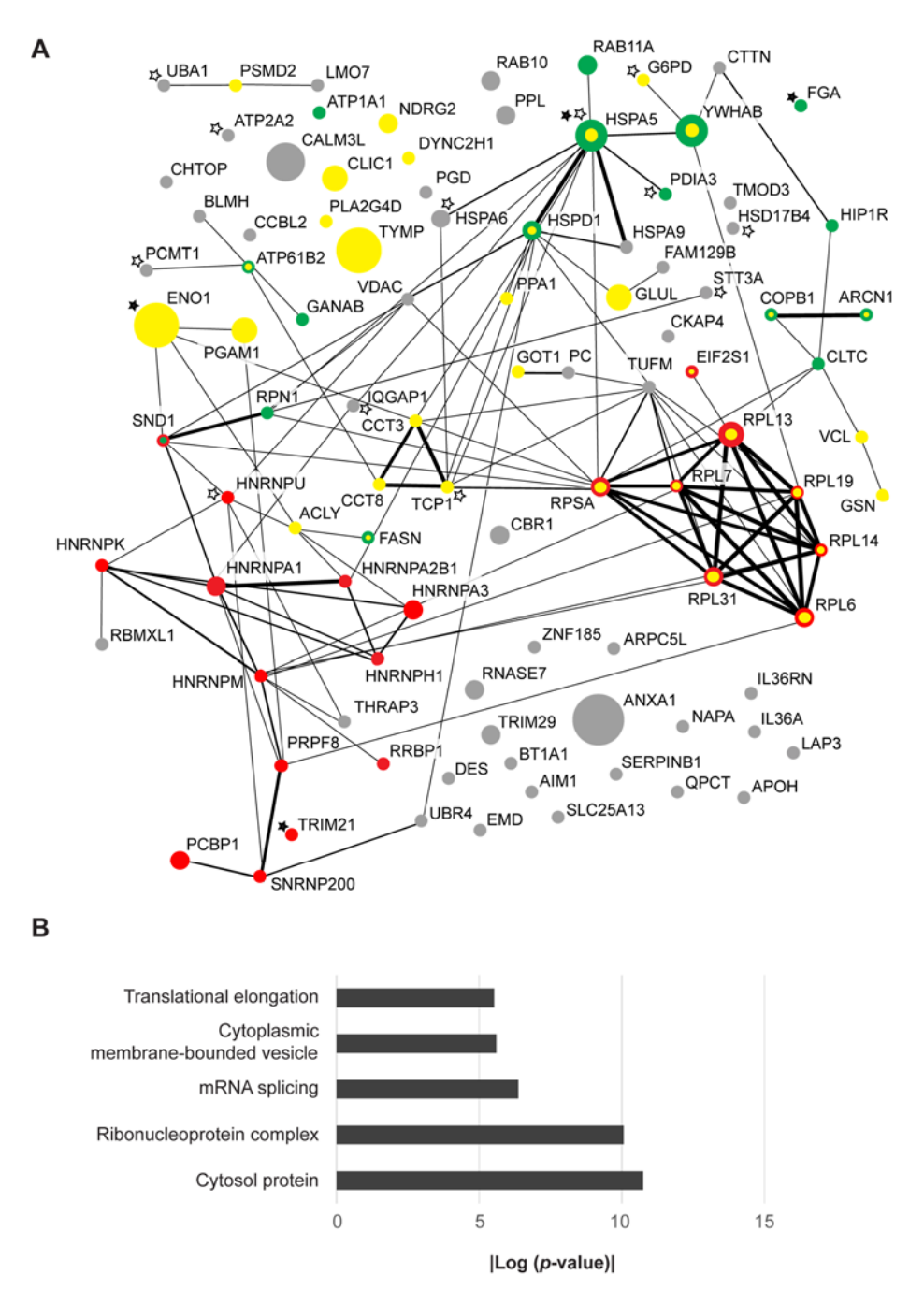


Figure 12. NS5 interactome in Huh-7 cells. (A) The protein-protein interaction network was reconstructed using the initial STRING 10.0 network as template. Colors indicate three enriched groups: yellow for non-membranous predominantly cytosolic proteins, red for ribonucleoproteins, and green for cytoplasmic membrane-bound vesicle proteins. Open and filled stars indicate proteins with altered expression levels and NS5 interactors identified in previous studies, respectively. Edge length and node placement are not of import. Isolated nodes should not be construed as irrelevant to infection. (B) List of enriched gene ontology groups using DAVID.

Our functional annotation showed highest enrichment in cytosolic proteins, a category that excluded membranous and subcellular components. Enrichment in cytosolic membranous components was also high, consistent with NS5's localization with the ER during replication. Ribonucleoproteins (RNPs), normally found in the nucleus, were abundant within the interactor list, with a subset of splicing-related hnRNPs (hnRNPM,

hnRNPA1, hnRNPA3, hnRNPU, hnRNPK, hnRNPH1, and hnRNPA2B1) showing particular enrichment. Interestingly, a previous study examining the infected Huh-7 proteome showed significant alterations in the abundance of RNA processing proteins; however, precise roles played by interaction of hnRNP with NS5 require further study. Another subset of RNP interactors was related to the translational elongation process. In particular, large ribosomal subunit members (RPL6, RPL7, RPL13, RPL14, RPL19, and RPL31) were identified as NS5 interaction partners, with only low levels of other ribosome proteins found in the control group.

We also divided the number of fragments detected by molecular weight and abundance (in parts per million of protein) in the liver (PaxDb Version 4.0) to reduce bias towards abundant proteins. The phospholipase 2 protein (PLA2G4D) came to the fore. Since it was shown that phospholipase 2 group 4C was involved in generation of the membranous web in HCV-infected cells, PLA2G4D could play a similar role in remodeling the ER membrane for DENV replication. In concord with this picture, fatty acid synthase (FASN), which was shown to be re-localized to viral replicase to remodel cytosolic membranes in DENV-infected cells, was also present in our interactome map. Other interactors involved in lipid metabolism included pyruvate carboxylase (PC), ATP citrate lyase (ACLY), and butyrophilin (BT1A1). Our results suggest tight association of fatty acid biosynthesis complex with viral replicase.

Table 3. DENV proteins identified by NS5 IP.			
Viral proteins	Peptides	MW (kDa)	
prM	1	18.92	
NS1	1	39.93	
NS3	10	69.26	
NS4A	1	13.96	
NS5	24	103.2	

Table 4. NS5 interactors identified in this study and other earlier reports.		
Symbols	Methodology	Functions
HSPA5	Y2H	Protein folding and protein assembly
ENO1	Y2H	Glycolysis enzyme and tumor suppressor
TRIM21	Y2H	Protein degradation process
FGA	Y2H	Blood coagulation

In order to further characterize potential vRNA-interacting proteins, 8 candidates were cloned into the Y3H protein expression vector, pACT2. Details of Y3H methodology are available in prior reports. The proteins of interest are ATP5a1, CCT6a, DDX19a, ENO1, HSPD1, LSM12, PCBP1, and TUB4b. Following standard methods, the appropriate sequences were inserted into pACT2 and validated by sequencing. Initial Y3H screening against

a library of DENV-2 fragments suggested some degree of interaction with DDX19a, LSM12, PCBP1, and TUB4b. Western blotting confirmed in-yeast expression of these four host-proteins. In another round of study, the RNA sequences associated with relatively strong interactions with PCBP1 were PCR-amplified from the RNA expression plasmids within yeast, and sequenced. The six resulting sequences, ranging in size from 38 to 78 nt, represented different regions of the viral genome, but all contained the canonical CCxxxCC PCBP1 binding motif, where x represents any nucleotide, with a weak preference toward U. Previous work has confirmed that the DENV Y3H RNA library is unbiased toward positive or negative strands, yet the six RNA sequences all aligned with the negative strand. Intriguingly, while 16 of these motifs are found on the DENV positive strand, 44 are found on the negative strand.

In addition to the molecular biological experiments, we are testing our new bioinformatics pipeline to analyze our interactome map in deep. We seek for any correlations between our interactome and any previous studies. The current database includes protein lists derived from proteomic pulldowns, microarray and RNA-seq results based on drug treatments or knockdown/overexpression of proteins, micro-RNA targets, transcripts/proteins that are over/underexpressed in various cancers, and more. The significance of overlap between protein lists in two studies can be summarized by a simple *p*-value via Fisher's exact test. Comparison of the proteins found in our vRNA interaction network with proteins in other studies generates the following overlaps of particular interest (Table 5).

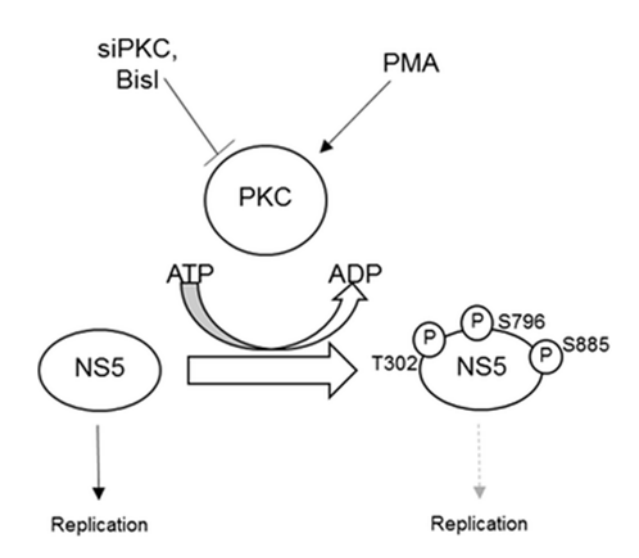
This study provides the two-dimensional interactome of DENV NS5 and vRNA for the first time. We are performing many experiments and bioinformatics to uncover the roles of human factor in DENV replication. We hope that our study will lead to a new design of antiviral drug and therapy in the future.

Table 5. Correlation between vRNA interactors from this study and other databases

Study	p-value
NS5 interactors (our own list)	-39.52194
proteins highly abundant in complexes (in Hela and Hek) (A Census of Human Soluble Protein Complexes)	-39.35706
cct complex interactors (New insights into the functions and localization of nuclear CCT protein complex)	-33.78848
MS study of proteins associated with IncRNA NORAD in hct116 cells (Noncoding RNA NORAD Regulates Genomic Stability)	-24.64325
HepG2 transcripts that tend to lack long poly-A tails (RNA-seq of long poly adenylated RNA and long non poly adenylated RNA from ENCOL	-24.56002
coding genes at which nearby IncRNAs are expressed at high levels (Divergent transcription of long noncoding)	-19.65059
300 proteins most abundant in whole humans (pax-db.org)	-17.46533
required for 40s ribosome assembly in hela cells (RNAi Screening Identifies Protein Modules)	-17.04015
u1 and/or u2 interactors: (Systematic Discovery of Xist RNA Binding Proteins)	-16.58041
upregulated in CHKV-infected HEK cells (High throughput proteomic analysis and a comparative review)	-15.1089
orf1 interactors (Mapping the LINE1 ORF1 protein interactome reveals)	-13.46899
CLASH targets of mir331-3p	-11.47353
most CLASH targets of mir484	-11.42136
CLASH targets of mir197-3p	-11.41606
downregulated in gastric cancer (Quantitative proteomic and genomic profiling reveals metastasis)	-11.40026
cyclin D1 interactors in 5 cancer types (SiwanonA function for cyclin D1 in DNA repair)	-11.32683
CLASH targets of mir744-5p#	-10.96968
abundant in whole human vs. seminal vesicle	-10.5289
chip-seq-based brca1/palb1 occupancy sites in breast cancer cells (Genome-wide analysis reveals a role for BRCA1)	-10.38773
CLASH targets of mir877-3p	-10.17469
CLASH targets of mir324-5p	-10.08301

The *p*-values above are unadjusted (i.e. no Bonferoni/Benjamini correction).

One more thing, we also collaborated with Dr. Siwanon Jirawatnotai (Siriraj hospital, Mahidol University) and Dr. Rutaiwan Tohtong (Faculty of Science, Mahidol University) to search for transient interaction between DENV RdRp and human kinases. We discovered that the human protein kinase C (PKC) phosphorylated DENV RdRp, and such phosphorylation reduced viral replication and increased viability of the DENV-infected cells. The results suggested that PKC may act as a restricting mechanism that modulates the DENV replication and represses the viral outburst in the host cells. The results were recently published [Noppakunmongkolchai W, Poyomtip T, Jittawuttipoka T, Luplertlop N, Sakuntabhai A, Chimnaronk S, Jirawatnotai S, Tohtong R. (2016) *Virol J.* 13, 35].



**Figure 13.** Inhibition of NS5 phosphorylation by PKC promotes viral replication. PKC is a host factor, which restricts intracellular DENV2 number by phosphorylating viral NS5. Inhibition of PKC by PKC inhibitor (BisI) or PKC-specific siRNA (siPKC) results in increased viral copy number

# Output ที่ได้จากโครงการ

In this study, we have developed many experimental procedures and obtained a number of significant results. We report here, for the first time, the two dimensional interactome map of DENV NS5 and vRNA in human Huh-7 cells using engineered tagged DENV. Our system completely mimic environment in human tissue than other studies that use only a plasmid to express a single viral protein. We are validating and bioinformatics analysis our interactome map to find essential pathways for DENV replication in human cells. We would like to summarize our output from the project as follows.

#### Technology developed or established

- 1. Two *in vitro* protein–RNA binding assay: Surface Plasmon Resonance (SPR) and Amplified Luminescent Proximity Homogeneous Assay (Alpha).
- 2. Engineered, tagged dengue virus (etDENV): Infectious DENV possessing His-FLAG tag inside NS5 gene.
- 3. Modified  $\underline{P}$ hoto $\underline{a}$ ctivatable- $\underline{R}$ ibonucleoside-Enhanced  $\underline{C}$ ross $\underline{l}$ inking and  $\underline{l}$ mmuno $\underline{p}$ recipitation (PAR-CLIP) that allows two dimensional omics analysis.

#### Novel knowledge

- 1. DENV-2 RdRp specifically binds to the 3´ SL RNA element with a dissociation constant  $K_d = 3.2$  nM (published).
- 2. Human PKC phosphorylates DENV-2 RdRp to suppress viral replication inside cells (published).
- 3. The high-confidence interactome map of DENV-2 RdRp with human factors (published).
- 4. The first interactome map of DENV-2 RNA with human factors (unpublished).

#### **Education**

- 1. Miss Maliwan Kamkaew obtained her M.Sc. degree.
- 2. Mr. Kenneth Hodge will defense his Ph.D. degree in this August.
- 3. Mr. Teera Poyomtip will defense his Ph.D. degree in this August.

#### **Publications**

- (1) Kamkaew M and **Chimnaronk S**. (2015) Characterization of soluble RNA-dependent RNA polymerase from dengue virus serotype 2: The polyhistidine tag compromises the polymerase activity. *Protein Expr. Purif.* **112**, 43-9.
- (2) Poyomtip T, Hodge K, Matangkasombut P, Sakuntabhai A, Pisitkun T, Jirawatnotai S, **Chimnaronk S.** (2016) Development of viable TAP-tagged dengue virus for investigation of host-virus interaction in viral replication. *J. Gen. Virol.* **97**(3), 646-58.
- (3) Noppakunmongkolchai W, Poyomtip T, Jittawuttipoka T, Luplertlop N, Sakuntabhai A, **Chimnaronk S**, Jirawatnotai S, Tohtong R. (2016) Inhibition of protein kinase C promotes dengue virus replication. *Virol J.* **13**, 35.
- (4) Hodge K, Tunghirun C, Kamkaew M, Limjindaporn T, Yenchitsomanus P, **Chimnaronk S.** (2016) Identification of a conserved RdRp–RNA interface required for flaviviral replication. *J Biol Chem.* In press.

### Other activities (การไปเสนอผลงาน การได้รับเชิญไปเป็นวิทยากร)

- 1.1. วิทยากรบรรยายเรื่อง "Exploration of An Interactive Layer of RNPomics" ที่ศูนย์ความเป็นเลิศทาง งานวิจัยสเต็มเซลล์ (SiSCR) อาคารเฉลิมพระเกียรติ 80 พรรษา 5 ธันวาคม 2550 (SiMR) ชั้น 7 รพ.ศิริราช เมื่อวันที่ 15 ตุลาคม พ.ศ. 2557
- 1.2. วิทยากรบรรยาย Molecular Club เรื่อง "RNPomics of Flavivirus: A search for interacting interfaces for drug development" ที่ห้องประชุม 304 ชั้น 3 ตึกอานันทมหิดล คณะแพทยศาสตร์ จุฬาลงกรณ์มหาวิทยาลัย เมื่อวันที่ 13 พฤศจิกายน พ.ศ. 2557
- 1.3. วิทยากรบรรยายเรื่อง "RNPomics of DENV for Drug Discovery" ในงาน System Biology Week ที่ ห้องประชุมชั้น 4 ห้องสมุดคณะแพทยศาสตร์ จุฬาลงกรณ์มหาวิทยาลัย เมื่อวันที่ 20 พฤศจิกายน พ.ศ. 2558
- 1.4. วิทยากรบรรยายเรื่อง "RNPomics of DENV for Drug Discovery" ในงาน SICMPH2016: Systems Biology ที่ห้องประชุม 201 ตึกศรีสวรินทิรา ชั้น 2 รพ.ศิริราช เมื่อวันที่ 15 มิถุนายน พ.ศ. 2559

# ภาคผนวก

ELSEVIER

Contents lists available at ScienceDirect

## Protein Expression and Purification

journal homepage: www.elsevier.com/locate/yprep



# Characterization of soluble RNA-dependent RNA polymerase from dengue virus serotype 2: The polyhistidine tag compromises the polymerase activity



Maliwan Kamkaew, Sarin Chimnaronk\*

Institute of Molecular Biosciences, Mahidol University, Salaya Campus, Phutthamonthon 4 Rd., Nakhon Pathom 73170, Thailand

#### ARTICLE INFO

Article history: Received 14 April 2015 and in revised form 19 April 2015 Available online 25 April 2015

Keywords:
Dengue virus
RNA-dependent RNA polymerase (RdRp)
Polyhistidine tag
In vitro polymerase assay
Surface plasmon resonance

#### ABSTRACT

The viral RNA polymerase is an attractive target for inhibition in the treatment of viral infections. In the case of dengue virus (DENV), a member of the genus *Flavivirus*, the RNA-dependent RNA polymerase (RdRp) activity resides in the C-terminal two-thirds of non-structural protein (NS) 5 responsible for the *de novo* synthesis of the viral RNA genome. Among four distinct, but closely related dengue serotypes, serotype 2 (DENV-2) produces more severe diseases than other serotypes. It has been reported that bacterial production of the recombinant DENV-2 RdRp was difficult due to its low expression and solubility levels. To facilitate functional and structural analyses, we here demonstrate complete protocols for overexpression and purification of soluble DENV-2 RdRp, increasing protein yields by a remarkable 10 times compared to earlier reports. Three different forms of DENV-2 RdRp as either N- or C-terminally His-tagged fusions, or without tag, were purified to homogeneity. We show here that the presence of both the N- and C-terminal His-tag had a deleterious effect on polymerase activity and, in contrast to earlier studies, our non-tagged RdRp did not require manganese ions to activate RNA polymerization. We also determined an apparent  $K_d$  value of 53 nM for binding to the 5'-UTR RNA by surface plasmon resonance (SPR). Our work provide a more suitable material for basic research of viral RdRp and for drug development.

© 2015 Elsevier Inc. All rights reserved.

#### Introduction

Dengue fever has become one of the most important mosquito-borne disease worldwide, accounting for approximately 96 million patients per year presenting several degrees of symptoms, including life-threatening dengue hemorrhagic fever (DHF)<sup>1</sup> and dengue shock syndrome (DSS) [1]. Currently, there is no commercially available vaccine or specific medication. The causative dengue virus (DENV) belongs to the *Flavivirus* genus and is classified into four distinct serotypes, DENV-1–4, which share ~60% genomic sequence identity [2]. It was reported that severe dengue cases were significantly associated with circulating infection by DENV-2 [3]. While accurate mechanisms for dengue severe

symptoms remain largely elusive, two viral non-structural (NS) proteins 3 and 5 were implicated in DHF as predominant T-cell antigens [4]. DENV possesses a single positive-sense stranded 10.7-kb RNA genome encoding a single long open reading frame (ORF) flanked by 5' and 3' untranslated regions (UTRs). The DENV ORF is translated into a pre-polyprotein having 3390 amino acids, which is subsequently proteolytically processed into three structural proteins: capsid (C), membrane (prM), and envelope (E), and seven non-structural proteins: NS1, NS2A, NS2B, NS3, NS4A, NS4B, and NS5 [5]. Of these, NS5 is the largest viral protein with the highest sequence conservation among serotypes [6]. NS5 is a multifunctional protein containing an N-terminal methyltransferase (MTase) and a C-terminal RNA-dependent RNA polymerase (RdRp), which play crucial roles in viral RNA synthesis in infected cells. Therefore, NS5 has been a primary target for antiviral drug development for a decade [7,8]. To date, crystal structures of the 73-kDa RdRp domain from DENV-3 have been determined to a high resolution of ~1.8 Å, revealing a classical polymerase right-hand conformation composed of fingers, thumb, and palm domains [6,9]. The fingers domain contains flexible loops that link together the fingers and thumb domains, and are likely to transmit conformational changes between these two

<sup>\*</sup> Corresponding author. Tel.: +66 2 441 9004x1468; fax: +66 2 441 9906. E-mail address: sarin.chi@mahidol.ac.th (S. Chimnaronk).

<sup>&</sup>lt;sup>1</sup> Abbreviations used: DHF, dengue hemorrhagic fever; DSS, dengue shock syndrome; DENV, dengue virus; NS, non-structural; ORF, open reading frame; UTRS, untranslated regions; MTase, methyltransferase; SLA, stem-loop A; IPTG, isopropyl-β-D-thiogalactopyranoside; PMSF, phenylmethylsulfonyl fluoride; PVDF, polyvinylidene fluoride; TAP, tandem affinity purification; CD, circular dichroism; EMSA, electrophoretic mobility shift assay; SPR, surface plasmon resonance.

domains. The thumb domain is involved in shaping the RNA template tunnel. There are two zinc-binding motifs in the fingers and thumb domains, where the zinc ion is thought to play a role in regulating conformational switches within the domain [6,9]. RdRp harbors the catalytic active site in the palm domain, comprised of an invariant Gly662–Asp663–Asp664 (GDD) motif and a coordinated Asp533 that binds to a catalytic Mg<sup>2+</sup> ion to locate incoming NTP substrates for RNA polymerization [6,9].

DENV RdRp is capable of de novo RNA polymerization without a primer, and is active on homopolymeric RNA template (for example, poly(rC)) in vitro in the presence of Mn<sup>2+</sup> ions [10]. Considerable Mn<sup>2+</sup> concentrations of 2–5 mM were also used in reactions with short genomic templates including the 3'-end of the positive strand [11]. Addition of Mn<sup>2+</sup> apparently accelerated RNA synthesis by significantly decreasing  $K_{\rm m}$  30-fold [10,12]. However, the Mn<sup>2+</sup> concentration exploited in the *in vitro* assay exceeded that in cytoplasm by three orders of magnitude [13]. On the other hand, it has been suggested that DENV RdRp required a specific interaction with the first 70-nt stem-loop A (SLA) RNA element in the 5'-UTR for initiation of RNA synthesis [14]. The RNA footprint experiments revealed the top and side loops of SLA as the RdRp-binding site; however, SLA alone did not bind to RdRp in an in vitro EMSA study [15]. These discrepancies imply substantial differences between in vitro studies and physiological conditions, and precise mechanisms for viral RNA synthesis still remain enigmatic.

Our interest is RdRp from DENV-2, for which the crystal structure is not available. This is due to difficulty in expression and solubilization of recombinant DENV-2 RdRp in *Escherichia coli* cells, with protein solubility only 10–20% in *E. coli* and protein yields was not higher than 0.3 mg per liter of culture [10,16]. Moreover, to our knowledge, RdRp has always been characterized in a form fused with a poly-histidine tag [10,12,14,15,17,18] that could affect the expression level, solubility, structure, and biological activity [19–23]. Here we describe preparation of the non-tagged DENV-2 RdRp with high quality and quantity. Characterization of our recombinant protein suggests intensive caution should be taken in interpretation of *in vitro* assays with the tagged protein.

#### **Materials and methods**

Cloning and expression of DENV-2 RdRps

The RdRp domain, residues 277-900, of NS5 was amplified from serotype 2 cDNA with a forward (5'-GGGCTAGCCCAAACCTAGATATAATTGG-3') and a reverse primer containing a stop codon (underline) (5'-GGGCTCGAGTTAACCACCCC ACAGAACTGGTGG-3') for the N-terminal tagged construct (N<sub>His</sub>-RdRp), or a tandem hexahistidine-FLAG tag (bold characters) (5'-GGGCTCGAGTTACTTATCATCATCATCCTTGTAATCACCACCACCGT GGTGGTGGTGGTGACCACCACCACAGAACTCCTGC-3') for the C-terminal tag fusion (RdRp-C<sub>HisFLAG</sub>). Resulting PCR products were digested with NheI and XhoI, gel-purified, and ligated into pET-28b and pET-21b vectors for  $N_{His}$ -RdRp and RdRp- $C_{HisFLAG}$ , respectively. Resultant plasmids were transformed into E. coli BL21 (DE3) and Rosetta (DE3) strains, grown at 37 °C in LB medium including 1% glucose, and challenged with various conditions of expression induction: (i) final concentrations (50-500 uM) isopropyl-β-p-thiogalactopyranoside (IPTG); (ii) the timing of IPTG induction (OD<sub>600</sub> = 0.6-1.0); (iii) the induction temperatures (18–37 °C); (iv) the presence/absence of 10 μM ZnSO<sub>4</sub>; and (v) the auto-induction media (0.5% glycerol, 0.05% glucose, and 0.2% lactose) [24]. Cells were harvested by centrifugation at 6000g for 10 min at 4 °C, and resuspended in lysis buffer containing 50 mM Tris pH 7.6, 500 mM KCl, 7 mM β-mercaptoethanol, 10% glycerol, 0.1% Triton X-100, and 1 mM phenylmethylsulfonyl fluoride (PMSF). Proteins were extracted via sonication on ice, and fractionated by centrifugation at 15,000g for 1 h at 4 °C.

#### Western blotting

Total cell lysate, soluble and insoluble fractions were separated on 10% SDS-PAGE followed by electroblotting onto polyvinylidene fluoride (PVDF) membranes. The membranes were blocked in 5% (w/v) skim milk in phosphate-buffered saline containing 0.1% (w/v) Tween-20 (PBS-T) overnight at 4 °C. Rabbit anti-NS5 polyclonal antibody (GeneTex) was used at a dilution of 1/2000 and incubated with the membranes for 1 h at room temperature. After washing with PBS-T, the membrane was incubated with an anti-rabbit secondary antibody-horseradish peroxidase (Dako) at a dilution of 1/2000 for 30 min at room temperature, and DENV RdRp was visualized using ECL reagents (GE Healthcare) according to the manufacturer's instructions.

#### Protein purification

Expression of the N- and C-terminal tagged RdRps were induced in E. coli Rosetta (DE3) and BL21 (DE3) with 200 and 50 µM IPTG at the early log phase (OD<sub>600</sub> = 0.6–0.7) at 18 °C and 25 °C, respectively, and proceeded for 16 h. Cells were harvested by centrifugation at 6000g for 10 min at 4 °C, and resuspended in 20 ml lysis buffer per approximately 3.6 g wet cell paste from 11 culture. Proteins were extracted from cells by sonication in the presence of 1 mM PMSF and 50 µg/ml lysozyme, and fractionated by ultracentrifugation at 100,000g for 1 h at 4 °C to completely remove cell debris, membrane fraction, and insoluble proteins. The supernatants were loaded onto the nickel-affinity HisTrap HP column (GE Healthcare). Unbound proteins were washed twice with the lysis buffer supplemented with 50 mM and 88 mM imidazole. His-tagged RdRps were eluted by a linear gradient of imidazole from 88 to 350 mM. In some cases, the His-tag was removed from N<sub>His</sub>-RdRp by addition of 2 units thrombin per 1 mg protein and dialysis against the lysis buffer for 2 days at 4 °C. The three different RdRp constructs were further purified via the anion exchange HiTrap Q column with a linear gradient of 50-900 mM KCl in solution containing 50 mM Tris-HCl pH 9.0, 0.2 mM EDTA, 2 mM DTT and 10% glycerol. The final purification process was performed with gel filtration chromatography using the Superdex 200 column (GE Healthcare) equilibrated with 50 mM Tris-HCl pH 7.6, 100 mM KCl, 2 mM DTT and 10% glycerol. Purified proteins were flash frozen by liquid nitrogen and stored at −80 °C until use.

#### Polymerase activity assay

We assayed the in vitro RdRp activity by measurement of accumulation of pyrophosphate (PPi) during the RNA polymerization reaction using a phosphate-based colorimetric method with malachite green-molybdate as the color-developing reagent. The reactions were prepared in 25  $\mu$ l solutions containing 2  $\mu$ M RdRp in 25 mM Tris-HCl pH 7.5, 2.5 mM MgCl<sub>2</sub>, 4 mM DTT, 0.1 μM poly (rC) template, 1 mM GTP, 20 U/ml RNase inhibitor, and 3 µM thermostable pyrophosphatase (PPase), and conducted at 30 °C. The reaction mixtures were quenched by heating at 70 °C for 20 min, where PPi was simultaneously converted to two molecules of inorganic phosphate (Pi) by PPase. Detection of Pi was performed by mixing 10 µl of the reaction mixture with 30 µl Milli Q water and 100 µl of the malachite green-molybdate reagent [25,26]. The phosphomolybdate complexes were measured by the absorbance at 650 nm in a microplate reader. The amount of Pi was quantified using a phosphate standard curve obtained from 25 to 125  $\mu$ M NaH<sub>2</sub>PO<sub>4</sub> standard solution. An inactive GDD  $\rightarrow$  GAA mutant of RdRp was used as a control for polymerase activity. For determination of steady kinetics, GTP concentrations were titrated from 0.2 mM to 1.4 mM, and each assay was performed at least in triplicate. The initial velocities at different GTP concentrations were used to determine the  $K_{\rm m}$  value via Michaelis–Menten equation [ $v_i$  =  $V_{\rm max}$ [GTP]/( $K_{\rm m}$  + [GTP])] using GraphPad Prism version 5.0.

#### SPR RNA-binding assay

The 5'-UTR (nucleotides 1–159) containing the SLA element was amplified from DENV-2 cDNA with a forward primer carrying the T7 class II promoter (underline) (5'-GAA AT<u>T AAT ACG ACT CAC TAT TAG</u> TTG TTA GTC TAC GTG GAC CGA C-3') and the AVG130

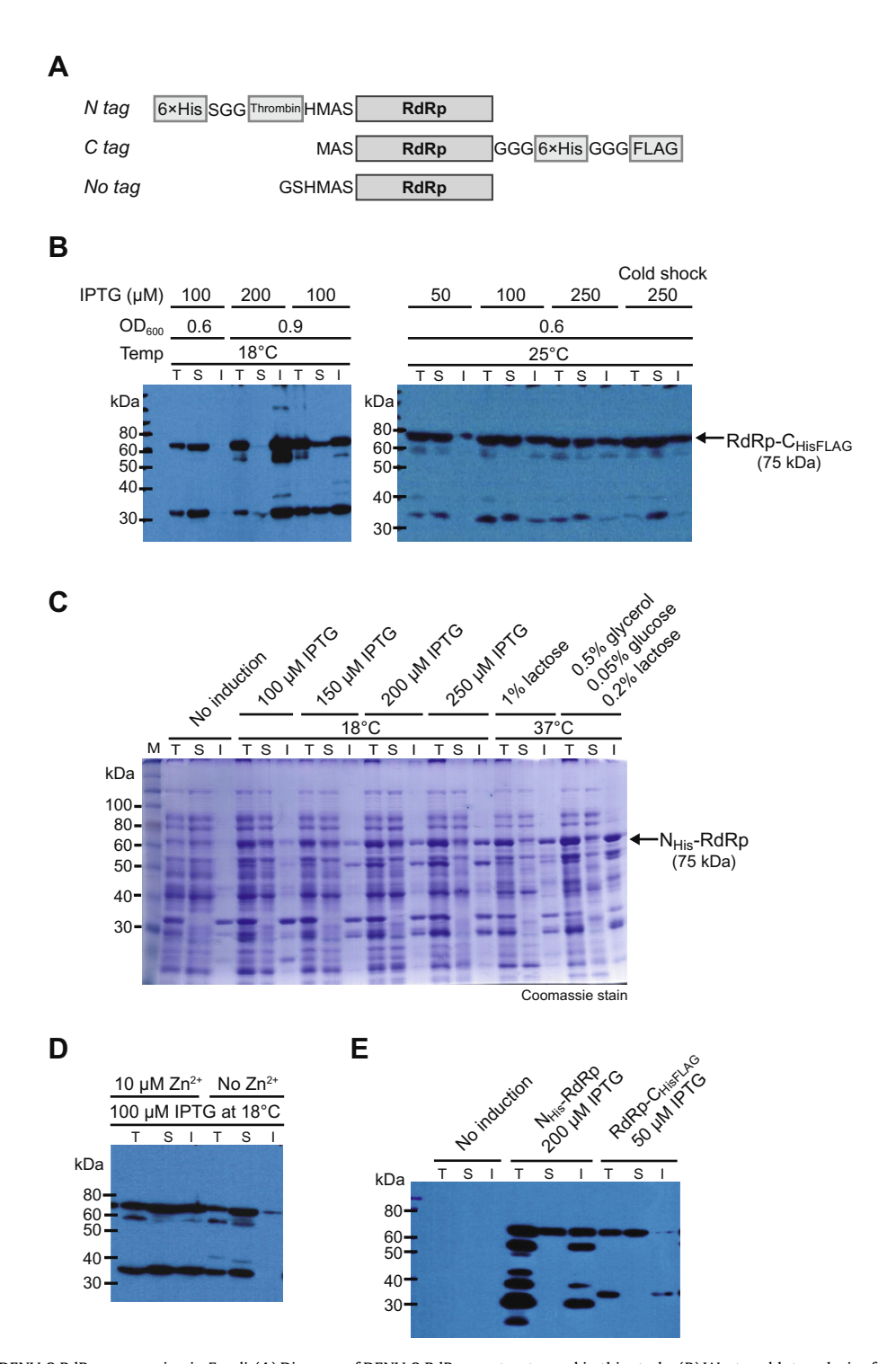


Fig. 1. Optimization of DENV-2 RdRps expression in *E. coli.* (A) Diagram of DENV-2 RdRp constructs used in this study. (B) Western blot analysis of expression of RdRp-C<sub>HisFLAG</sub> at two different temparatures of 18 °C (left panel) and 25 °C (right panel). Each IPTG concentration and inducing OD point are indicated above the lane. T, total cell lysate; S, soluble fraction; and I, insoluble fraction. (C) SDS-PAGE analysis of N<sub>His</sub>-RdRp expression. (D) Effect of zinc ion in the solubility of RdRp. (E) Final conditions for expression of N<sub>His</sub>-RdRp and RdRp-C<sub>HisFLAG</sub>.

reverse primer as earlier described [14]. PCR products were subjected to the *in vitro* run-off transcription with T7 RNA polymerase. Transcibed products were separated on long denaturing acrylamide gels, and visualized by staining with 0.1% toluidine blue O. Desired RNA bands were excised, and extracted from gels with a solution containing 0.3 M NaOAc pH 6.0, 0.5 mM EDTA, 5 mM Mg(OAc)<sub>2</sub>, and 0.1% SDS overnight at 4 °C with shaking. 5′-UTR RNA pellets were collected via ethanol precipitation, washed several times with 70% ethanol, and stored at -30 °C.

The SLA-binding ability of the recombinant RdRp was determined by surface plasmon resonance (SPR) analysis using the Biacore X100 biosensor (GE Healthcare). N<sub>His</sub>-RdRp was immobilized on a CM5 sensor chip by the amine coupling method according to manufacturer's instructions. In brief, 1.8 µg RdRp was diluted in 70 ul of the solution containing 10 mM sodium acetate pH 6.5, 150 mM NaCl, 0.5 mM MgCl<sub>2</sub>, and 0.05% surfactant P20, and injected with a flow rate of 5 ul/min for 360 s. The total immobilization level was adjusted to about 3000 RU. Binding analyses were determined at 25 °C at a flow rate of 40 μl/min in solution containing 10 mM HEPES pH 7.5, 150 mM NaCl, 0.5 mM MgCl<sub>2</sub>, and 0.05% surfactant P20. The association phase was followed for 60 s, while dissociation phase was followed for 180 s. SLA RNA was injected with increasing concentrations (6.25, 12.5, 25, 50 and 75 nM) in a single analysis cycle without regeneration. The experiments were repeated in triplicate for each protein concentration. The tRNAmix from baker's yeast was used as a negative control for non-specfic RNA-binding activity of RdRp. Dissociation constants ( $K_d$ ) were estimated by Scatchard plot analysis using Biacore X100 evaluation software.

#### Results and discussion

Expression of soluble His-tagged DENV-2 RdRps

Our initial attempt to insert a hexahistidine tag into the C-terminus of NS5 in the viral genome was not successful because the insertion abolished viral replication in BHK-21 and HEK-293T cells (unpublished data). It was earlier described that RdRp from the dengue virus serotype 2 was expressed mostly as insoluble forms in E. coli [6,10]. It is likely that locations of the His tag might negatively affect protein solubility and function. Therefore, we constructed two recombinant RdRps fused with either N- or C-terminal tags. A C-terminal tandem affinity purification (TAP) tag (RdRp-C<sub>HisFLAG</sub>) comprised of a hexahistidine and a FLAG peptide (DYKDDDDK) [27] for dual purification via nickel-affinity chromatography and anti-FLAG antibodies was employed for the C-tagged RdRp. A glycine linker (GGG) was introduced at the border between His and FLAG tags (Fig. 1A) for improving flexibility and accessibility of tags without interfering with folding and function of the protein [28]. On the other hand, the N-terminal His-tag construct possessed a hexahistidine tag linked with a thrombin cleavage site (Fig. 1A) to enable tag removal. After thrombin treatment, the resultant non-tagged RdRp had only six extra residues (Gly-Ser-His-Met-Ala-Ser) at its N-terminus, derived from the vector, which should barely affect protein structure and function.

RdRp-C<sub>HisFLAG</sub> expression in *E. coli* was initially induced with  $100-500 \, \mu M$  IPTG at  $18 \, ^{\circ}C$  and  $37 \, ^{\circ}C$  in LB medium containing 1% glucose to prevent expression leak from the *lac* operon [29]. As expected, DENV-2 RdRp was expressed only in insoluble form at  $37 \, ^{\circ}C$  but was partially soluble at  $18 \, ^{\circ}C$ . We then varied IPTG

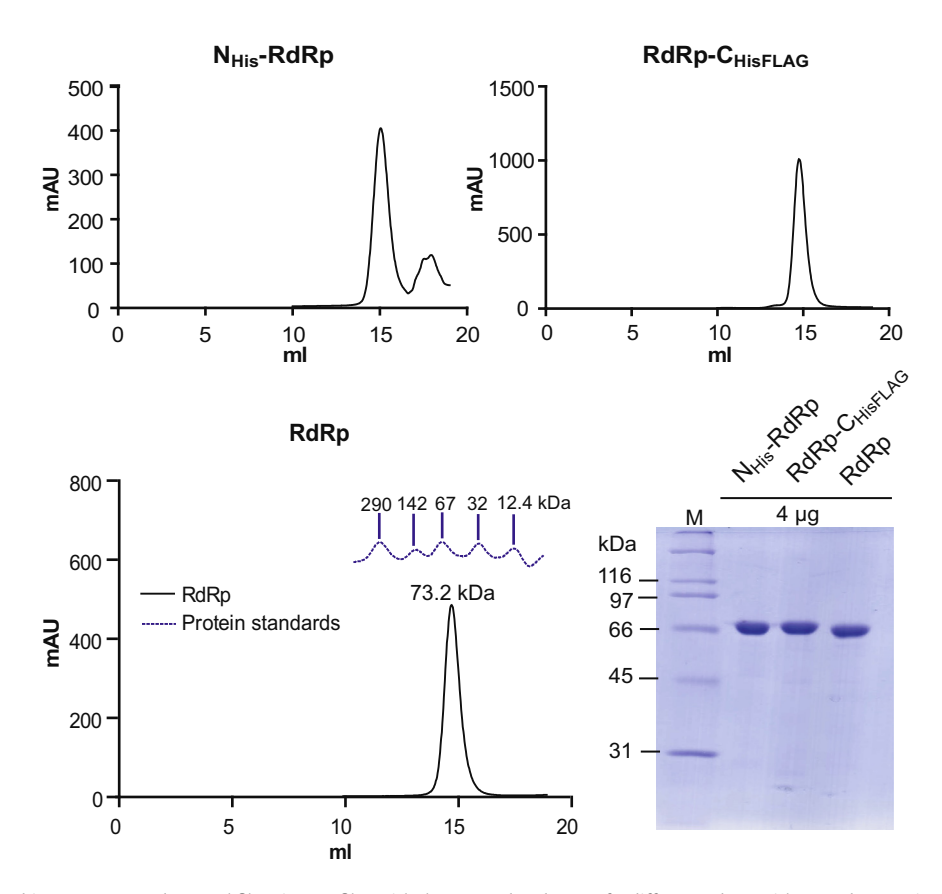


Fig. 2. Quality of three recombinant DENV-2 RdRps. Gel filtration profiles with the UV<sub>280</sub> absorbance of 3 different RdRps with N- and C-terminal tags, and without a tag. The size of non-tagged RdRp was calculated to be  $\sim$ 60 kDa according to the protein standards, which was smaller than its theoretical size of 73.2 kDa. Protein purity was quantitated using SDS-PAGE stained with Coomassie Blue (right bottom).

concentrations and the timing of induction during cell growth, and found that soluble RdRp- $C_{HisFLAG}$  could be achieved upon 100  $\mu$ M IPTG induction at 18 °C at an early log phase (OD<sub>600</sub> = 0.6–0.7) (Fig. 1B left panel). Induction at the later log phase (OD = 0.8–0.9) significantly increased insoluble RdRp. Our results revealed that the concentration of IPTG and the timing of induction were critical for RdRp solubilization. Although cell growth at 18 °C could greatly improve protein solubility, the yield of RdRp production was not ideal for further structural analysis likely due to decreases in bacterial replication, transcription, and translation [30,31]. To this end, the highest yield of soluble RdRp- $C_{HisFLAG}$  was achieved in the *E. coli* BL21 (DE3) strain by increasing temperature to 25 °C and reducing the concentration of IPTG to 50  $\mu$ M (Fig. 1B right panel). The cold shock method used in a previous study did not obviously improve protein solubility in our study [10,17].

We further used the same conditions to express  $N_{His}$ -RdRp. Unfortunately,  $N_{His}$ -RdRp expression was extremely low in the BL21 (DE3) strain, and mostly insoluble in the Rosetta (DE3) strain. To improve solubility, expression induction was performed at OD $_{600}$  = 0.6 at 18 °C with various IPTG concentrations. We also examined two auto-inducing media that contained 1% lactose or 0.05% glucose, 0.2% lactose, and 0.5% glycerol at 37 °C. Glucose prevented lactose induction in the early stage, whereas glycerol was an energy source to support cell growth and prevented *E. coli* from using lactose as energy source during the induction period [24]. Our results showed that IPTG of 200  $\mu$ M rendered the optimal condition for  $N_{His}$ -RdRp expression (Fig. 1C). Moreover, we

investigated the effect of zinc ion in the solubility of RdRp, as the crystal structure possesses two zinc-binding motifs. We found that zinc only slightly improved the solubility of the protein (Fig. 1D), possibly helping protein folding. To conclude, the highest yields of soluble  $N_{\rm His}$ -RdRp and RdRp- $C_{\rm HisFLAG}$  could be obtained by 200 and 50  $\mu$ M IPTG inductions at the early log phase (OD<sub>600</sub> = 0.6–0.7) in Rosetta (DE3) and BL21 (DE3) strains at 18 °C and 25 °C, respectively (Fig. 1E). In these optimal conditions, there were at least three smaller bands of ~60, 40, and 33 kDa observed in the Western blot. These might represent products of abandoned protein synthesis and/or protein degradation. It was noted that the soluble fraction did not contained these small bands (Fig. 1E).

#### Purification of DENV-2 RdRps with and without tag

The larger-scale expressions of  $N_{His}$ -RdRp and RdRp- $C_{HisFLAG}$  confirmed protein solubility as in small-scale optimization. Soluble proteins were separated by ultracentrifugation and tagged RdRps were purified to homogeneity through nickel-affinity, anion exchange, and size-exclusion chromatography.  $N_{His}$ -RdRp and RdRp- $C_{HisFLAG}$  showed distinct elution profiles in nickel-affinity chromatography, with RdRp- $C_{HisFLAG}$  binding more weakly to the resin and eluting at a lower imidazole concentration. This might suggest that the C-terminal tag made contacts with the protein and was less exposed to the solvent. To produce non-tagged RdRp,  $N_{His}$ -RdRp was treated with thrombin protease during dialysis for 2 days at 4 °C to completely remove the tag after

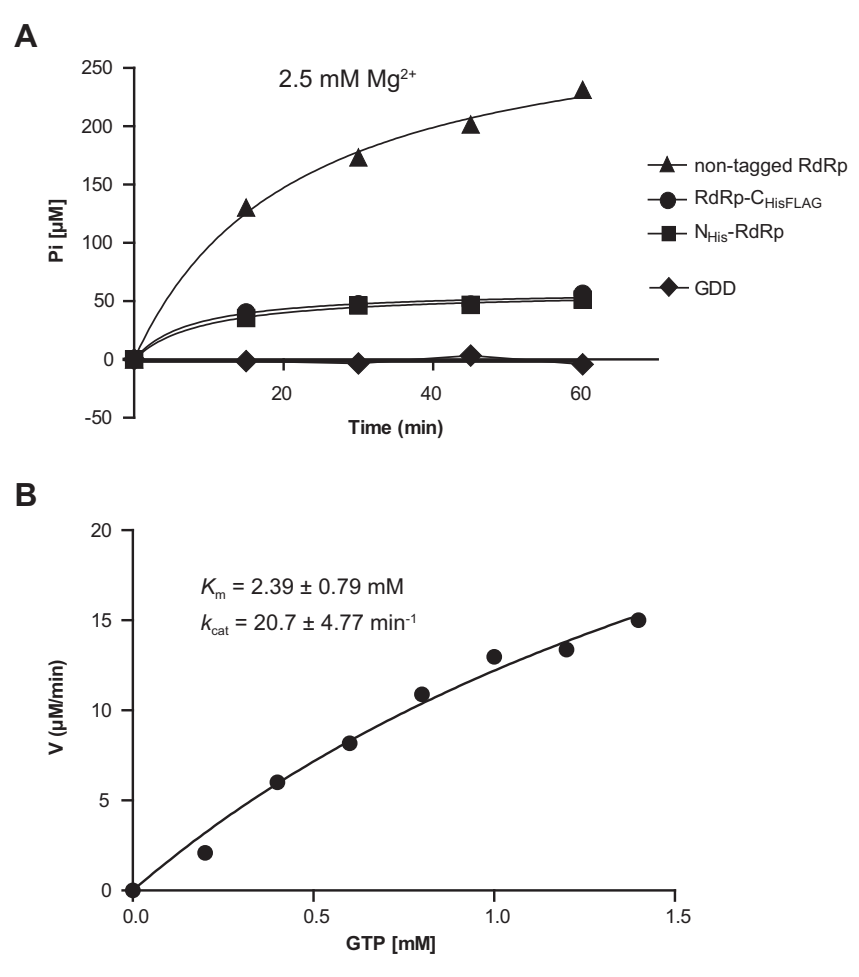


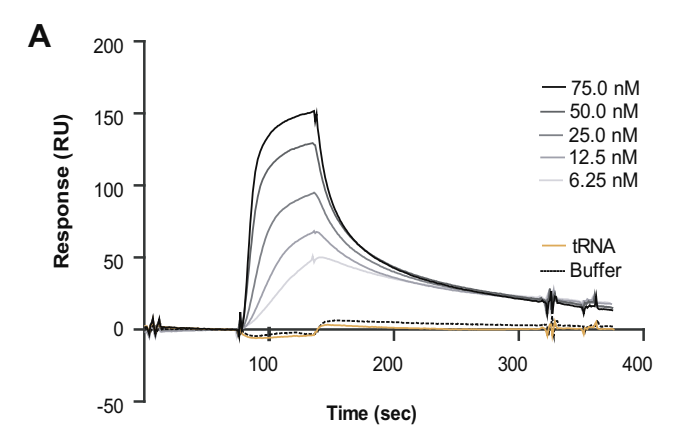
Fig. 3. Kinetics study of non-tagged DENV-2 RdRp. (A) Comparison of tagged and non-tagged RdRps' activities via the *in vitro* polymerase assay. An inactive GDD mutant served as negative control. Each RdRp was used at constant concentration of 2  $\mu$ M. (B) Steady-state kinetics of non-tagged RdRp at 30 °C, pH 7.5. Data were fitted to the Michaelis-Menten equation.

nickel-affinity purification. Non-tagged RdRp was separated from a trace of undigested RdRp via a repeated treatment with the nickel-affinity resin, and the flow-through fractions were recovered. The final gel filtration purification was indispensable to eliminate a trace of RNase contamination. The profiles showed single symmetric peaks of RdRps as monomer compared to the protein standards (Fig. 2). All DENV-2 RdRp constructs showed over 95% purity as assessed by SDS-PAGE (Fig. 2 right bottom panel). Typical yields of N<sub>His</sub>-RdRp (75 kDa), RdRp-C<sub>HisFLAG</sub> (75 kDa), and non-tagged RdRp (73.2 kDa) after three-step purification were 4, 1.5, and 3 mg per liter culture (or about 1.1, 0.5, and 0.8 mg/g wet cell), respectively. We note here that protein yields were improved by a remarkable 10-fold over earlier report [10,16], and their purity were sufficient for future application to X-ray crystallization screen.

#### Tags interferes with the polymerase activity

In this study, we employed a nonradioactive phosphate-based colorimetric assay to measure the in vitro polymerase activity of RdRp, which may be more suitable for high-throughput screening of inhibitors using microplates in the future [26]. We initially compared N<sub>His</sub>-RdRp, RdRp-C<sub>HisFLAG</sub>, and non-tagged RdRp together with a GDD → GAA mutant that has no RNA polymerase activity by assays using homopolymeric poly(rC) template in the presence of 2.5 mM Mg<sup>2+</sup> (Fig. 3A). Interestingly, the results revealed drastic differences in polymerase activity between non-tagged RdRp and His-tagged RdRps, strongly suggesting that the tag interfered with RdRp. However, there was no discernable conformational difference in their overall structures as measured by circular dichroism (CD) spectrum (data not shown). The N- and C-terminal His-tags were located in fingers and thumb domains, respectively, and were distant from the active site in the palm domain. Given that the fingers and thumb domains likely contribute to conformational changes in shaping of RNA template tunnel [6], it might be possible that the His-tag interfered with conformational changes between these two domains. Moreover, our assay revealed high polymerase activity when only Mg<sup>2+</sup> was present in the reaction (Fig. 3A). This is in contrast to previous studies using the N-terminal His-tagged RdRp including Selisko et al. that showed a requirement of 2 mM Mn<sup>2+</sup> for the polymerase activity, and suggested that Mn<sup>2+</sup> might modulate overall RdRp activity [10]. Mn<sup>2+</sup> ions are known to modulate the substrate specificity and cause nucleotide misincorporation, reducing fidelity of viral RdRp [32]. Moreover, in the presence of Mn<sup>2+</sup>, a previous study showed that DENV-2 RdRp failed to precisely discriminate the 3'-CU dinucleotide end of the viral template in de novo initiation of RNA synthesis [33]. Given that the intracellular Mg<sup>2+</sup> concentration is three orders higher that of Mn<sup>2+</sup> [13,34], it remains controversial whether RdRp preferentially binds Mn<sup>2+</sup> in vivo. Nonetheless, our results highlight a need for caution when interpreting in vitro assays with tagged

Next, we performed a steady-state kinetics analysis of non-tagged DENV-2 RdRp in the presence of constant poly(rC) and  $\mathrm{Mg^{2+}}$  concentrations. To our knowledge, this is the first report of a kinetics study of non-tagged DENV-2 RdRp. The non-tagged RdRp revealed  $V_{\mathrm{max}}$ ,  $K_{\mathrm{m}}$ , and  $k_{\mathrm{cat}}$  being 41.4 ± 9.54  $\mu$ M/min, 2.39 ± 0.79 mM, and 20.7 ± 4.77 min<sup>-1</sup>, respectively (Fig. 3B).Very recently, Potisopon et al. demonstrated a  $K_{\mathrm{m}}$  (CTP) of 0.3 mM and  $k_{\mathrm{cat}}$  of 0.12 min<sup>-1</sup> in the elongation step of RNA synthesis with N-terminal His-tagged DENV-2 RdRp in the presence of  $\mathrm{Mg^{2+}}$  [12]. Reduction in substrate affinity by 8-fold increase of  $K_{\mathrm{m}}$  was not unexpected because the 3' last 20 nt of the DENV genome was used in Potisopon et al.'s study instead of the poly(rC) in our assay. Interestingly, our non-tagged RdRp showed a greater than 60-fold increase in  $k_{\mathrm{cat}}$  compared to His-tagged RdRp and the full



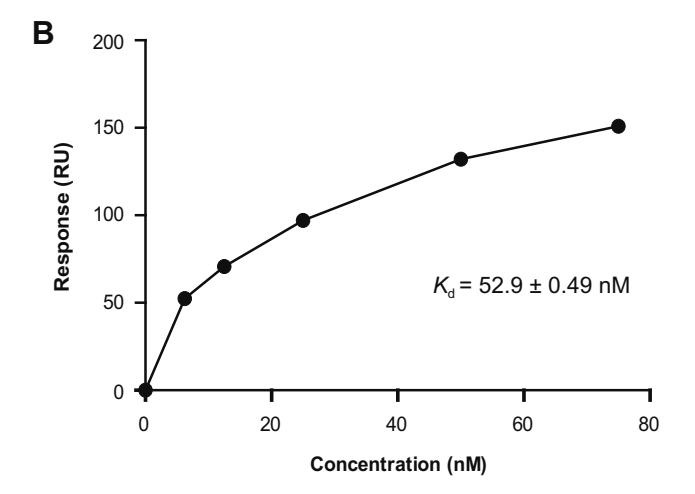


**Fig. 4.** SPR-based binding analysis of DENV-2 RdRp with 5′-UTR. (A) SPR sensorgrams of RNA-binding of  $N_{\rm His}$ -RdRp, and (B) fitted saturation binding curves. Equilibrium dissociation constant ( $K_{\rm d}$ ) was determined from the binding curves at various concentrations of DENV 5′-UTR RNA from 6.25 nM to 75 nM.

length NS5 ( $k_{\rm cat} \sim 0.31~{\rm min}^{-1}$ ) [12]. These facts support our speculation that the His-tag might interfered with conformational changes between two RdRp domains, thus reducing the enzyme turnover rate. Indeed, extension of distance between the tag and the RdRp core elevated enzymatic activity 2.6-fold (as measured by  $k_{\rm cat}$ ) when compared to the N-terminal tagged full-length NS5 and RdRp [12].

#### RdRp specifically binds to the viral UTR

Interactions between viral RdRps and their RNA elements have been widely studied in vitro using electrophoretic mobility shift assay (EMSA). In particular, the dissociation constant  $(K_d)$  of DENV RdRp against the 70-nt SLA element in the 5'-untranslated region (UTR) was determined to be 11 nM [15]. It was also suggested that the polymerase active site and the RNA-binding site are separated in DENV RdRp [35]. In this study, we exploited surface plasmon resonance (SPR) analysis to monitor RNA binding in real time in solution (Fig. 4A). RdRp was coated on a CM5 chip via random covalent bonds to prevent biases in protein orientation and conformation. The first SPR K<sub>d</sub> against the 5'-UTR RNA fragment (159 nt) was determined by Scatchard plot to be  $52.9 \pm 0.49$  nM (Fig. 4B), which was in the same order of magnitude as EMSA [15]. No binding curve was observed with control tRNAs, suggesting RNA-specificity of DENV RdRp (Fig. 4A). Our SPR approach should be useful for future high-throughput screening of inhibitors that block interaction of RdRp with RNAs, and thus, viral replication.

#### Conclusions

Soluble DENV-2 RdRp was successfully expressed and purified to homogeneity from  $E.\ coli$  in the N- and C-terminally His-tagged forms, and without any tags. We found that non-tagged RdRp did not require  $Mn^{2+}$  ions for efficient polymerization, and both N- and C-terminal tags impaired the polymerase activity, likely due to interference with structural switches and thus significantly reducing  $k_{\text{cat}}$ . DENV RdRp specifically bound to the viral 5'-UTR with an apparent  $K_{\text{d}}$  of 53 nM. Our results highlighted the importance of the use of non-tagged viral RdRps in functional characterization and screening for antiviral inhibitors.

#### Acknowledgments

We greatly thank Chatchawan Srisawat for helpful advices in SPR experiments. This work was supported by Grants-in-Aids for scientific research from Mahidol University (Thailand) and by the Mid-Career Grant (RSA5680054) from Thailand Research Fund (TRF) to S.C. M.K. was supported by scholarships from the 60th Year Supreme Reign of his Majesty King Bhumibol adulyadej Scholarship (Mahidol University), SHELL Centennial Education Fund (Shell Thailand), and from Thermo Fisher Scientific Company, Thailand.

#### References

- [1] S. Bhatt, P.W. Gething, O.J. Brady, J.P. Messina, A.W. Farlow, C.L. Moyes, J.M. Drake, J.S. Brownstein, A.G. Hoen, O. Sankoh, M.F. Myers, D.B. George, T. Jaenisch, G.R. Wint, C.P. Simmons, T.W. Scott, J.J. Farrar, S.I. Hay, The global distribution and burden of dengue. Nature 496 (2013) 504–507.
- [2] J. Blok, Genetic relationships of the dengue virus serotypes, J. Gen. Virol. 66 (1985) 1323–1325.
- [3] B.E.E. Martina, P. Koraka, A.D.M.E. Osterhaus, Dengue virus pathogenesis: an integrated view, Clin. Microbiol. Rev. 22 (2009) 564–581.
- [4] T. Duangchinda, W. Dejnirattisai, S. Vasanawathana, W. Limpitikul, N. Tangthawornchaikul, P. Malasit, J. Mongkolsapaya, G. Screaton, Immunodominant T-cell responses to dengue virus NS3 are associated with DHF, Proc. Natl. Acad. Sci. USA 107 (2010) 16922–16927.
- [5] T.J. Chambers, C.S. Hahn, R. Galler, C.M. Rice, Flavivirus genome organization, expression, and replication, Annu. Rev. Microbiol. 44 (1990) 649–688.
- [6] T.L. Yap, T. Xu, Y.-L. Chen, H. Malet, M.-P. Egloff, B. Canard, S.G. Vasudevan, J. Lescar, Crystal structure of the dengue virus RNA-dependent RNA polymerase catalytic domain at 1.85-angstrom resolution, J. Virol. 81 (2007) 4753–4765.
- [7] A. Sampath, R. Padmanabhan, Molecular targets for flavivirus drug discovery, Antiviral Res. 81 (2009) 6–15.
- [8] H. Malet, N. Massé, B. Sélisko, J.-L. Romette, K. Alvarez, J.C. Guillemot, H. Tolou, T.L. Yap, S.G. Vasudevan, J. Lescar, B. Canard, The flavivirus polymerase as a target for drug discovery, Antiviral Res. 80 (2008) 23–35.
- [9] C.G. Noble, S.P. Lim, Y.-L. Chen, C.W. Liew, L. Yap, J. Lescar, P.-Y. Shi, Conformational flexibility of the dengue virus RNA-dependent RNA polymerase revealed by a complex with an inhibitor, J. Virol. 87 (2013) 5291–5295.
- [10] B. Selisko, H. Dutartre, J.-C. Guillemot, C. Debarnot, D. Benarroch, A. Khromykh, P. Desprès, M.-P. Egloff, B. Canard, Comparative mechanistic studies of *de novo* RNA synthesis by flavivirus RNA-dependent RNA polymerases, Virology 351 (2006) 145–158.
- [11] S.P. Lim, J.H. Koh, C.C. Seh, C.W. Liew, A.D. Davidson, L.S. Chua, R. Chandrasekaran, T.C. Cornvik, P.Y. Shi, J. Lescar, A crystal structure of the dengue virus non-structural protein 5 (NS5) polymerase delineates interdomain amino acid residues that enhance its thermostability and de novo initiation activities, J. Biol. Chem. 288 (2013) 31105–31114.

- [12] S. Potisopon, S. Priet, A. Collet, E. Decroly, B. Canard, B. Selisko, The methyltransferase domain of dengue virus protein NS5 ensures efficient RNA synthesis initiation and elongation by the polymerase domain, Nucleic Acids Res. (2014).
- [13] R.Q. Zhang, K.J. Ellis, In vivo measurement of total body magnesium and manganese in rats, Am. J. Physiol. 257 (1989) R1136–R1140.
- [14] C.V. Filomatori, M.F. Lodeiro, D.E. Alvarez, M.M. Samsa, L. Pietrasanta, A.V. Gamarnik, A 5' RNA element promotes dengue virus RNA synthesis on a circular genome, Genes Dev. 20 (2006) 2238–2249.
- [15] C.V. Filomatori, N.G. Iglesias, S.M. Villordo, D.E. Alvarez, A.V. Gamarnik, RNA sequences and structures required for the recruitment and activity of the dengue virus polymerase, J. Biol. Chem. 286 (2011) 6929–6939.
- [16] T.L. Yap, Y.L. Chen, T. Xu, D. Wen, S.G. Vasudevan, J. Lescar, A multi-step strategy to obtain crystals of the dengue virus RNA-dependent RNA polymerase that diffract to high resolution, Acta Crystallogr. Sect. F 63 (2007) 78–83.
- [17] Z. Jin, J. Deval, K.A. Johnson, D.C. Swinney, Characterization of the elongation complex of dengue virus RNA polymerase: assembly, kinetics of nucleotide incorporation, and fidelity, J. Biol. Chem. 286 (2011) 2067–2077.
- [18] M.R. Szymanski, M.J. Jezewska, P.J. Bujalowski, C. Bussetta, M. Ye, K.H. Choi, W. Bujalowski, Full-length dengue virus RNA-dependent RNA polymerase-RNA/DNA complexes: stoichiometries, intrinsic affinities, cooperativities, base, and conformational specificities, J. Biol. Chem. 286 (2011) 33095–33108.
- [19] A. Chant, C.M. Kraemer-Pecore, R. Watkin, G.G. Kneale, Attachment of a histidine tag to the minimal zinc finger protein of the Aspergillus nidulans gene regulatory protein AreA causes a conformational change at the DNA-binding site, Protein Expr. Purif. 39 (2005) 152–159.
- [20] Y. Yeon, H. Park, H.-Y. Park, Y. Yoo, Effect of His-tag location on the catalytic activity of 3-hydroxybutyrate dehydrogenase, Biotechnol. Bioprocess Eng. 19 (2014) 798–802.
- [21] M. Amor-Mahjoub, J.P. Suppini, N. Gomez-Vrielyunck, M. Ladjimi, The effect of the hexahistidine-tag in the oligomerization of HSC70 constructs, J. Chromatogr. B 844 (2006) 328–334.
- [22] F. Renzi, G. Panetta, B. Vallone, M. Brunori, M. Arceci, I. Bozzoni, P. Laneve, E. Caffarelli, Large-scale purification and crystallization of the endoribonuclease XendoU: troubleshooting with His-tagged proteins, Acta Crystallogr. Sect. F 62 (2006) 298–301.
- [23] D.S. Waugh, Making the most of affinity tags, Trends Biotechnol. 23 (2005) 316–320
- [24] F.W. Studier, Protein production by auto-induction in high density shaking cultures, Protein Expr. Purif. 41 (2005) 207–234.
- [25] J. Feng, Y. Chen, J. Pu, X. Yang, C. Zhang, S. Zhu, Y. Zhao, Y. Yuan, H. Yuan, F. Liao, An improved malachite green assay of phosphate: mechanism and application, Anal. Biochem. 409 (2011) 144–149.
- [26] H.T.D. Nguyen, Y. Chong, D.-K. Oh, Y.-S. Heo, P.T. Viet, L.-W. Kang, S.-J. Jeon, D.-E. Kim, An efficient colorimetric assay for RNA synthesis by viral RNA-dependent RNA polymerases, using thermostable pyrophosphatase, Anal. Biochem. 434 (2013) 284–286.
- [27] T.P. Hopp, K.S. Prickett, V.L. Price, R.T. Libby, C.J. March, D. Pat Cerretti, D.L. Urdal, P.J. Conlon, A short polypeptide marker sequence useful for recombinant protein identification and purification, Nat. Biotechnol. 6 (1988) 1204–1210.
- [28] M. Sabourin, C.T. Tuzon, T.S. Fisher, V.A. Zakian, A flexible protein linker improves the function of epitope-tagged proteins in *Saccharomyces cerevisiaei*, Yeast 24 (2007) 39–45.
- [29] W.F. Loomis Jr., B. Magasanik, Glucose-lactose diauxie in Escherichia coli, J. Bacteriol. 93 (1967) 1397–1401.
- [30] C.H. Schein, Production of soluble recombinant proteins in bacteria, Nat. Biotechnol. 7 (1989) 1141–1149.
- [31] M.K. Shaw, J.L. Ingraham, Synthesis of macromolecules by *Escherichia coli* near the minimal temperature for growth, J. Bacteriol. 94 (1967) 157–164.
- [32] J.J. Arnold, D.W. Gohara, C.E. Cameron, Poliovirus RNA-dependent RNA polymerase (3Dpol): pre-steady-state kinetic analysis of ribonucleotide incorporation in the presence of Mn<sup>2+</sup>, Biochemistry 43 (2004) 5138–5148.
- [33] B. Selisko, S. Potisopon, R. Agred, S. Priet, I. Varlet, Y. Thillier, C. Sallamand, F. Debart, J.-J. Vasseur, B. Canard, Molecular basis for nucleotide conservation at the ends of the dengue virus genome, PLoS Pathog. 8 (2012) e1002912.
- [34] G.A. Quamme, L.J. Dai, S.W. Rabkin, Dynamics of intracellular free Mg<sup>2+</sup> changes in a vascular smooth muscle cell line, Am. J. Physiol. 265 (1993) H281–288.
- [35] N.G. Iglesias, C.V. Filomatori, A.V. Gamarnik, The F1 motif of dengue virus polymerase NS5 is involved in promoter-dependent RNA synthesis, J. Virol. 85 (2011) 5745–5756.

# Development of viable TAP-tagged dengue virus for investigation of host-virus interactions in viral replication

Teera Poyomtip,<sup>1</sup>† Kenneth Hodge,<sup>2</sup>† Ponpan Matangkasombut,<sup>1,3</sup> Anavaj Sakuntabhai,<sup>3,4,5</sup> Trairak Pisitkun,<sup>6</sup> Siwanon Jirawatnotai<sup>3,7</sup> and Sarin Chimnaronk<sup>2,3</sup>

Dengue virus (DENV) is a mosquito-borne flavivirus responsible for life-threatening dengue haemorrhagic fever (DHF) and dengue shock syndrome (DSS). The viral replication machinery containing the core non-structural protein 5 (NS5) is implicated in severe dengue symptoms but molecular details remain obscure. To date, studies seeking to catalogue and characterize interaction networks between viral NS5 and host proteins have been limited to the yeast twohybrid system, computational prediction and co-immunoprecipitation (IP) of ectopically expressed NS5. However, these traditional approaches do not reproduce a natural course of infection in which a number of DENV NS proteins colocalize and tightly associate during the replication process. Here, we demonstrate the development of a recombinant DENV that harbours a TAP tag in NS5 to study host-virus interactions in vivo. We show that our engineered DENV was infective in several human cell lines and that the tags were stable over multiple viral passages, suggesting negligible structural and functional disturbance of NS5. We further provide proof-of-concept for the use of rationally tagged virus by revealing a high confidence NS5 interaction network in human hepatic cells. Our analysis uncovered previously unrecognized hnRNP complexes and several low-abundance fatty acid metabolism genes, which have been implicated in the viral life cycle. This study sets a new standard for investigation of host-flavivirus interactions.

Correspondence Siwanon Jirawatnotai

siwanon.jir@mahidol.ac.th Sarin Chimnaronk sarin.chi@mahidol.ac.th

Received 16 November 2015 Accepted 11 December 2015

### **INTRODUCTION**

Dengue virus (DENV), Japanese encephalitis virus, West Nile virus and yellow fever virus are flaviviruses of well-publicized epidemiological importance. Of these, DENV is the world's most common arthropod-borne virus, afflicting approximately 390 million individuals per year (Bhatt et al., 2013). DENV is most prevalent in tropical and subtropical regions such as South and SouthEast Asia,

†These authors contributed equally to this work.

Three supplementary tables are available with the online Supplementary Material.

the Western Pacific and Central and South America. Advances in biotechnology have thus far failed to stem a net increase in infections over the past 50 years; the World Health Organization reported that from 1955 to 2007, the number of DENV-infected patients increased over 1000-fold (WHO, 2009). DENV causes a wide range of diseases in humans, from a self-limiting dengue fever to a lifethreatening syndrome called dengue haemorrhagic fever (DHF) or dengue shock syndrome (DSS). No vaccines or drugs are currently approved for therapeutic treatment.

The genome of DENV is an approximately 10.7 kb positive ssRNA that is composed of a long ORF of a viral

<sup>&</sup>lt;sup>1</sup>Department of Microbiology, Faculty of Science, Mahidol University, Bangkok 10400, Thailand

<sup>&</sup>lt;sup>2</sup>Institute of Molecular Biosciences, Mahidol University, Salaya Campus, Phutthamonthon, Nakhon Pathom 73170, Thailand

<sup>&</sup>lt;sup>3</sup>Systems Biology of Diseases Research Unit, Faculty of Science, Mahidol University, Bangkok 10400, Thailand

<sup>&</sup>lt;sup>4</sup>Functional Genetics of Infectious Diseases Unit, Institute Pasteur, Paris, France

<sup>&</sup>lt;sup>5</sup>Centre National de la Recherche Scientifique (CNRS), URA3012, F-75015 Paris, France

<sup>&</sup>lt;sup>6</sup>Systems Biology Center, Faculty of Medicine, Chulalongkorn University, Bangkok 10330, Thailand

<sup>&</sup>lt;sup>7</sup>Department of Pharmacology, Faculty of Medicine, Siriraj Hospital, Mahidol University, Bangkok 10700, Thailand

polyprotein of 3390 amino acids. The polyprotein is proteolytically processed into three structural proteins (C, prM and E) and seven non-structural (NS) proteins (NS1, NS2A, NS2B, NS3, NS4A, NS4B and NS5) at the endoplasmic reticulum (ER) membrane. Among viral proteins, NS5 is the largest protein, possessing methyltransferase (MTase) and RNA-dependent RNA polymerase (RdRp) activities in its N- and C-termini, responsible for capping the 5' end and generation of new genomic viral RNA in infected cells, respectively (Dong et al., 2014). NS5 recruits at least NS3 and a subset of host cellular proteins to form the replication complex or 'replicase' in virus-induced membranous compartments for productive viral RNA synthesis (Bidet & Garcia-Blanco, 2014). NS5 also plays important roles as an immune suppressor by downregulating type I IFN responses through interacting with STAT2 (Ashour et al., 2009). Moreover, both NS3 and NS5 were implicated in DHF as they were found to be the immunodominant T-cell antigens compared to other viral proteins (Duangchinda et al., 2010). Hence, NS5 has long been considered an attractive drug target due to its multiple crucial roles in viral replication (Dong et al., 2008), and its cellular interaction partners may also reveal new therapeutic avenues for fatal DHF or DSS (Krishnan & Garcia-Blanco, 2014).

A number of approaches have been used to identify NS5-interacting partners (Carpp et al., 2014; Doolittle & Gomez, 2011; Khadka et al., 2011; Le Breton et al., 2011; Mairiang et al., 2013). The yeast two-hybrid system (Y2H) offers the advantage of rapid large-scale screening of protein pairs. However, the method usually does not take into account both cellular localization and abundance of particular interactions in specific cell types. Flaviviral Y2H studies conducted by different groups have, thus far, shown a curious lack of overlap in their datasets. For example, Khadka et al. (2011) and Le Breton et al. (2011) both generated DENV NS5 interaction networks, with no overlapping data (Krishnan & Garcia-Blanco, 2014).

Affinity isolation of ectopically expressed viral proteins is another approach to analyse the host-virus interactome, which frequently renders extensive lists of interactors. However, overexpression of NS5 alone should not mimic physiological conditions (Rigaut et al., 1999). Such an approach downplays a body of work that suggests that viral RNA and proteins are tightly associated from translation to later stages in the viral life cycle; for example, ectopically expressed NS5 was not able to complement viruses carrying various NS5 mutants (Khromykh et al., 1999). Presumably, the introduced NS5 failed to insinuate itself into existing viral replicases which, depending on the stage of infection, might be protected by membranous compartments in the ER (Welsch et al., 2009). Recent work with tobacco mosaic virus has demonstrated a tight association between its RdRp and genome from the time of translation through replication (Kawamura-Nagaya et al., 2014). The limitations of ectopic expression have also been reported with the other replicase component

NS3, showing that the inability of introduced WT NS3 to overcome the deficiencies of mutant viral NS3 could be observed at the assembly stage of the viral life cycle (Liu *et al.*, 2002).

To eliminate or minimize the aforementioned deficiencies, immunoprecipitation (IP) of NS5 polymerase from infected cells via an anti-NS5 antibody could be achieved; however, acquisition of a monoclonal antibody that recognizes epitopes in a native form of protein with high specificity and affinity is a key bottleneck and challenge. A viable recombinant virus with a tagged NS5 polymerase would be ideal for investigation of its interacting partners. Moreover, the endogenous tag would permit studies of the cellular localization of NS5 and its partners, as well as the timing of NS5-related events in the viral life cycle, with physiological relevance. In this study, we demonstrate, to our knowledge for the first time, a rational design of infectious DENV carrying a tandem affinity purification (TAP) tag inside NS5, allowing the identification of a landscape of NS5-interacting proteins in infected hepatic cells, a natural target of DENV.

#### **RESULTS**

# **Design and production of recombinant NS5-tagged DENV**

A previous study attempting to incorporate a tag into NS5 in viable DENV was unsuccessful (Carpp et al., 2014). Initially, we attempted to generate an infectious recombinant DENV carrying a tag following the NS5 polyprotein cleavage site (GTGNIG) immediately downstream of the N-terminus, and a tag at the C-terminus of NS5. However, tags at these locations completely disabled viral replication and propagation. Therefore, we selected a more rational approach to seek possible tag locations. NS5 sequences from ten flaviviruses were aligned and scored. In our scheme, there were seven regions at which a conservation value, calculated over 31 residue windows, was obviously low (Fig. 1a). These regions were then mapped onto the crystal structure of DENV NS5 to winnow out insert sites that could interfere with structures (i.e.  $\alpha$ -helices or  $\beta$ -sheets) or that would be located inside the protein core. A final screening procedure examined potential insert sites for the presence of eukaryotic linear motifs that might be of importance (Dinkel et al., 2012). Finally, the positions of interest were required to have a minimum 10 Å distance from the two active sites (MTase and RdRp) of NS5. Combining the above criteria, we identified suitable regions at N172-N177 of the MTase domain and Q633-T636 of the RdRp domain. The TAP tag containing a poly-histidine (eight amino acids) and FLAG (eight amino acids) tags, which facilitate a two-step protein purification and reduce non-specific background, was inserted following N173 in MTase or T636 in DENV-2 RdRp (Fig. 1b). We also placed a glycine linker between the

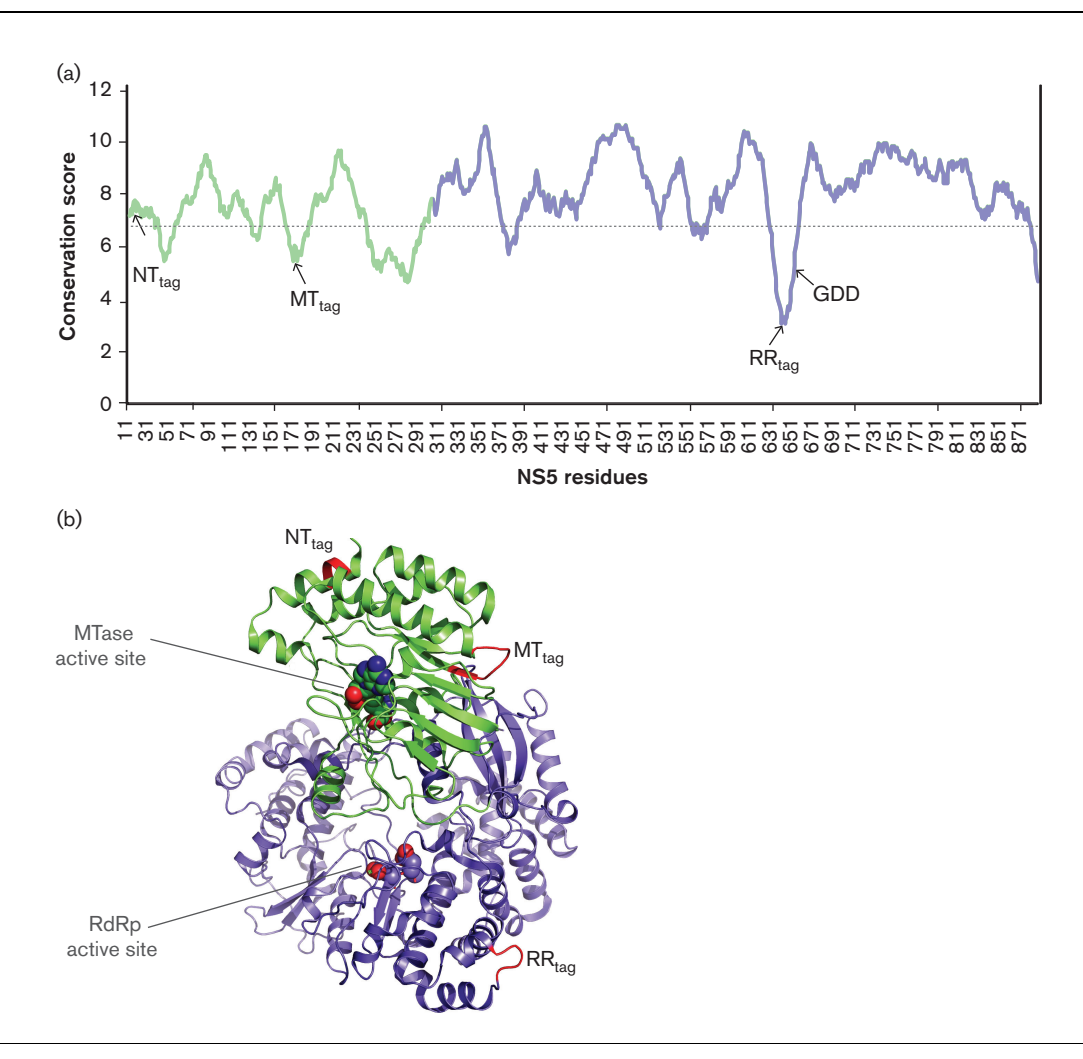


**Fig. 1.** Rational design for tagging DENV NS5. (a) Analysis of amino acid conservation among 11 flaviviral NS5s. Means of summed CLUSTAL Omega conservation scores over all 31 amino acid frames are plotted against NS5 residues including MTase (green) and RdRp (blue) domains. The dotted line is positioned one SD unit (1.23) below the mean conservation value (7.95); note the seven troughs below this cut-off. (b) DENV-3 NS5 crystal structure. Red colour represents the insertion position of the TAP tag. The polymerase active site is indicated by the GDD catalytic triad.

poly-histidine and FLAG epitopes to increase their flexibility and accessibility (Sabourin et al., 2007).

The full-length DENV-2 RNA genome with tagged NS5 (10.7 kb) was synthesized *in vitro* using T7 RNA polymerase (Fig. 2a). DENV transcripts from pD2-IC (WT) and three recombinant constructs each carrying the TAP tag at the N-terminus of NS5 (NT<sub>tag</sub>), inside MTase (MT<sub>tag</sub>) or in RdRp (RR<sub>tag</sub>), were transfected into BHK-21 cells, and their effects on viral production inside the cells were investigated at 2, 4 and 7 days post-infection via immunofluorescence signals of DENV E protein. Only the MT<sub>tag</sub> construct showed E protein expression in a time-dependent manner similar to that of WT, whereas the NT<sub>tag</sub> and RR<sub>tag</sub> rendered negative results (Fig. 2b) similarly to our earlier C-terminally tagged NS5 construct (data not shown). Our results indicated that understanding of the protein sequence and structure is essential for success in insertion

of an extra sequence into the compact viral genome, and our rational approach should be useful for tag insertion into other viral proteins.

Next, we examined the production of infectious DENV from our NS5-tagged constructs. The foci formation assays were performed with supernatants obtained 7 days post RNA transfection into BHK-21 cells. The results were consistent with the E protein expression profiles, revealing that the MT<sub>tag</sub> clone could produce infectious viral particles comparable to the WT clone from pD2-IC (Fig. 2c). We also generated an MT<sub>tag</sub> construct that possessed an alternative HA–FLAG tag epitope in the same position, and this tagged version also gave infectious particles (data not shown). Therefore, the N172–N177 loop of MTase is a suitable location, with the tag having a minimal effect on viral replication and production, for general tag insertion into flaviviral NS5s.

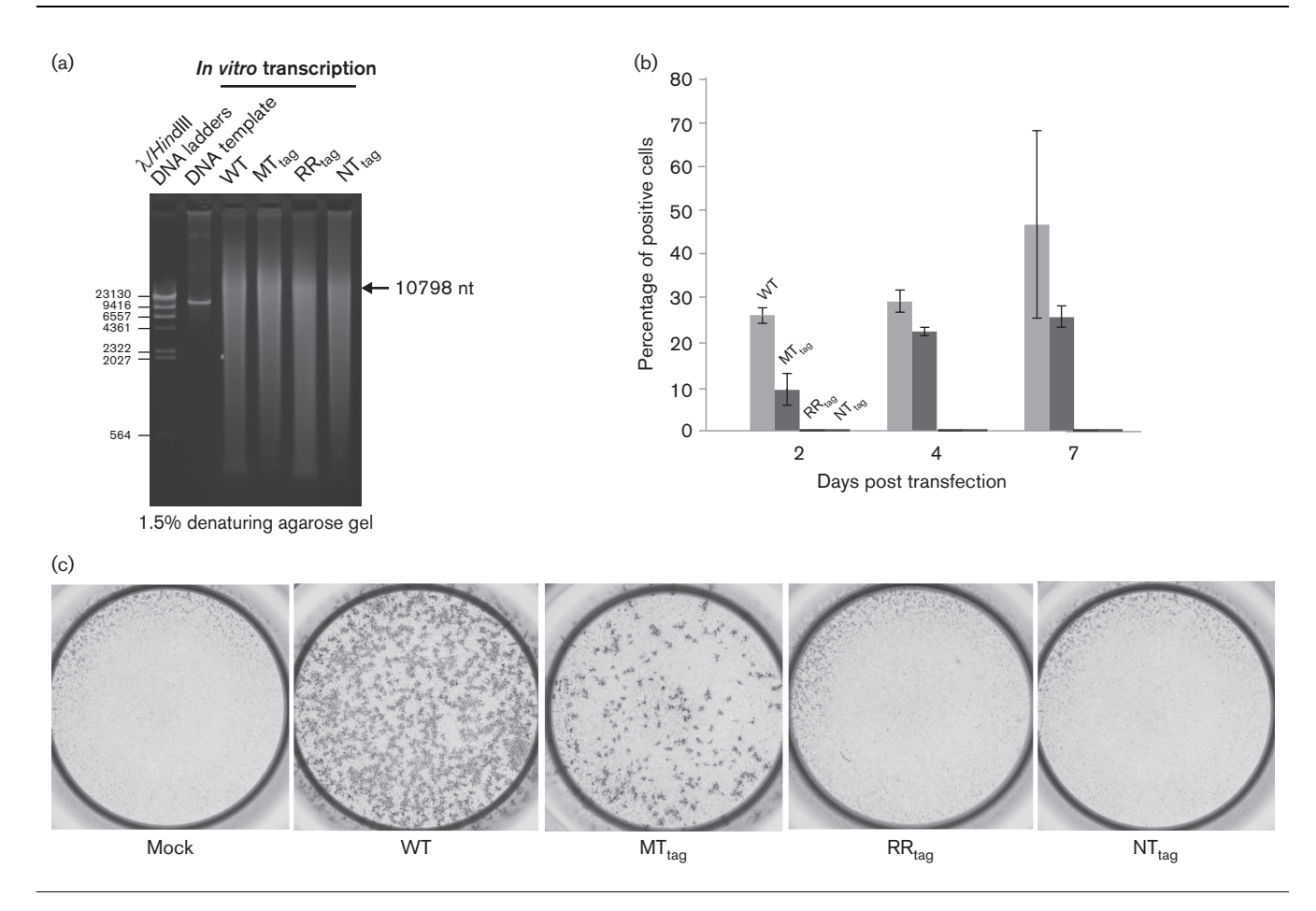


**Fig. 2.** Screening of various tagged DENV constructs. (a) Formamide gel electrophoresis shows the quality of *in vitro* transcribed products. Arrow shows the size of the full-length DENV genome. (b) DENV transcripts were electroporated into BHK-21 cells and the synthesis of E protein in transfected cells was measured via immunofluorescence. Light and dark grey bars represent WT and MT<sub>tag</sub> transfections, respectively. Blank spaces highlight the absence of detected E protein in RR<sub>tag</sub> and NT<sub>tag</sub> constructs. Hereafter, the graphs show means of experiments performed in triplicate, and the error bars show sp. (c) Representative data from two independent experiments show focus forming assays of culture media from RNA-transfected cells at day 7.

#### Characterization of MTase-tagged DENV

We collected supernatants obtained at 7 days post RNA transfection and increased the viral titre by another three passages in BHK-21. Then, engineered tagged DENV particles recovered from the MT<sub>tag</sub> construct (hereafter designated etDENV) were used to infect BHK-21 at an m.o.i. of 1 and 0.01 for observation of phenotype and viral kinetics, respectively. Our etDENV induced rounded cell shapes which represent a cytopathic effect in cell culture at day 2 post-infection similar to the natural DENV-2 strain 16681 (Fig. 3a). Production of infectious etDENV showed an identical pattern to those of DENV-2 from natural strain 16681 and virions derived from supernatant of RNA-transfected cells (WT), reaching peaks of viral titre of approximately 10<sup>6</sup> FFU ml<sup>-1</sup> at day 4 (Fig. 3b). Besides BHK-21 cells, flow cytometry analysis showed that our etDENV also possessed infectivity in A549, HEK-293 and Huh-7 cell lines, representing virus targeting of human

lung, kidney and liver, respectively. However, the infectivity is about 60 % of that of WT (Fig. 3c).

Next, we confirmed that the tags would not interfere with the localization of NS5 between nucleus and cytoplasm that has been demonstrated for DENV serotypes 2 and 4 (Hannemann et al., 2013). At day 2 post-infection in BHK-21 cells at an m.o.i. of 1, NS5s of both WT and etDENV mainly localized in the nucleus as described earlier (Uchil et al., 2006) (Fig. 3d). Finally, we validated the stability of the tag in etDENV, since the possibility that the virus could remove or modify the epitope tag after several passages has been proposed (Schoggins et al., 2012; Usme-Ciro et al., 2014). The etDENV collected after seven passages in BHK-21 was sequenced (Fig. 3e). No mutation or deletion was found around the insertion region, indicating a high stability of these insertion clones. These results also suggested that the tag insertion did not disturb the folding and function of NS5 in infected cells. Taken together, our etDENV showed

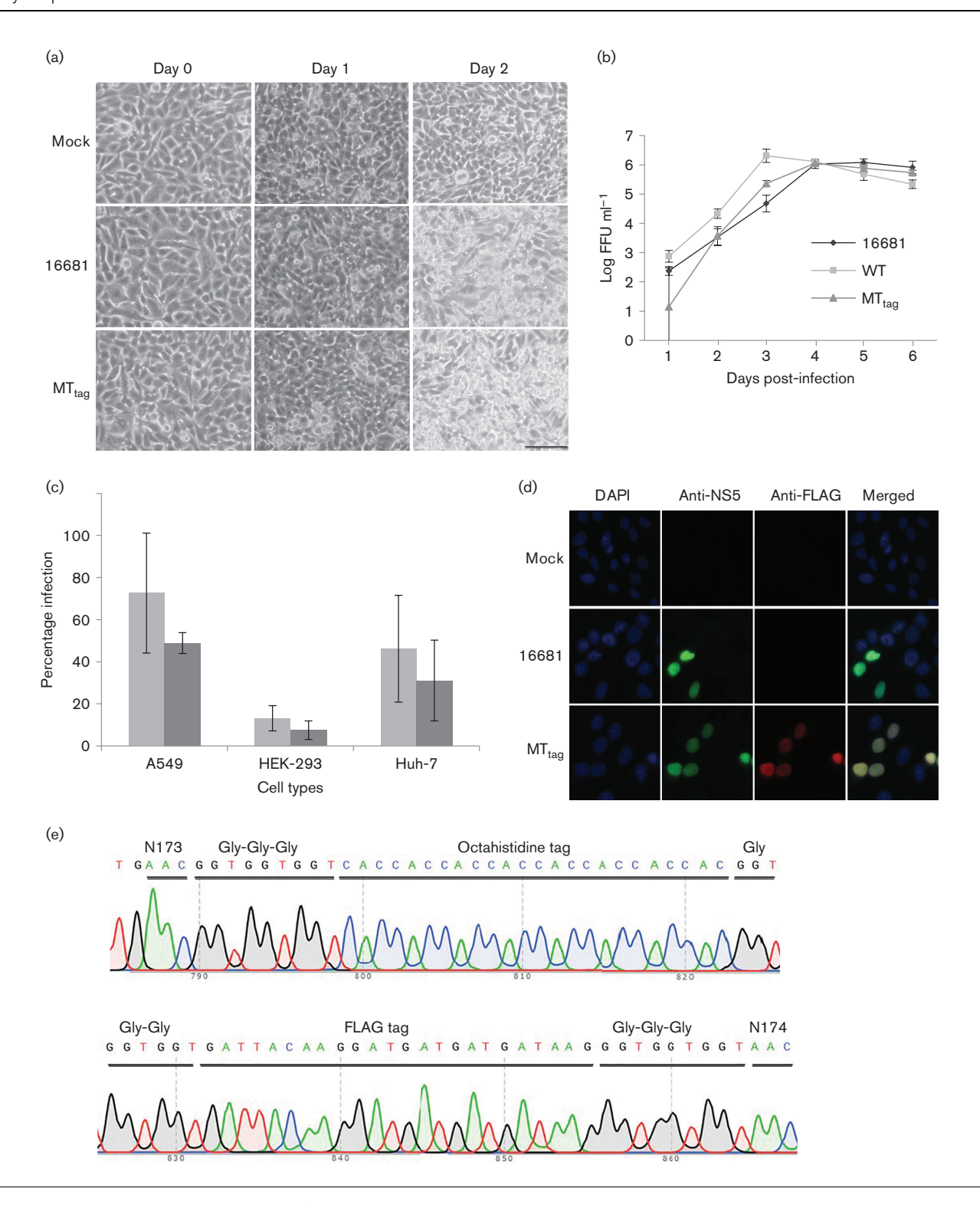


**Fig. 3.** Characterization of etDENV. (a) BHK-21 cells were infected with DENV-2 strain 16681 or etDENV at an m.o.i. of 1. Cytopathic effect represented by rounding and detachment of cells was observed 2 days after infection. Bar, 30 μm. (b) Growth kinetics of etDENV in BHK-21 were compared with DENV from laboratory stock (16681) and RNA transfection (WT). A constant m.o.i. of 0.01 was used. Bars represent means of three independent experiments. (c) Flow cytometry analysis with anti-E antibody revealed that etDENV could infect several human cell lines. Light and dark grey bars represent DENV-2 16681 and etDENV. (d) Localization of NS5 in infected BHK-21 cells was observed 2 days post-infection by immunofluorescence. (e) The chromatogram of etDENV sequence showed no mutations in the tag sequences after seven passages in BHK-21 cells.

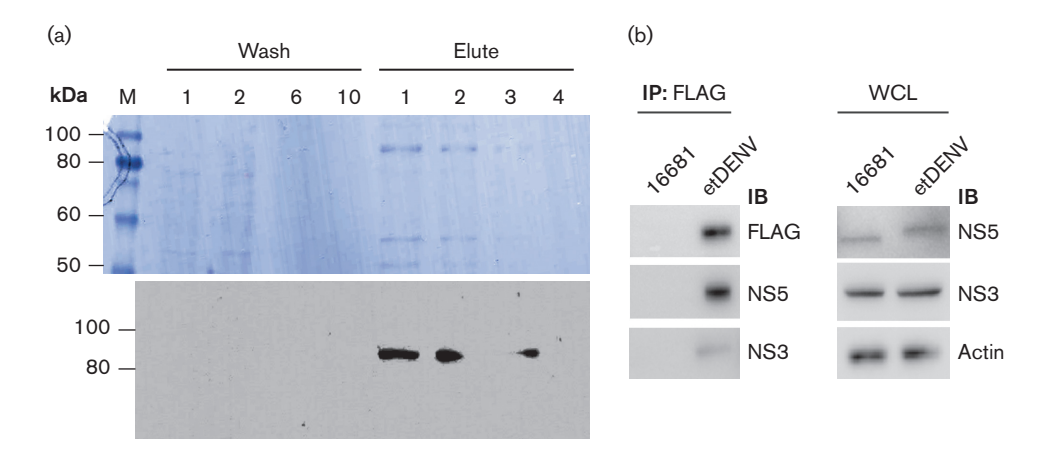


**Fig. 4.** Purification of NS5 via the internal TAP tag. (a) Ni affinity purified fractions were analysed by SDS-PAGE (top panel) and immunoblotting (IB) (lower panel). Wash and elution fractions are indicated above the lanes. (b) FLAG IP fractions were subjected to IB with specific antibodies. WCL, Whole cell lysate.

identical properties to WT DENV-2, and is suitable for studying the NS5 interactome in different cell types. To our knowledge, this is the first report of stable, infectious recombinant NS5-tagged flavivirus.

### Isolation of tagged NS5 from infected cells

Since the TAP tag existed inside the MTase domain, we validated its ability to isolate NS5-interacting complexes via both His and FLAG tag pull downs. For Ni affinity, we infected Huh-7 cells with etDENV at an m.o.i. of 5, and extracted the total protein 48 h after infection. After Ni affinity purification, the results showed clear NS5 bands in both SDS-PAGE and Western blot analyses, suggesting that this internal tag was exposed to the solvent and useful for isolation (Fig. 4a). Based on purified recombinant DENV RdRp as standards in Western blot analysis (Kamkaew & Chimnaronk, 2015), we calculated the total amount of NS5 as approximately 500 ng from 10<sup>7</sup> cells; therefore, giving  $9.4 \times 10^5$  NS5 molecules (infected cell)<sup>-1</sup> (a molecular mass of  $1.06 \times 10^5$  Da or  $1.76 \times 10^{-19}$  g). Furthermore, we also performed IP of NS5 via the FLAG tag from BHK-21 cells which were infected at an m.o.i. of 1. As with Ni affinity, the IP with a FLAG antibody was highly effective in pulling down NS5 with a very low background (Fig. 4b). NS3, a well-known NS5 interactor, was detected in the co-IP fraction of etDENV. Taken together, we have here provided a new biological tool for studying host-DENV interactions.

#### Interactome of DENV NS5 in human liver cells

To explore an interaction landscape of NS5 in liver cells, Huh-7 cells were infected with either etDENV or DENV-2 16681 at an m.o.i. of 5, and the NS5 complexes were isolated via FLAG IP at 48 h post-infection followed by mass spectrometry. Only DENV NS5 interactors that

were found in etDENV IP samples, but not in the control, were considered. Moreover, we utilized two distinct algorithms for peptide identification, and only 97 proteins overlapping between 554 X! Tandem and 199 SEQUEST candidates were considered, and mapped by STRING 10.0 software (Table S2). To reveal a high-confidence interactome, this network was reconstructed to include two forms of information (Fig. 5a). First, STRING's proteinprotein interaction confidence levels were shown as edge widths. Secondly, relative peptide abundances from mass spectrometry were indicated by node sizes. In addition to the host proteins, the NS3 helicase was identified, confirming its role as the major viral protein interacting with NS5 (Table 1). Our NS5 interaction network contained only four proteins that were also reported as NS5 interactors in recent genome-wide studies (Table 2). Intriguingly, heterogeneous nuclear ribonucleoproteins (hnRNPs) were identified as the main NS5 complex for the first time. Several NS5 interactors related to the protein-folding pathway have already been shown to be upregulated upon DENV infection (Fig. 5a and Table 3). Though our interactome map was constructed with proteins found only in the etDENV IP, we did examine the control-only protein list for possible insights. However, none of the predicted functional control-only groups reached the significance of the top 15 etDENV IP groups, with one exception (enrichment in desmosome-related proteins in the control group). Further, comparing the top 15 enriched groups derived from etDENV and control IP, no overlap was observed, with enriched groups from control IP focusing on celljunction related functions (e.g. 'anchoring junction', 'desmosome' and 'cell-cell junction'), whereas cytosol and RNA-binding functions dominated in the etDENV IP (Fig. 5b and Table S3). The clear difference in the contents of control versus etDENV pulldowns again points to the efficacy of etDENV in isolating NS5-specific interactors.

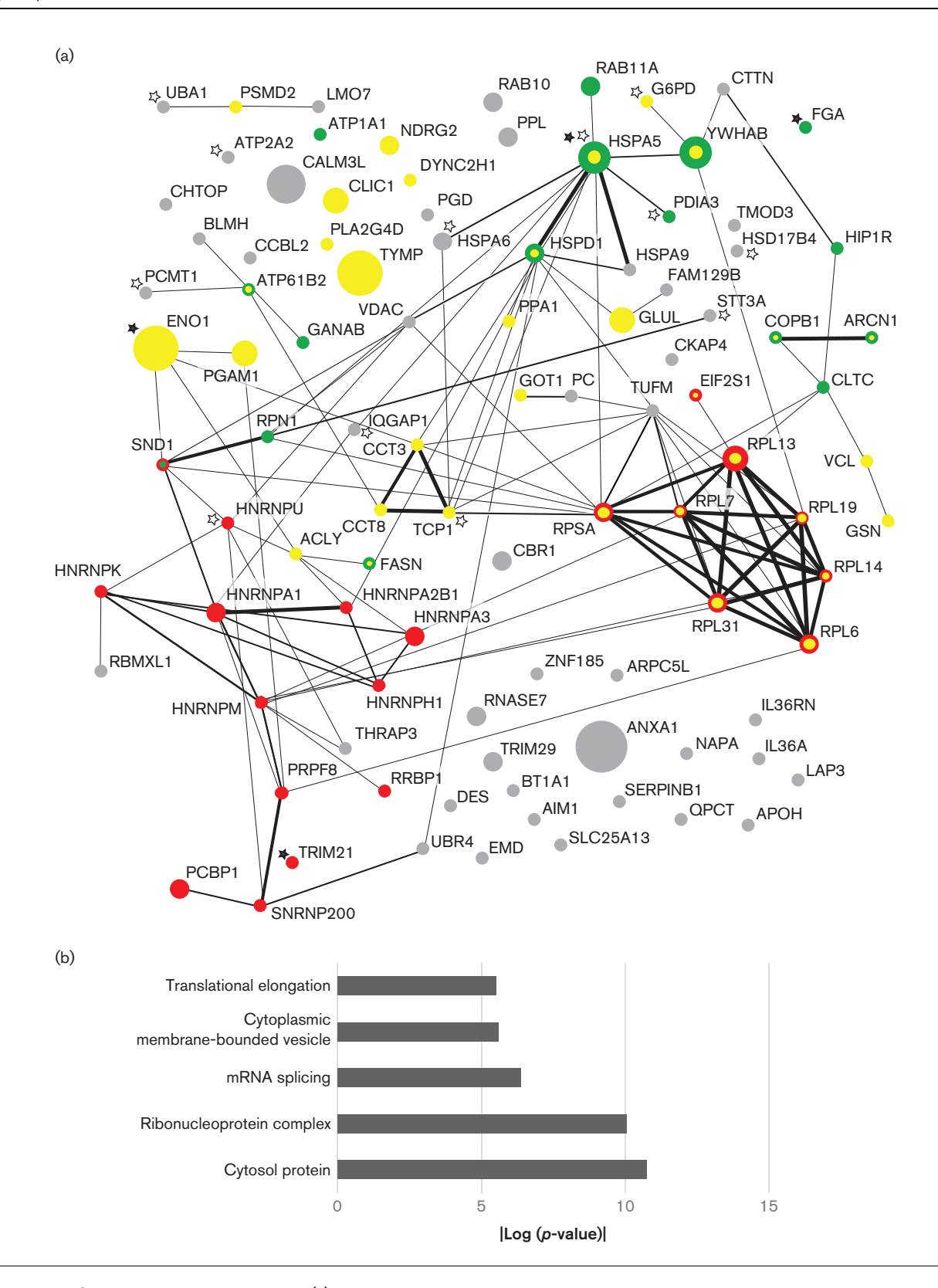


**Fig. 5.** NS5 interactome in Huh-7 cells. (a) The protein–protein interaction network was reconstructed using the initial STRING 10.0 network as template. Colours indicate three enriched groups: yellow for non-membranous predominantly cytosolic proteins, red for ribonucleoproteins and green for cytoplasmic membrane-bound vesicle proteins. Open and filled stars indicate proteins with altered expression levels and NS5 interactors identified in previous studies, respectively (Table 3). Edge length and node placement are not of importance. Isolated nodes should not be construed as irrelevant to infection. (b) List of enriched gene ontology groups using DAVID.

Table 1. DENV proteins identified by NS5 IP

Peptides	Molecular mass (kDa)
1	18.92
1	39.93
10	69.26
1	13.96
24	103.2
	1 1 10 1

#### **DISCUSSION**

In the early stages of our work, we unsuccessfully attempted to place epitope tags into the N- and C-termini of several DENV proteins. The vast majority of TAP-tag experiments have placed the tag at a protein's N- or C-terminus. Generally, such an approach should offer minimal disruption of the protein structure and function. Carpp *et al.* (2014) also pointed out an inability to insert tags into DENV NS3 and NS5 proteins in the context of viable virus, and their subsequent work, therefore, depended on ectopic expression. On the other hand, Teterina *et al.* (2011) used a transposon-based method to

randomly insert 15 nt sequences into the poliovirus genome. Viable viruses were then found to contain tags predominantly within regions of low conservation and at surface-exposed loops. These results were later successfully applied to specifically tag foot-and-mouth disease virus protein 3a (Li *et al.*, 2012). This work highlighted the potential for a rational tagging strategy based on both sequence conservation and tertiary structure.

Our success in tag insertion within NS5's MTase indicated that internal insertions may be underrated in their utility. In the context of a viral genome, such tags are particularly useful, as terminal insertions may interfere with polyprotein processing. At the same time, virus with a rationally designed internal RdRp tag was not viable, highlighting the still unpredictable effects of tag insertion. One simple factor that may have contributed to our final success, however, would be the size of the tags, with 8 × His and FLAG combo contributing less than 25 residues to NS5. Previous work has established that insert size and type certainly could be a factor in viral viability; in one case, a relatively large luciferase insert within WNV capsid was quickly eliminated over passaging, while a 75 nt portion of a TAT insert (from HIV) remained stable over multiple

Table 2. NS5 interactors identified in this study and other earlier reports

Gene ID	Symbol	Methodology	Function(s)	Reference
ENSG00000044574	HSPA5	Y2H	Protein folding and protein assembly	Mairiang et al. (2013)
ENSG00000074800	ENO1	Y2H	Glycolysis enzyme and tumour suppressor	Le Breton et al. (2011)
ENSG00000132109	TRIM21	Y2H	Protein degradation process	Le Breton et al. (2011)
ENSG00000171560	FGA	Y2H	Blood coagulation	Khadka et al. (2011)

Table 3. Identified NS5 interactors that showed alteration of gene expression upon DENV infection

Gene ID	Symbol	Expression	Function(s)	Reference(s)
ENSG00000044574	HSPA5	Upregulation in Huh-7 and A549	Folding and protein assembly	Chiu <i>et al.</i> (2014); Pando-Robles <i>et al.</i> (2014)
ENSG00000120265	PCMT1	Downregulation in ECV	Type II carboxyl methytransferase enzyme	Liew & Chow (2006)
ENSG00000120438	TCP1	Upregulation in Huh-7	Chaperone protein	Pando-Robles et al. (2014)
ENSG00000130985	UBA1	Upregulation in Huh-7	Protein degradation process	Pando-Robles et al. (2014)
ENSG00000133835	HSD17B4	Upregulation in A549	Peroxisomal $\beta$ -oxidation	Chiu et al. (2014)
ENSG00000134910	STT3A	Upregulation in A549	N-Oligosaccharyltransferase complex	Chiu et al. (2014)
ENSG00000140575	IQGAP1	Upregulation in Huh-7	Reorganization of cytoskeleton process	Pando-Robles et al. (2014)
ENSG00000153187	HNRNPU	Upregulation in Huh-7	mRNA processing	Pando-Robles et al. (2014)
ENSG00000160211	G6PD	Upregulation in Huh-7	Energy generation	Pando-Robles et al. (2014)
ENSG00000167004	PDIA3	Upregulation in A549 and HepG2	Folding and disulfide isomerase enzyme	Chiu et al. (2014); Higa et al. (2008)
ENSG00000174437	ATP2A2	Upregulation in A549	Hydrolysis of ATP in ER	Chiu et al. (2014)
ENSG00000173110	HSPA6	Upregulation in HepG2	Protein folding	Fink et al. (2007)

passages (Vandergaast *et al.*, 2014). Similarly, a C-terminal GFP tag of Sindbis virus's RdRp failed to infect cells, but virus was viable when the tag was switched to 3 × FLAG (Cristea *et al.*, 2010). Yet another study showed that insertion of the smaller luciferase gene into the dengue genome rendered more stable recombinant virus, while the epitope was lost over a series of passages when the GFP gene was exploited instead (Schoggins *et al.*, 2012; Usme-Ciro *et al.*, 2014). The luciferase gene could also be successfully inserted into the N-terminal region of the capsid in DENV genome despite possible concerns that it would disrupt viral packaging (Zou *et al.*, 2011).

DENV infects several organs in humans, altering host homeostasis and counteracting the host response (Aye et al., 2014; Póvoa et al., 2014). These events suggest complex interactions between host and virus where viral proteins play roles in several networks. However, current systems for studying the host–DENV interaction network may not be up to the task of emulating actual infection conditions. By placing a tag sequence within an organism's genome, the protein in question can be expressed, localized and regulated under natural infection conditions and, at the same time, isolated along with its protein partners with high specificity.

Our functional annotation showed highest enrichment in cytosolic proteins, a category that excluded membranous and subcellular components. Enrichment in cytosolic membranous components was also high, consistent with NS5's localization with the ER during replication. RNPs were abundant within the interactor list, with a subset of splicing-related hnRNPs (hnRNPM, hnRNPA1, hnRNPA3, hnRNPU, hnRNPK, hnRNPH1 and hnRNPA2B1), which are generally localized to the nucleus, showing particular enrichment. Earlier work suggested that DENV genomic RNA lacks splicing sites (Brunak et al., 1991), although one study predicted a candidate donor splicing present on the DENV genome (Usme-Ciro et al., 2014). Interestingly, a previous study examining the infected Huh-7 proteome showed significant alterations in the abundance of RNA processing proteins (Pando-Robles et al., 2014). While DENV-2 NS5 could shuttle between the nucleus and cytoplasm, and thus hnRNPs might not be necessarily associated with the replication complex, it has been revealed that the hnRNPK and hnRNPA1 proteins accumulated in the cytoplasm and promoted DENV production (Anwar et al., 2009; Brunetti et al., 2015; Jiang et al., 2009). However, precise roles played by interaction of hnRNPs with NS5 require further study. Another subset of RNP interactors was related to the translational elongation process. In particular, large ribosomal subunit members (RPL6, RPL7, RPL13, RPL14, RPL19 and RPL31) were identified as NS5 interaction partners, with only low levels of other ribosome proteins found in the control group. Though translational elongation and viral replication are processes that, logically, cannot occur simultaneously, Germain et al. (2014) also found ribosomal proteins interacting with the **HCV** polymerase.

Conceivably, the NS5-ribosome interaction might enhance and/or inhibit translation according to a need for protein versus RNA, without any conflicts between translation and replication.

We also divided the number of fragments detected by molecular mass and abundance (in p.p.m. of protein) in the liver (PaxDb version 4.0) to reduce bias towards abundant proteins (Wang et al., 2015). The phospholipase 2 protein (PLA2G4D) came to the fore. Since it was shown that phospholipase 2 group 4C was involved in generation of the membranous web in HCV-infected cells (Xu et al., 2012), PLA2G4D could play a similar role in remodelling the ER membrane for DENV replication. In concord with this picture, fatty acid synthase (FASN), which was shown to be relocalized to viral replicase to remodel cytosolic membranes in DENV-infected cells (Heaton et al., 2010), was also present in our interactome map. Other interactors involved in lipid metabolism included pyruvate carboxylase (PC), ATP citrate lyase (ACLY) and butyrophilin (BT1A1). Our results suggest tight association of fatty acid biosynthesis complex with viral replicase.

It might be informative to compare our interactome with that of Carpp et al. (2014), in which DENV-2 NS5 was ectopically expressed in infected cells as a C-terminally GFP tagged fusion. Taking the Carpp et al. (2014) data, we selected proteins with light/heavy ratios of at least 5.0, proteins that appeared in all independent NS5 experiments and proteins that were found in GFP control pulldowns not more than two times, generating a list of 73 candidates against our 97. Here, no overlap in datasets was found (Fisher's exact test; P value=0.70). On the other hand, the overlap between our data and that in Germain et al. (2014) using N-terminal FLAG-tagged NS5B in distantly related HCV was far more significant (P value= $7.2 \times 10^{-9}$ ), underlining the importance of tag size. While our list was enriched in cytosolic proteins, Carpp et al. (2014) showed enrichment in nuclear import and transport system proteins. While DENV-2 NS5 does localize to the nucleus, mutations that eliminate this localization showed little effect on viral replication, casting doubt on the notion of critical interactions with nuclear proteins (Hannemann et al., 2013). It is also possible that ectopic expression of an extra 28 kDa GFP tag could alter protein folding in cells. We have shown that even a short hexahistidine tag at either N- or C-termini of DENV RdRp markedly impaired the polymerase activity (Kamkaew & Chimnaronk, 2015).

In conclusion, we highlighted stringent criteria for effective design of protein tagging, and provided proof-of-concept evidence by generation of viable tagged recombinant DENV-2 possessing an internal TAP tag in NS5. Utilizing our tagged DENV, we revealed here a high-confidence protein interaction network with NS5 in infected human hepatic cells, in which RNP and fatty acid biosynthesis complexes were recruited into DENV replicase. This work provides a general method for tagging of viral proteins and a standard for future studies of virus–host interactions.

#### **METHODS**

Primary and tertiary structure analyses of NS5. To seek candidate tag insertion sites with minimal conservation, ten flaviviral NS5-containing polyprotein sequences were aligned using ClustalW2, representing DENV-1 (NCBI accession AHG23185), DENV-2 (AHG23127), DENV-3 (ABG73588.1), DENV-4 (AIG60035.1), West Nile virus (AAT02759.1), Japanese encephalitis virus (AAD20233), yellow fever virus (AAC35903), St. Louis encephalitis virus (AEN02430), Omsk haemorrhagic fever virus (AAR98531) and tickborne encephalitis virus (ACL97686.1). The alignment results generated integer conservation values for each residue position (Thompson et al., 1994), and subsequently, the means of the data were taken over all 31 residue windows, clarifying regions of particularly high and low conservation.

Following identification of potential conservation-based insertion sites, the available crystal structure of DENV-3 NS5 (PDB ID: 4V0R) was examined to screen out candidates that would be located in structured or hydrophobic regions. Finally, short sequences that various tags would straddle were interrogated against the ELM database (http://elm.eu.org/) to reduce the chances that critical linear motifs would be interrupted. Only two internal NS5 locations fulfilled all the above criteria, and were selected for tag insertion.

Insertion of the TAP tag sequences into NS5 of a DENV-2 16681 clone. The cDNA from DENV serotype 2 strain 16681 in the pD2-IC plasmid was used as the template for the insertion of the epitope tag (Kinney et al., 1997). In this work, the TAP tag comprised an octahistidine (His<sub>8</sub>) tag, a tri-glycine spacer and FLAG sequence (DYKDDDDK) which was inserted into the NS5 gene in pD2-IC via a standard QuikChange procedure. Briefly, the tag sequences in the forward and reverse primers overlapped by at least 20 nt (Table S1, available in the online Supplementary Material), while the 3' portions of the primers were required to overlap the DENV genome with an annealing temperature of not less than 70 °C. Reactions were conducted in 20 µl volumes with 0.4 U Phusion polymerase (NEB) and not more than 10 ng of template. Twenty-two PCR cycles were performed, with a 10 s denaturation period at 98 °C, a 30 s annealing period at 55 °C and an extension period of 4.5 min at 72 °C. The resulting PCR product was treated with DpnI (NEB) prior to bacterial transformation. Colony PCR was used to screen clones for successful mutagenesis, as the tags added 75 nt to the NS5 gene. Positively screened plasmids were sequenced to verify in-frame insertions.

In vitro transcription, transfection and viral titration. DNA templates for *in vitro* run-off transcription were generated by PCR using Phusion polymerase with the forward primer: 5'-GAAATTAATACG-ACTCACTATTAGTTGTTAGTCTACGTGGACCGAC-3', carrying a T7 promoter sequence (italics) and the reverse primer: 5'-AGAACCTGTTGATTCAACAGCACC-3'. The 10.75 kb PCR product was purified with a QIAquick Gel Extraction kit (Qiagen). WT and tagged DENV RNAs were synthesized in a 50  $\mu$ l reaction with 5  $\mu$ g purified templates using a RiboMax Large Scale RNA Production kit (Promega) at 37 °C for 4 h. The dsDNA template was removed by DNase I (NEB) treatment, and transcripts were purified via an RNeasy Mini kit (Qiagen). The quality of transcribed RNAs was analysed on denaturing formamide agarose gels.

Ten micrograms of transcribed product was electroporated into  $2\times 10^6$  BHK-21 cells following the protocol of Leardkamolkarn *et al.* (2012). Supernatant of transfected cells was collected for foci formation assay at 7 days post-transfection. The supernatant was incubated with BHK-21 cells in 96-well plates for 2 h, and subsequently 200  $\mu$ l of 1.5 % carboxymethylcellulose and 2 % FBS in Dulbecco's modified Eagle's media (DMEM) was added to cover the cells, and incubated at 37 °C for 3 days. The infected BHK-21 cells were then washed with PBS three times and fixed with 3.7 %

formaldehyde for 10 min at room temperature. The cells were permeabilized by 1 % Triton X-100 in PBS for 10 min and washed with PBS five times. Anti-DENV E protein (Millipore) was diluted 1:1000 in PBS supplied with 2 % FBS and 0.05 % Tween-20, and incubated at 37 °C for 2 h. Thereafter, the cells were washed with PBS five times before incubation with goat anti-mouse conjugated HRP antibody at a 1:1000 dilution for 45 min at 37 °C. The foci were visualized through Sigma*FAST* DAP (Sigma) and counted under microscopy.

**Cell culture and infection.** BHK-21 (baby hamster kidney cells), Huh-7 (human hepatocyte cells), A549 (lung carcinoma cells) and HEK-293 (human embryonic kidney cells) were cultured in DMEM supplemented with 10 % FBS at 37 °C with 5 % CO<sub>2</sub>. When the confluences were 75–90 %, the cells were incubated with DENV for 90 min in 2 % FBS DMEM media at 37 °C, 5 % CO<sub>2</sub>.

**Immunofluorescence assay.** At indicated time points, transfected or infected cells were washed with PBS, and then fixed with 3 % paraformaldehyde and 2 % sucrose in PBS. After three washes with PBS, the samples were permeabilized by incubation with Triton X-100 solution (0.5 % Triton X-100, 20 mM HEPES pH 7.8, 50 mM NaCl, 3 mM MgCl<sub>2</sub> and 300 mM sucrose) for 5 min on ice. Cells were washed with PBS four times, and incubated with an anti-NS5 rabbit antibody (Thermo) or an anti-FLAG mouse antibody (Sigma) diluted 1:1000 in PBS with 5 % BSA for 2 h at room temperature. Thereafter, the slides were washed three times with PBS, and probed by a goat anti-rabbit conjugated Alexa Fluor 488 (Invitrogen) or goat antimouse Alexa Fluor 594 (Jackson ImmunoResearch) antibodies in the dark for 1 h at room temperature before mounting with Prolong Gold Antifade with DAPI (Invitrogen). Protein expression and localization were observed on fluorescence microscopy (Nikon).

Co-immunoprecipitation and immunoblotting. For His tagaffinity purification, infected cells were lysed by incubation with 50 mM HEPES pH 7.2, 150 mM KCl, 25 mM imidazole, 1 % NP-40, 10 % glycerol, 5 mM  $\beta$ -mercaptoethanol (2-ME), 1 × EDTA-free protease inhibitor (GE Healthcare), 1 % Triton X-100, 1 × Phosphatase Inhibitor (Thermo) and 7 U ml<sup>-1</sup> DNase (NEB) for 30 min on ice. Cell lysate was cleared via centrifugation at 15 000 r.p.m. for 15 min, and the supernatant was applied to Ni-NTA agarose beads (Qiagen) pre-equilibrated with Ni wash buffer (50 mM HEPES pH 7.2, 150 mM KCl, 25 mM imidazole, 1 % NP-40, 10 % glycerol, 5 mM 2-ME and  $1 \times$  EDTA-free protease inhibitor). A 10  $\mu$ l bed volume of beads was suitable for approximately 10<sup>7</sup> cells. The resin was gently agitated at 4 °C for 1 h for binding. Unbound materials were removed by at least six cycles of 5 min washing at 4 °C. Elution proceeded with four cycles of treatment with 100 µl elution buffer. In cases where subsequent FLAG purification was not desired, elution buffer was the wash buffer supplied with a final 250 mM imidazole concentration. Otherwise, the elution buffer omitted 2-ME and NP-40, as these components could interfere with FLAG purification.

For the FLAG pull down, infected cells were carefully washed with PBS, and cell pellets were incubated with 2 mM dimethyl pimelimidate at room temperature for 20 min to cross-link protein–protein complexes. Cells were lysed with CLB buffer (50 mM Tris/HCl pH 7.4, 250 mM NaCl, 0.5 % NP-40, 1 mM glycerophosphate, 1 mM sodium orthovanadate and 5 mM EDTA). The total cell lysates were pre-cleared with protein G agarose (Roche) to reduce non-specific binding for 60 min at 4 °C, and subsequently gently mixed with EZview Red Anti-FLAG M2 affinity gels (Sigma) for 4 h at 4 °C. After washing three times with 50 mM Tris/HCl pH 7.4 and 150 mM NaCl, bound proteins were eluted with 30  $\mu$ l of 1 M glycine pH 2.5 three times. The samples were neutralized by adding 10  $\mu$ l 1 M Tris/HCl pH 8.0, and concentrated using 10 kDa-cut-off Amicon Ultra filters (Millipore).

Total cell lysates and pulled-down fractions were analysed with 10 % SDS-PAGE, and transferred onto a PVDF membrane. The membranes were blocked with 5 % skim milk in 0.01 % Tween-20, 10 mM Tris/ HCl pH 8.0 and 150 mM NaCl (TBST buffer). The membranes were incubated with primary antibody for 12–16 h at 4 °C, washed three times at room temperature with TBST, and probed with a goat anti-rabbit (Thermo) or goat anti-mouse (Novagen) conjugated HRP antibodies for 2 h. The protein bands were detected via chemiluminescence according to the manufacturer's instructions (ECL, GE Healthcare Life Sciences).

**Flow cytometry.** Cells were collected by centrifugation at 1800 *g* after treatment with 0.25 % trypsin-EDTA for 3–5 min. The cell pellets were fixed with 3.7 % formaldehyde in PBS for 15 min, and permeabilized with FACS solution containing 0.5 % saponin, 2 % FBS, 2 mM EDTA and 0.05 % AB human serum in PBS for 20 min at room temperature. The DENV E protein was probed by a mouse anti-E primary antibody and a goat anti-mouse FITC-labelled secondary antibody (Dako) for 60 min at 4 °C. Then cells were washed three times with FACS solution, and fixed with 1 % formaldehyde in PBS before analysing with a FACS Caliber (BD). The percentage of DENV-infected cells was calculated using Flowing Software version 2.5.1.

Mass spectrometry. Concentrated samples from FLAG IP were separated on a 10 % SDS-PAGE, and in-gel trypsin digestion was performed as follows. Small gel slices were washed with 25 mM ammoniumbicarbonate (Ambic) in 50 % acetonitrile (ACN) two times. Dehydration proceeded with 100 % ACN two or three times until gel pieces were white, followed by speed vacuum treatment to evaporate the solution. A reducing step was performed by adding 10 mM DTT and 25 mM Ambic and incubating at 56 °C for 45 min. The supernatant was then removed, and gel pieces were incubated with 55 mM iodoacetamine and 25 mM Ambic in the dark for 30 min at room temperature. After washing with 25 mM Ambic for 10 min followed by 100 % ACN, gel pieces were dried by speed-vac for 15 min. Proteins were digested by incubation with 12.5 ng μl<sup>-1</sup> trypsin (Promega) for 1 h on ice, and processed at 37 °C in 25 mM Ambic overnight. Tryptic peptides were extracted with 50 % ACN two or three times and concentrated via a vacuum centrifuge. Peptide pools were desalted with an octadecyl C<sub>18</sub> resin before injection into a tandem mass spectrometer (Q-Exactive Plus, Thermo).

**Data analysis.** Mass spectrometry results were analysed using the X! Tandem algorithm in the Global Proteome Machine software (Craig et al., 2004) and the SEQUEST algorithm in the Proteome Discoverer (PD) software (Thermo). Ensembl and UniProt databases were used in these software packages, respectively. Precursor and fragment mass errors were set to 10 p.p.m. NS5 protein partners were included in the list using a false discovery rate of lower than 1 % as a cut-off based on target-decoy analysis. Only proteins identified by both software approaches were included in the final list of potential NS5 interactors. For the label-free quantification, the list of peptides from PD was further subjected to analysis by Skyline software (MacLean et al., 2010). For Skyline, isotope dot product, a measure that compares apparent isotope ratios in experimental peptides with naturally occurring expected ratios, was used to exclude peptides with isotope dot product value of less than 0.8. The NS5-interacting network was generated using the STRING 10.0 database, with co-occurrence, database and text mining excluded from analysis (Szklarczyk et al., 2015). This network was used as a template to construct a refined network that indicated the number of peptide fragments weighted against molecular mass for all nodes, and also indicated the confidence of STRING interactions at levels 0.9, 0.7 and 0.4 as edge widths. DAVID (Huang et al., 2009a, b) was used for gene-ontology analysis.

#### **ACKNOWLEDGEMENTS**

This work was supported by Grants-in-Aid for scientific research from Mahidol University (Thailand) and by the Mid-Career Grant from Thailand Research Fund (TRF) (RSA5680054) to S. C.; S. J. was supported by the Chalermphrakiat Grant, Faculty of Medicine, Siriraj Hospital, Mahidol University. S. J. and S. C. were also supported by the Advanced Research on Pharmacology Fund, Siriraj Foundation (D003421). This work was also funded by the Office of the Higher Education Commission and Mahidol University under the National Research Universities initiative (NRU), and the DENFREE project (The European Union Seventh Framework Programme, FP7/2007/ 2011 under Grant Agreement no. 282 378) to A. S. and P. M. T. Pisitkun was supported by Chulalongkorn Academic Advancement into its 2nd Century Project (CUAASC) grant. T. Poyomtip was supported by a scholarship from Science Achievement Scholarship of Thailand (SAST). We thank Poorichaya Somparn for helping in all aspects of mass spectrometry, and Vijittra Learkamolkarn for kindly providing the pD2-IC plasmid.

#### REFERENCES

Anwar, A., Leong, K. M., Ng, M. L., Chu, J. J. & Garcia-Blanco, M. A. (2009). The polypyrimidine tract-binding protein is required for efficient dengue virus propagation and associates with the viral replication machinery. *J Biol Chem* 284, 17021–17029.

**Ashour, J., Laurent-Rolle, M., Shi, P. Y. & García-Sastre, A. (2009).** NS5 of dengue virus mediates STAT2 binding and degradation. *J Virol* **83**, 5408–5418.

Aye, K. S., Charngkaew, K., Win, N., Wai, K. Z., Moe, K., Punyadee, N., Thiemmeca, S., Suttitheptumrong, A., Sukpanichnant, S. & other authors (2014). Pathologic highlights of dengue hemorrhagic fever in 13 autopsy cases from Myanmar. *Hum Pathol* 45, 1221–1233.

Bhatt, S., Gething, P. W., Brady, O. J., Messina, J. P., Farlow, A. W., Moyes, C. L., Drake, J. M., Brownstein, J. S., Hoen, A. G. & other authors (2013). The global distribution and burden of dengue. *Nature* 496, 504–507.

**Bidet, K. & Garcia-Blanco, M. A. (2014).** Flaviviral RNAs: weapons and targets in the war between virus and host. *Biochem J* **462**, 215–230.

Brunak, S., Engelbrecht, J. & Knudsen, S. (1991). Prediction of human mRNA donor and acceptor sites from the DNA sequence. *J Mol Biol* 220, 49–65.

Brunetti, J. E., Scolaro, L. A. & Castilla, V. (2015). The heterogeneous nuclear ribonucleoprotein K (hnRNP K) is a host factor required for dengue virus and Junín virus multiplication. *Virus Res* 203, 84–91.

Carpp, L. N., Rogers, R. S., Moritz, R. L. & Aitchison, J. D. (2014). Quantitative proteomic analysis of host-virus interactions reveals a role for Golgi brefeldin A resistance factor 1 (GBF1) in dengue infection. *Mol Cell Proteomics* 13, 2836–2854.

Chiu, H. C., Hannemann, H., Heesom, K. J., Matthews, D. A. & Davidson, A. D. (2014). High-throughput quantitative proteomic analysis of dengue virus type 2 infected A549 cells. *PLoS One* 9, e93305.

Craig, R., Cortens, J. P. & Beavis, R. C. (2004). Open source system for analyzing, validating, and storing protein identification data. *J Proteome Res* 3, 1234–1242.

Cristea, I. M., Rozjabek, H., Molloy, K. R., Karki, S., White, L. L., Rice, C. M., Rout, M. P., Chait, B. T. & MacDonald, M. R. (2010). Host factors associated with the Sindbis virus RNA-dependent RNA polymerase: role for G3BP1 and G3BP2 in virus replication. *J Virol* 84, 6720–6732.

- Dinkel, H., Michael, S., Weatheritt, R. J., Davey, N. E., Van Roey, K., Altenberg, B., Toedt, G., Uyar, B., Seiler, M. & other authors (2012). ELM—the database of eukaryotic linear motifs. *Nucleic Acids Res* 40 (D1), D242–D251.
- **Dong, H., Zhang, B. & Shi, P. Y. (2008).** Flavivirus methyltransferase: a novel antiviral target. *Antiviral Res* **80**, 1–10.
- Dong, H., Fink, K., Züst, R., Lim, S. P., Qin, C. F. & Shi, P. Y. (2014). Flavivirus RNA methylation. *J Gen Virol* 95, 763–778.
- **Doolittle, J. M. & Gomez, S. M. (2011).** Mapping protein interactions between Dengue virus and its human and insect hosts. *PLoS Negl Trop Dis* **5**. e954
- Duangchinda, T., Dejnirattisai, W., Vasanawathana, S., Limpitikul, W., Tangthawornchaikul, N., Malasit, P., Mongkolsapaya, J. & Screaton, G. (2010). Immunodominant T-cell responses to dengue virus NS3 are associated with DHF. *Proc Natl Acad Sci U S A* 107, 16922–16927.
- Fink, J., Gu, F., Ling, L., Tolfvenstam, T., Olfat, F., Chin, K. C., Aw, P., George, J., Kuznetsov, V. A. & other authors (2007). Host gene expression profiling of dengue virus infection in cell lines and patients. *PLoS Negl Trop Dis* 1, e86.
- Germain, M. A., Chatel-Chaix, L., Gagné, B., Bonneil, É., Thibault, P., Pradezynski, F., de Chassey, B., Meyniel-Schicklin, L., Lotteau, V. & other authors (2014). Elucidating novel hepatitis C virus-host interactions using combined mass spectrometry and functional genomics approaches. *Mol Cell Proteomics* 13, 184–203.
- Hannemann, H., Sung, P. Y., Chiu, H. C., Yousuf, A., Bird, J., Lim, S. P. & Davidson, A. D. (2013). Serotype-specific differences in dengue virus non-structural protein 5 nuclear localization. *J Biol Chem* 288, 22621–22635.
- Heaton, N. S., Perera, R., Berger, K. L., Khadka, S., Lacount, D. J., Kuhn, R. J. & Randall, G. (2010). Dengue virus nonstructural protein 3 redistributes fatty acid synthase to sites of viral replication and increases cellular fatty acid synthesis. *Proc Natl Acad Sci U S A* 107, 17345–17350.
- Higa, L. M., Caruso, M. B., Canellas, F., Soares, M. R., Oliveira-Carvalho, A. L., Chapeaurouge, D. A., Almeida, P. M., Perales, J., Zingali, R. B. & Da Poian, A. T. (2008). Secretome of HepG2 cells infected with dengue virus: implications for pathogenesis. *Biochim Biophys Acta* 1784, 1607–1616.
- **Huang, W., Sherman, B. T. & Lempicki, R. A. (2009a).** Bioinformatics enrichment tools: paths toward the comprehensive functional analysis of large gene lists. *Nucleic Acids Res* **37**, 1–13.
- **Huang, W., Sherman, B. T. & Lempicki, R. A. (2009b).** Systematic and integrative analysis of large gene lists using DAVID bioinformatics resources. *Nat Protoc* **4**, 44–57.
- Jiang, L., Yao, H., Duan, X., Lu, X. & Liu, Y. (2009). Polypyrimidine tract-binding protein influences negative strand RNA synthesis of dengue virus. *Biochem Biophys Res Commun* 385, 187–192.
- Kamkaew, M. & Chimnaronk, S. (2015). Characterization of soluble RNA-dependent RNA polymerase from dengue virus serotype 2: The polyhistidine tag compromises the polymerase activity. *Protein Expr Purif* 112, 43–49.
- Kawamura-Nagaya, K., Ishibashi, K., Huang, Y. P., Miyashita, S. & Ishikawa, M. (2014). Replication protein of tobacco mosaic virus cotranslationally binds the 5' untranslated region of genomic RNA to enable viral replication. *Proc Natl Acad Sci U S A* 111, E1620–E1628.
- Khadka, S., Vangeloff, A. D., Zhang, C., Siddavatam, P., Heaton, N. S., Wang, L., Sengupta, R., Sahasrabudhe, S., Randall, G. & other authors (2011). A physical interaction network of dengue virus and human proteins. *Mol Cell Proteomics* 10, 012187.

- Khromykh, A. A., Sedlak, P. L., Guyatt, K. J., Hall, R. A. & Westaway, E. G. (1999). Efficient trans-complementation of the flavivirus kunjin NS5 protein but not of the NS1 protein requires its coexpression with other components of the viral replicase. *J Virol* 73, 10272–10280.
- Kinney, R. M., Butrapet, S., Chang, G. J., Tsuchiya, K. R., Roehrig, J. T., Bhamarapravati, N. & Gubler, D. J. (1997). Construction of infectious cDNA clones for dengue 2 virus: strain 16681 and its attenuated vaccine derivative, strain PDK-53. *Virology* 230, 300–308.
- Krishnan, M. N. & Garcia-Blanco, M. A. (2014). Targeting host factors to treat West Nile and dengue viral infections. *Viruses* 6, 683–708.
- Le Breton, M., Meyniel-Schicklin, L., Deloire, A., Coutard, B., Canard, B., de Lamballerie, X., Andre, P., Rabourdin-Combe, C., Lotteau, V. & Davoust, N. (2011). Flavivirus NS3 and NS5 proteins interaction network: a high-throughput yeast two-hybrid screen. *BMC Microbiol* 11, 234.
- **Leardkamolkarn, V., Sirigulpanit, W., Chotiwan, N., Kumkate, S. & Huang, C. Y. (2012).** Development of Dengue type-2 virus replicons expressing GFP reporter gene in study of viral RNA replication. *Virus Res* **163**, 552–562.
- Li, P., Bai, X., Cao, Y., Han, C., Lu, Z., Sun, P., Yin, H. & Liu, Z. (2012). Expression and stability of foreign epitopes introduced into 3A nonstructural protein of foot-and-mouth disease virus. *PLoS One* 7, e41486.
- **Liew, K. J. & Chow, V. T. (2006).** Microarray and real-time RT-PCR analyses of a novel set of differentially expressed human genes in ECV304 endothelial-like cells infected with dengue virus type 2. *J Virol Methods* **131**, 47–57.
- Liu, W. J., Sedlak, P. L., Kondratieva, N. & Khromykh, A. A. (2002). Complementation analysis of the flavivirus Kunjin NS3 and NS5 proteins defines the minimal regions essential for formation of a replication complex and shows a requirement of NS3 in cis for virus assembly. *J Virol* 76, 10766–10775.
- MacLean, B., Tomazela, D. M., Shulman, N., Chambers, M., Finney, G. L., Frewen, B., Kern, R., Tabb, D. L., Liebler, D. C. & MacCoss, M. J. (2010). Skyline: an open source document editor for creating and analyzing targeted proteomics experiments. *Bioinformatics* 26, 966–968.
- Mairiang, D., Zhang, H., Sodja, A., Murali, T., Suriyaphol, P., Malasit, P., Limjindaporn, T. & Finley, R. L. Jr. (2013). Identification of new protein interactions between dengue fever virus and its hosts, human and mosquito. *PLoS One* 8, e53535.
- Pando-Robles, V., Oses-Prieto, J. A., Rodríguez-Gandarilla, M., Meneses-Romero, E., Burlingame, A. L. & Batista, C. V. (2014). Quantitative proteomic analysis of Huh-7 cells infected with Dengue virus by label-free LC-MS. *J Proteomics* 111, 16–29.
- Póvoa, T. F., Alves, A. M., Oliveira, C. A., Nuovo, G. J., Chagas, V. L. & Paes, M. V. (2014). The pathology of severe dengue in multiple organs of human fatal cases: histopathology, ultrastructure and virus replication. *PLoS One* 9, e83386.
- Rigaut, G., Shevchenko, A., Rutz, B., Wilm, M., Mann, M. & Séraphin, B. (1999). A generic protein purification method for protein complex characterization and proteome exploration. *Nat Biotechnol* 17, 1030–1032.
- Sabourin, M., Tuzon, C. T., Fisher, T. S. & Zakian, V. A. (2007). A flexible protein linker improves the function of epitope-tagged proteins in *Saccharomyces cerevisiae*. Yeast 24, 39–45.
- Schoggins, J. W., Dorner, M., Feulner, M., Imanaka, N., Murphy, M. Y., Ploss, A. & Rice, C. M. (2012). Dengue reporter viruses reveal viral dynamics in interferon receptor-deficient mice and sensitivity to interferon effectors in vitro. *Proc Natl Acad Sci U S A* 109, 14610–14615.

- Szklarczyk, D., Franceschini, A., Wyder, S., Forslund, K., Heller, D., Huerta-Cepas, J., Simonovic, M., Roth, A., Santos, A. & other authors (2015). STRING v10: protein-protein interaction networks, integrated over the tree of life. *Nucleic Acids Res* 43 (D1), D447–D452.
- Teterina, N. L., Lauber, C., Jensen, K. S., Levenson, E. A., Gorbalenya, A. E. & Ehrenfeld, E. (2011). Identification of tolerated insertion sites in poliovirus non-structural proteins. *Virology* 409, 1–11
- Thompson, J. D., Higgins, D. G. & Gibson, T. J. (1994). CLUSTAL W: improving the sensitivity of progressive multiple sequence alignment through sequence weighting, position-specific gap penalties and weight matrix choice. *Nucleic Acids Res* 22, 4673–4680.
- **Uchil, P. D., Kumar, A. V. & Satchidanandam, V. (2006).** Nuclear localization of flavivirus RNA synthesis in infected cells. *J Virol* **80**, 5451–5464.
- Usme-Ciro, J. A., Lopera, J. A., Enjuanes, L., Almazán, F. & Gallego-Gomez, J. C. (2014). Development of a novel DNA-launched dengue virus type 2 infectious clone assembled in a bacterial artificial chromosome. *Virus Res* 180, 12–22.

- Vandergaast, R., Hoover, L. I., Zheng, K. & Fredericksen, B. L. (2014). Generation of West Nile virus infectious clones containing amino acid insertions between capsid and capsid anchor. *Viruses* 6, 1637–1653.
- Wang, M., Herrmann, C. J., Simonovic, M., Szklarczyk, D. & von Mering, C. (2015). Version 4.0 of PaxDb: protein abundance data, integrated across model organisms, tissues, and cell-lines. *Proteomics* 15, 3163–3168.
- Welsch, S., Miller, S., Romero-Brey, I., Merz, A., Bleck, C. K., Walther, P., Fuller, S. D., Antony, C., Krijnse-Locker, J. & Bartenschlager, R. (2009). Composition and three-dimensional architecture of the dengue virus replication and assembly sites. *Cell Host Microbe* 5, 365–375.
- **WHO (2009).** Dengue: Guidelines for Diagnosis, Treatment, Prevention and Control: New Edition. Geneva: World Health Organization.
- Xu, S., Pei, R., Guo, M., Han, Q., Lai, J., Wang, Y., Wu, C., Zhou, Y., Lu, M. & Chen, X. (2012). Cytosolic phospholipase A2 gamma is involved in hepatitis C virus replication and assembly. *J Virol* 86, 13025–13037.
- Zou, G., Xu, H. Y., Qing, M., Wang, Q. Y. & Shi, P. Y. (2011). Development and characterization of a stable luciferase dengue virus for high-throughput screening. *Antiviral Res* 91, 11–19.

RESEARCH Open Access



# Inhibition of protein kinase C promotes dengue virus replication

Warobon Noppakunmongkolchai<sup>1†</sup>, Teera Poyomtip<sup>2†</sup>, Thichakorn Jittawuttipoka<sup>2</sup>, Natthanej Luplertlop<sup>3</sup>, Anavai Sakuntabhai<sup>4,5,7</sup>, Sarin Chimnaronk<sup>6,7</sup>, Siwanon Jirawatnotai<sup>7,8\*</sup> and Rutaiwan Tohtong<sup>1\*</sup>

### Abstract

**Background:** Dengue virus (DENV) is a member of the *Flaviviridae* family, transmitted to human *via* mosquito. DENV infection is common in tropical areas and occasionally causes life-threatening symptoms. DENV contains a relatively short positive-stranded RNA genome, which encodes ten viral proteins. Thus, the viral life cycle is necessarily rely on or regulated by host factors.

**Methods:** *In silico* analyses in conjunction with *in vitro* kinase assay were used to study kinases that potentially phosphorylate DENV NS5. Potential kinase was inhibited or activated by a specific inhibitor (or siRNA), or an activator. Results of the inhibition and activation on viral entry/replication and host cell survival were examined.

**Results:** Our *in silico* analyses indicated that the non-structural protein 5 (NS5), especially the RNA-dependent RNA polymerase (RdRp) domain, contains conserved phosphorylation sites for protein kinase C (PKC). Phosphorylation of NS5 RdRp was further verified by PKC *in vitro* kinase assay. Inhibitions of PKC by a PKC-specific chemical inhibitor or siRNA suppressed NS5 phosphorylation *in vivo*, increased viral replication and reduced viability of the DENV-infected cells. In contrary, activation of PKC effectively suppressed intracellular viral number.

**Conclusions:** These results indicated that PKC may act as a restricting mechanism that modulates the DENV replication and represses the viral outburst in the host cells.

**Keywords:** Dengue virus (DENV), Protein kinase C (PKC), Phosphorylation, Non-structural protein 5 (NS5), Viral replication, Flavivirus

#### **Background**

DENV infection is among major life-threatening infectious diseases in tropical countries. A fraction of infected human will develop severe life-threatening symptoms, which are recognized as dengue hemorrhagic fever (DHF). This composes of bleeding, low levels of blood platelets and blood plasma leakage. It can develop into dengue shock syndrome (DSS), where dangerously low blood pressure occurs. These are normally followed by mortality, since there is no specific management for it, except the symptomatic treatments. Currently, there is

no effective vaccine that can prevent the infection. Therefore, information on the pathogenesis and the biology of the virus is required to build novel strategies to reduce the death rate caused by this virus.

DENV is a relatively simple virus. Its genome encodes 10 viral proteins, including 3 structural proteins; envelope (E), capsid, prM, and 7 non-structural (NS) proteins; NS1, NS2A, NS2B, NS3, NS4A, NS4B, and NS5. To reproduce in the host cells, DENV requires host's components to propagate [1–4]. Thus, virus-host interaction is one of the major processes that influence viral life cycle, and is being extensively investigated.

Accumulating evidences have shown that many viral proteins interact with host proteins. Viral proteins, such as NS1, NS4A, NS5, E, and capsid, were demonstrated by yeast two-hybrid or by co-immunoprecipitation coupled with Mass spectrometry to physically associate with host proteins [5–7]. Many of these interactions were proven to

Full list of author information is available at the end of the article



<sup>\*</sup> Correspondence: siwanon.jir@mahidol.ac.th; rutaiwan.toh@mahidol.ac.th  $^\dagger \text{Equal contributors}$ 

<sup>&</sup>lt;sup>7</sup>Systems Biology of Diseases Research Unit, Faculty of Science, Mahidol University, Bangkok, Thailand

<sup>&</sup>lt;sup>1</sup>Department of Biochemistry, Faculty of Sciences, Mahidol University, Bangkok, Thailand

be physiologically relevant [6, 8, 9]. Functional interactions, such as phosphorylation and methylation, are also subjected for examinations. Recent evidences indicated that host proteins functionally interact with, and regulate the viral proteins, and *vice versa* [10–13].

NS5s from various flaviviruses have long been distinctively characterized as a phosphoprotein which contains several possible phosphorylation sites [14], suggesting a significance of this phospho regulation for the viruses. The protein is composed of 2 functional domains, namely the N-terminal methyltransferase, which catalyzes guanine N-7 and ribose 2'-OH methylations of the 5' terminal cap 1 structure (m7GpppAmG) during viral cap formation [15], and the C-terminal RNA-dependent RNA polymerase (RdRp), which is an enzyme that synthesizes viral RNAs during viral replication [16].

Identification of kinases that responsible for the phosphorylation has been a topic of interest. Recent reports showed that NS5 is phosphorylated by Casein Kinase I (CK I) or protein kinase G (PKG) at the methyltransferase domain [10, 17]. The phosphorylations appeared to be essential for the normal function of NS5, since blocking the phosphorylation either by chemical inhibitor or amino acid substitution of the potential phosphorylation site suppressed viral replication and viral production [17]. These findings also suggested that NS5 is a central protein, which mediates functional interactions between host and virus proteins. Detailed study of NS5 phosphorylation may provide a better understanding of the viral life cycle, and may lead to intervention approaches that are based on viral-host interaction. In this study, we performed in silico analyses to identify human kinases that potentially regulate DENV2 NS5. We identified that there were several possible PKC phosphorylation sites on the NS5. We then also studied the physiological relevance of the phosphorylations for the virus and host cells.

#### **Results**

# NS5 contains possible protein kinase C phosphorylation sites

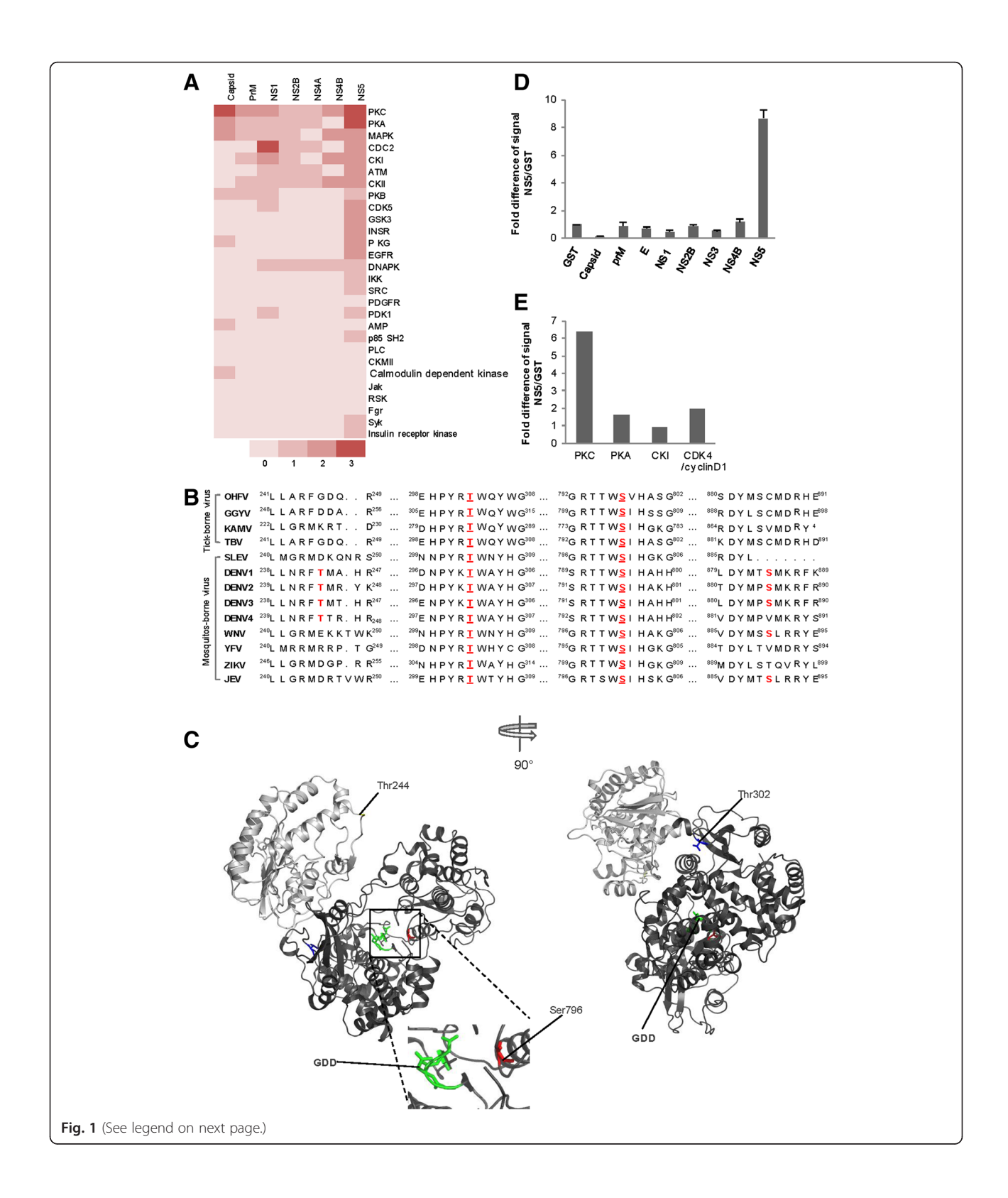
To investigate possible amino acids on NS5 that might be phosphorylated by human kinases, we analyzed amino acid sequence of dengue serotype 2 (DENV2) NS5 by three phospho-algorithms; Scansite™ [18], NetPhosK 2.0 [19], and KinasePhos 2.0 [20]. In accordance with the previous notion describing NS5 as phosphoprotein, the analyses revealed many potential candidate phosphorylation sites on NS5 for several kinases, when compared to other DENV proteins (Fig. 1a). Protein kinases predicted to phosphorylate NS5 by at least one algorithm included PKC, PKA, CDKs (CDCs), MAPK, ATM, CK II, PKB, and others (Fig. 1a). Our analyses also identified 2 kinases that were previously reported to phosphorylate NS5, i.e. Casein Kinase I (CK I), and protein

kinase G (PKG) [10, 17, 21]. Among the candidates, we focused on possible functional interaction between NS5 and PKC (predicted by all 3 algorithms). We found that 4 potential phosphorylation sites, in particular Thr244, Thr302, Ser796, and Ser885, were recognized by at least 2 predicting algorithms on DENV2 NS5. Among the 4 candidates, Thr302 and Ser796 are conserved in all vector-borne flaviviruses (Fig. 1b). Thr244, and Ser885 were not in the other mosquito-borne or tick-borne viruses, but were rather limited within the DENVs (Fig. 1b). While Thr244 resides in the methyltransferase domain of NS5, Thr302 Ser796 and Ser885 reside in the RdRp domain of NS5. These 4 candidate sites are exposed to solvent, thus, are potentially be phosphorylated (Fig. 1b, c).

Since RdRp domain contains several of the possible phosphorylation sites for PKC, we set up a PKC in vitro kinase assay using purified recombinant DENV2 RdRp domain, containing Thr302 Ser796 and Ser885, as a substrate. The kinase assay showed that PKC efficiently phosphorylated RdRp in vitro. The signal was approximately 9 folds higher than that of GST (used as nonrelevant control). Under these conditions, PKC kinase assay gave a very low signals for the other DENV proteins, such as capsid, prM, E, NS1, NS2B, NS3, NS4B (Fig. 1d). Interestingly, protein kinase C appeared to produce relatively high phosphorylation signal compared with the other potential NS5 kinases, namely PKA, CK I, and CDK4/cyclinD1 (Fig. 1e). Thus, PKC can efficiently phosphorylated the NS5 RdRp domain in vitro. Of note, although the methyltransferase domain contains only one possible PKC phosphorylation site, Thr244, which is not conserved in all of the vectorborne flaviviruses, it is entirely possible that this site may be phosphorylated by PKC. We have yet to test this possibility.

# Silencing of PKC $\alpha$ reduced Ser and Thr phosphorylation of NS5 in vivo

To investigate the functional interaction between host PKC and DENV NS5 *in vivo*, we depleted PKCα using PKCα-specific siRNAs and examined the level of NS5 phosphorylation *in vivo*. We first, tested the efficiency of siRNA-mediated PKC depletion. We found that at 24, 48, and 72 h after PKC-specific siRNA transfection, more than 70 % of the endogenous PKC levels were downregulated (Fig. 2a), while host cell viability was unaffected (data not shown). We selected to examine NS5 phosphorylation at the 24 h after siRNA transfection. We expressed His-FLAG-tagged NS5 in host cells by infecting the cells with recombinant DENV expressing the His-FLAG-NS5 protein (etDENV), then pulled down the NS5 using anti-FLAG antibody. The phosphorylation on the His-FLAG-NS5 was analyzed by anti phospho-



(See figure on previous page.)

Fig. 1 In silico analyses revealed possible protein kinase C phosphorylation sites on dengue NS5. a Prediction of possible NS5 kinases. A heat map showed possible human kinases that phosphorylate DENV2 NS5 based on in silico predictions by Scansite™, NetPhosK 2.0, and KinasePhos 2.0 (upper panel). Names of possible kinases were listed vertically on the right of the panel. DENV2 proteins were listed horizontally on the top. Color codes (lower panel) indicated numbers of hit from the predicting algorithms; from 0 (very light red) to 3 (dark red). b Sequence conservation of the predicted PKC phosphorylation sites across flaviviruses. Partial amino acid sequences of flaviviruses were listed as indicated by name; Omsk hemorrhagic fever virus (OHFV), Gadgets Gully virus (GGYV), Kama virus (KAMV), and tick-borne encephalitis virus (TBV), St. Louis encephalitis virus (SLEV), dengue 1–4 (DENV1–4), West Nile virus (WNV), yellow fever virus (YFV), Zika virus (ZIKA), Japanese Encephalitis virus (JEV). Predicted PKC phosphorylation sites were showed in RED. In addition, Thr302, and Ser796 that were conserved were underlined. c Three-dimension models of DENV2 NS5 protein. Colored in light gray is the methyltransferase domain, dark gray is the RNA-dependent RNA polymerase (RdRp) domain. Highlighted in yellow, red, and blue are possible PKC phosphorylation sites; Thr244, Ser796, andThr302, respectively. Highlighted in fluorescent green is the GDD RNA polymerase active site. d PKC in vitro kinase assays. Purified DENV2 proteins were used as substrate. Purified GST was used as a non-relevant control for the reaction. Bars represented means of 3 independent experiments, error bars; S.D. e In vitro kinase assays, several human kinases were tested including PKC, PKA, CKI, and CDK4/cyclin D1, as indicated. The signal was normalized by the signal from reactions with GST. Bars represented data from a representative experiment

Ser and phospho-Thr immunoblottings. We found that under this condition, silencing of the PKC clearly decreased Serine and Threonine phosphorylations of NS5 (Fig. 2b, c).

# Inhibition of PKC by Bisl reduced Ser and Thr phosphorylation of NS5 in vivo

To confirm the effect of PKC depletion on NS5 phosphorylation, we inhibited PKC activity of host cells using bisindolylmaleimide I (BisI), a specific chemical inhibitor of conventional and novel PKCs. We found that various concentrations of BisI, (up to 1  $\mu M$  of BisI) were not toxic to the cells for at least up to 72 h (Fig. 3a). As early as 24 h after treatment, 0.1 and 1  $\mu M$  of BisI clearly suppressed the activity of PKC, as indicated by a complete loss of the phosphorylation of PEA15, an established PKC substrate (Fig. 3b, c). Importantly, FLAG immunoprecipitation of the tagged-NS5 followed by phospho-Ser or phospho-Thr immunoblotings showed that Serine and Threonine phosphorylations were decreased, when the cells were treated with non-toxic dose (1  $\mu M$ ) of BisI (Fig. 3d, e).

# PKC blockage enhanced DENV viral replication, but not viral entry into host cells

To examine the biological effects of PKC blockage on the viral replication, we quantitated the viral copy number in the host cells pre-treated with BisI using RT-qPCR. BisI, which blocked the PKC activities, significantly increased the viral copy of DENV2 strain 16681 in human hepatocellular carcinoma HepG2 cells, with the highest copy number of the virus attained by the 0.1 and 1  $\mu$ M BisI treatments (Fig. 4a). On the contrary, we detected a very lowering of dengue virus copy number in HepG2 cells pretreated with 0.1 nM of a PKC activator Phorbol 12-myristate 13-acetate (PMA) (Fig. 4b). We found that, at this dose of PMA, activity of PCK was induced indicated by an upregulation of phospho-PEA15 (Fig. 4c).

To further investigate whether the PKC inhibitor altered DENV entry into the host cells, we assessed the viral copy number in the cells at early time points, i.e. at 2, 5 and 8 h after viral infection. During these time points, the viral replication was not yet fully operated. Therefore, the viral copy number would represent the number of virus entering the host cells after the infections [22]. We found that the amounts of virus in BisItreated cells were comparable to those in the vehicle-treated cells, during these early time points (Fig. 4d). Therefore, it is likely that the activity of PKC was not involved with DENV entry into the host cells, and inhibition of PKC activity does not interfere with this process.

In contrast to the results from early time points, viral copy numbers at the later time points were augmented by at least 10 folds (after 12 h of BisI-treatment), when compared to that of the vehicle-treated cells. The viral copy numbers continued to be higher at every time point examined until 72 h post infection (Fig. 4e).

These results indicated that inhibition of the PKC activity promotes viral replication, showing in an increase of the viral copy number, whereas stimulation of the PKC activity may be involved in suppression of the DENV replication in the host cells.

Promotion of the viral replication by PKC blockage was also confirmed using siRNA-mediated silencing of PKC $\alpha$ . This also resulted in a significant increase of dengue viral copy number and the amounts of viral NS5 and NS3 proteins in host cells (Fig. 5a, b). Although not statistically significant, we detected an increase of secreted virus into the culture medium of BisI-treated cells as well (Fig. 5c).

#### Inhibition of PKC reduced host cell viability

The above data showed that depletion of PKC significantly enhanced the dengue viral replication in the host cells. To further assess whether PKC depletion also had an effect on the host cells, we monitored growth of the infected HepG2 cells in the presence or absence of PKC

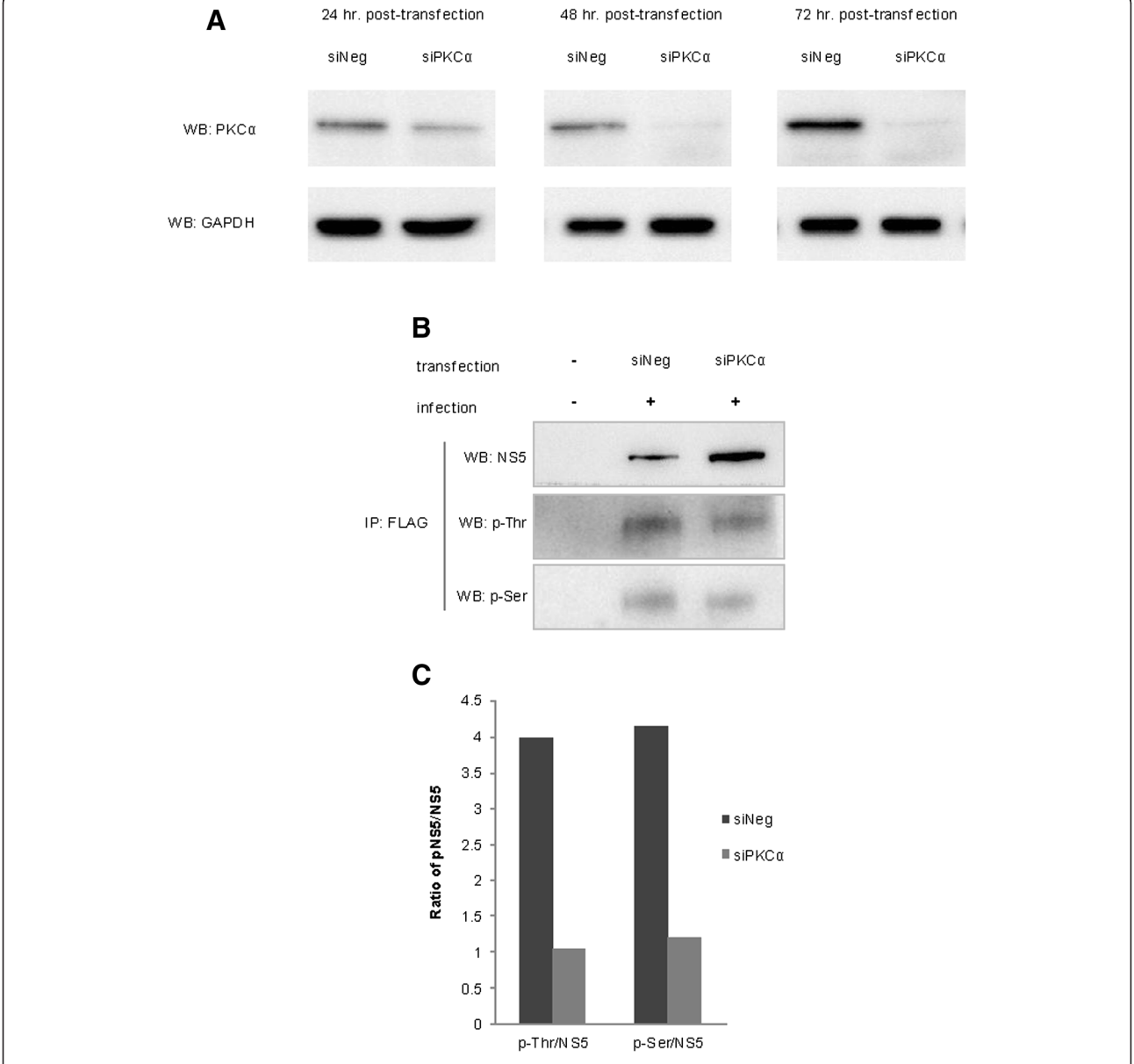
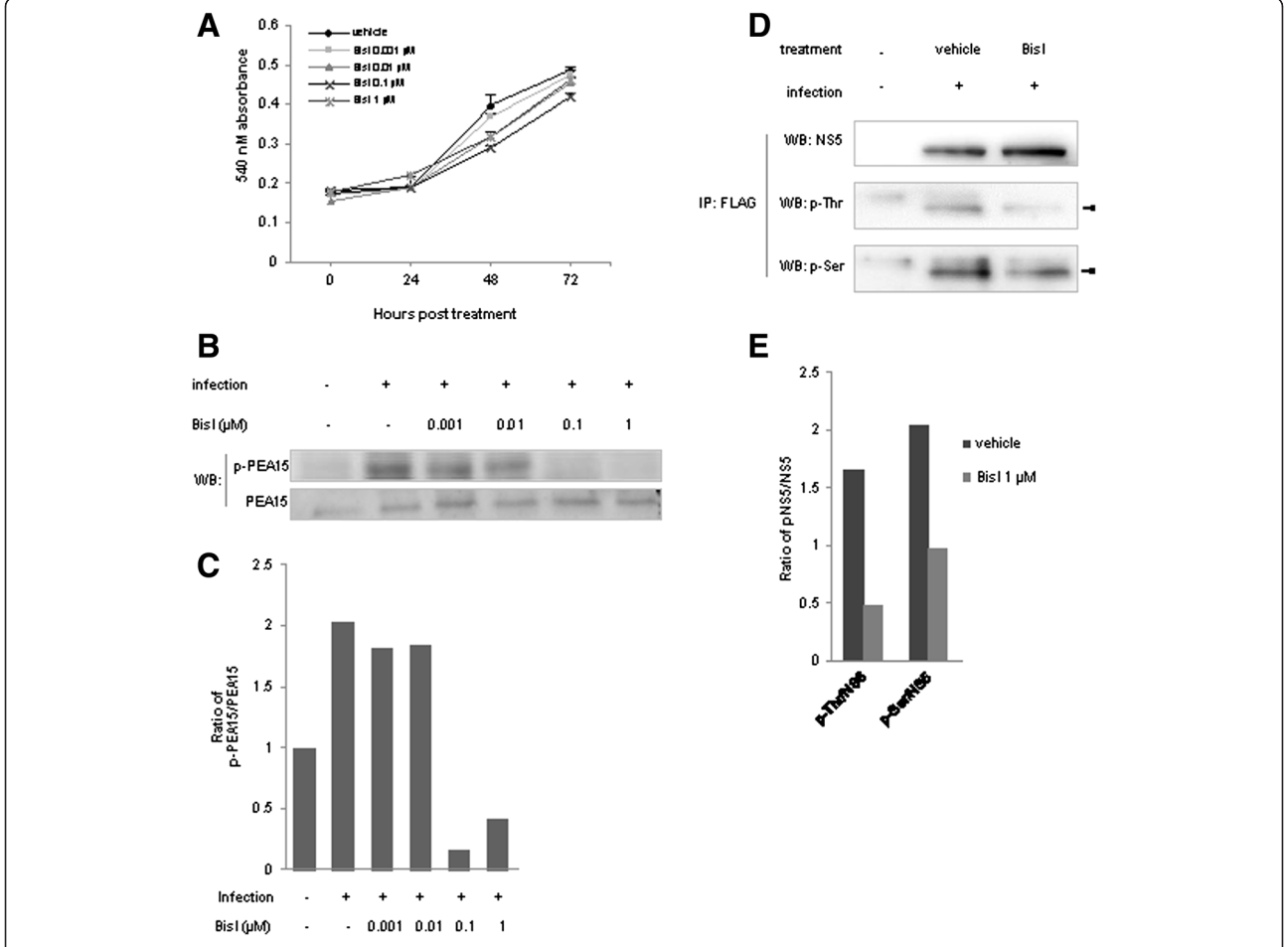


Fig. 2 Inhibitions of PKC by PKCα siRNA or a chemical inhibitor (Bisl) suppressed NS5 RdRp phosphorylations. a PKCα-specific siRNA depleted endogenous PKCα at 24, 48, 72 h after siRNA transfection. A pool of PKCα siRNAs (siPKCα) was transfected into the BHK-21 cells. The levels of PKCα were detected by PKCα immunoblotting. A non-targeting siRNA (siNeg) was used as a control. GAPDH immunoblots were used as a loading control. b PKCα depletion by siRNA downregulated NS5 Threonine and Serine phosphorylations. BHK-21 cells were infected with recombinant DENV expressing His-FLAG-tagged NS5. The His-FLAG-tagged NS5 was pulled down (IP) from BHK-21 cell lysate by anti-FLAG antibody, and Threonine/Serine phosphorylations (p-Thr/p-Ser) were examined by p-Thr or p-Ser-specific antibodies. c Quantifications of p-Thr/NS5 and p-Ser/NS5 from (b)

depletion. To this end, HepG2 cells, which either pretreated with non-targeting (control) siRNA or PKC-specific siRNA, were infected with DENV2 16681. We found that, viability of the non-targeting siRNA-treated control cells without viral infection consistently increased over 3 days (Fig. 5d, dashed black line). Infection of dengue virus, or PKC siRNA transfection alone, significantly reduced HepG2 cell viability by 72 h after the

PKC knockdown (Fig. 5d, dashed red line and solid black line, respectively). Importantly, depletion of PKC by siRNA together with DENV-infection accelerated suppression of HepG2 cell viability to 48 h after transfection. The loss of host cells became more clearly evident at the 72 h time point (Fig. 5d, solid red line). Inhibition of PKC by BisI also caused a marked reduction of host cell viability at 48 h after DENV infection (Fig. 5e).



**Fig. 3** Inhibition of PKC by Bisl. **a** Inhibition of PKC by Bisl did not alter host cell growth. HepG2 cells were treated with various concentrations of Bisl. Average cell viability from right after the treatment (0 h), 24, 48, and 72 h was monitored by MTT assays. Error bars represented S.D. from 3 independent experiments. **b** Bisl effectively inhibited PKC activity. Phosphorylation of PEA15, a known substrate of PKC. Levels of phospho-PEA15 at 24 h after Bisl treatment were examined by immunoblotting using a phospho-PEA15 (p-PEA15) specific antibody. Concentrations of Bisl used were indicated. PEA15 immunoblot was used to examine the total amount of PEA15. **c** Quantification of p-PEA15 from **b** Amounts of p-PEA15 were normalized by total PEA15. **d** PKC inhibition by 1 μM of Bisl downregulated NS5 Threonine and Serine phosphorylations. BHK-21 cells were infected with recombinant DENV expressing His-FLAG-NS5, and tagged protein was then pulled down by anti-FLAG antibody. The p-Thr and p-Ser were examined by immunobloting as in Fig. 2b. Arrow heads indicated specific p-Thr or p-Ser signals. **e** Quantifications of p-Thr/NS5 and p-Ser/NS5 from (**d**)

Altogether, these data indicated that inhibition of PKC led to an enhancement of the DENV growth and suppression of host cell viability.

#### Discussion

Significance of the interaction between virus and host cells have been established, especially that of positive-strand RNA viruses, such as the DENV and the host cells. The simplicity of the viruses, and limited number of viral proteins have made the host factors indispensable for the virus. Physical interactions between host proteins and several viral proteins have been widely studied. Yeast-two-hybrid and immunoaffinity-purification/Mass spectrometry experiments revealed

extensive physical networks of viral-host interactomes [23]. Biochemical reactions between biomolecule are often transient, and sometimes fastidiously hard to detect. Hence, there are fewer numbers of report describing functional interactions among the host-viral proteins. However, functional interactions are of importance, since all of them are virtually regulative and physiologically meaningful for the co-existing of the virus and the host cell.

In this study, we used an *in silico* screening approach, which relied on three different phospho-scanning tools, to search for novel phosphor regulatory sites on DENV NS5 protein. None of the screening tools to these days can accurately predict phosphorylation for all kinases.

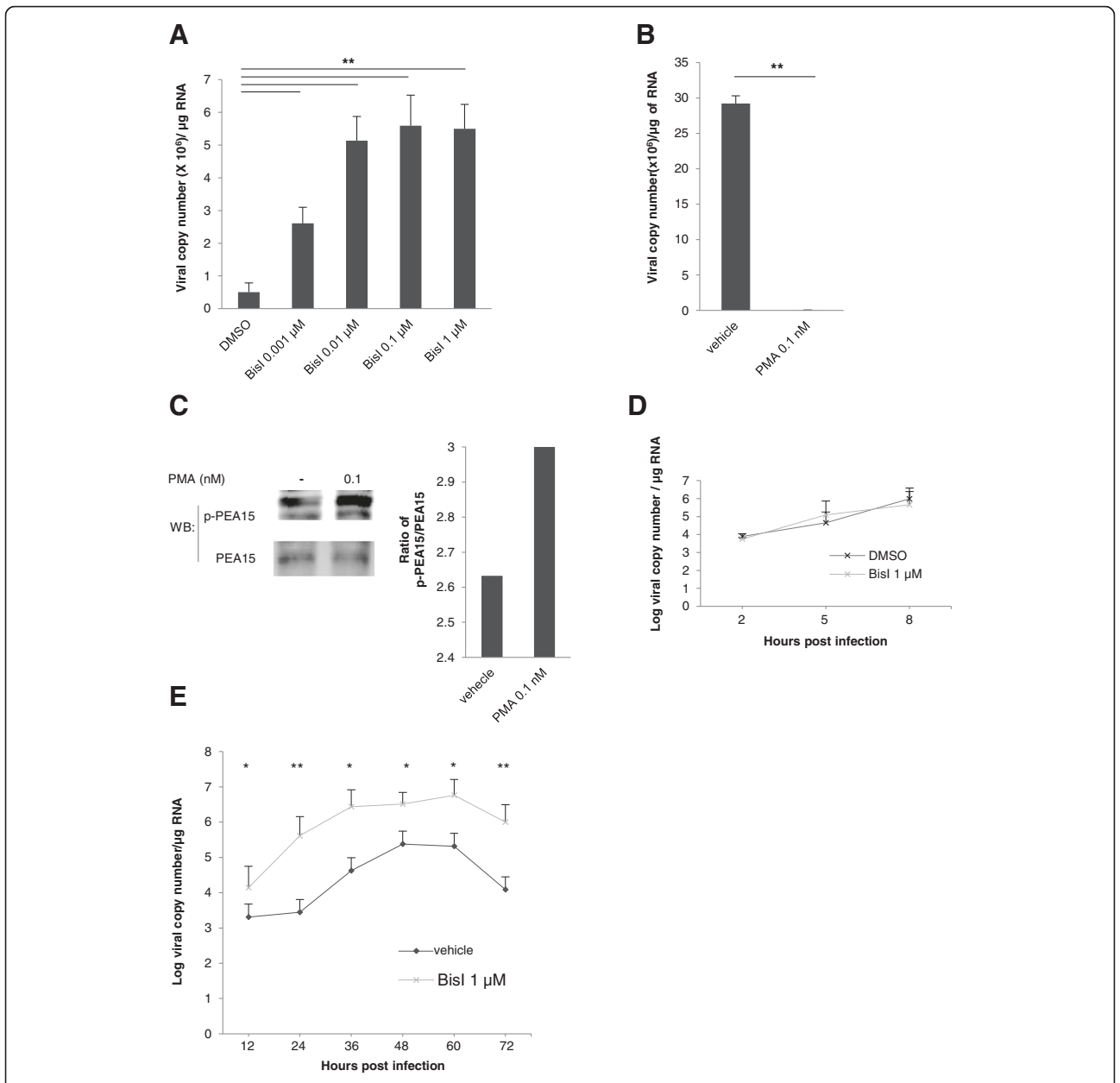


**Fig. 4** PKC activity restricted DENV viral number in host cells. **a** Viral copy numbers in HepG2 cells treated with various Bisl concentrations. Cells were treated with various concentrations of Bisl for 30 min, prior to a 1.5-h infection by DENV strain 16681. Cells were kept in medium with Bisl for a total of 24 h, before harvesting. Viral copy numbers were quantified by quantitative PCR. Bars represent means viral copy number from 3 independent experiments. Error bars represent S.D., \*\*\*; p-value ≤ 0.01. Concentrations of Bisl used were not toxic to the host cells. **b** Reduction of DENV copy number in host cells by PKC activator. HepG2 cells were treated with 0.1 nM of a PKC activator PMA or vehicle for 30 min, prior to a 2-h infection by DENV strain 16681 (MOI of 5). Cells were then kept in the activator (or vehicle) for 24 h before harvesting to quantify the viral copy numbers. Bars represent means of 3 independent experiments. Error bars represent S.D., \*\*\*; p-value ≤ 0.01. **c** PMA promoted PKC activity. Levels of total PEA15 and phospho-PEA15 at 24 h after PMA treatment were examined using immunoblotting (left panel). Ratios of the signals p-PEA15/PEA15 from the immunoblots were shown on the right. **d** Bisl had no effect on entering of virus in to the host cells (HepG2). Average viral copy numbers at the early time points after viral infection, 2, 5, 8 h. Viral infection and Bisl treatment was performed as indicated in **a** Three independent experiments were performed. Error bars represent S.D. **e** DENV copy numbers in HepG2 cells during indicated time pointed were represented as mean of 3 independent experiments. Error bars represent S.D., \*; p-value ≤ 0.05, \*\*; p-value ≤ 0.01. Bisl treatment and viral infection was performed as indicated in (**a**)

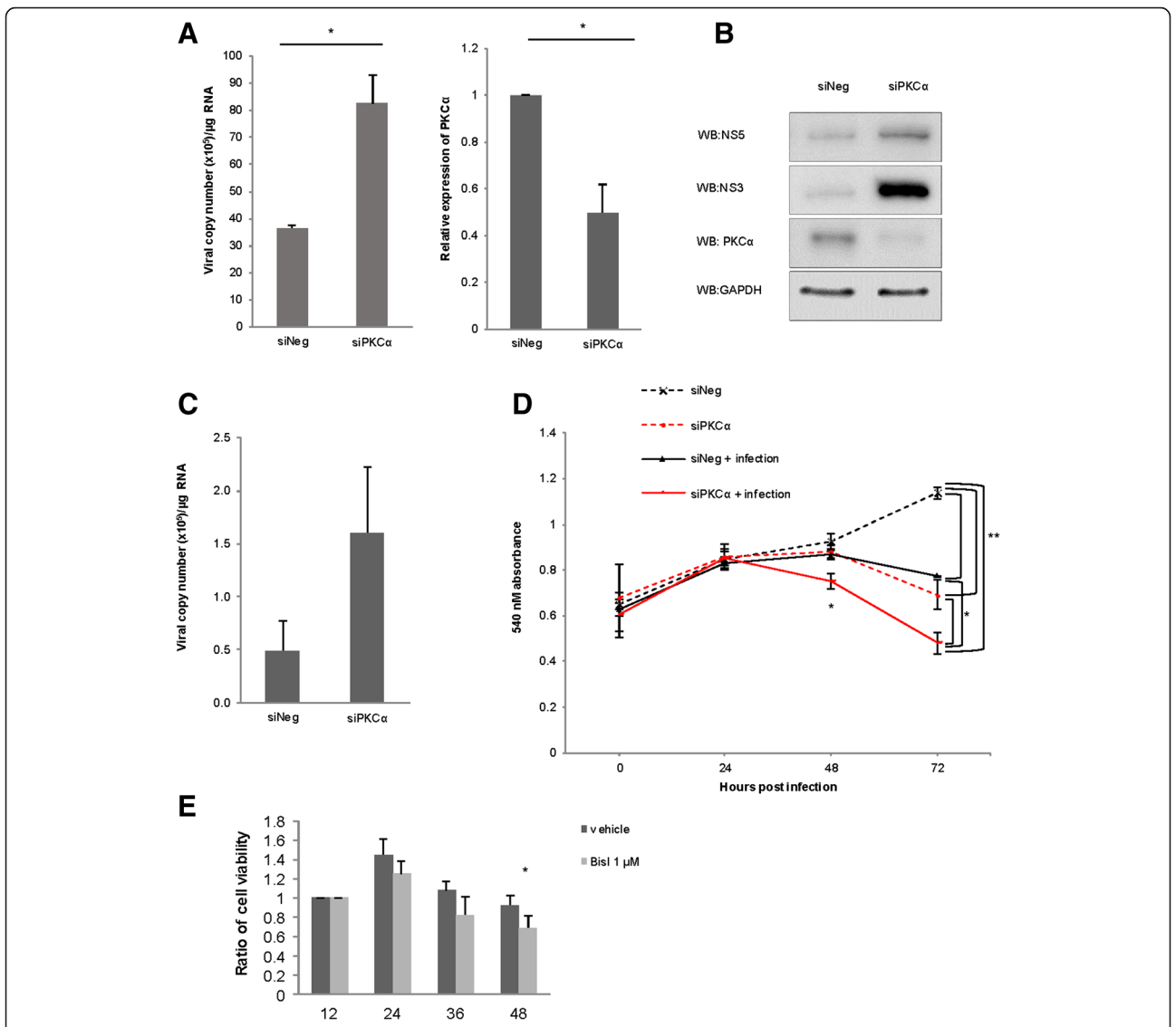


Fig. 5 Depletion of PKC increased viral-induced host cell damage. a siRNA-mediated depletion of PKCα resulted in increased intracellular DENV copy number. HepG2 cells were transfected with PKCα-specific siRNA (siPKCα) or non-targeting siRNA (siNeg) for 24 h prior to a 2-h infection of DENV strain 16681. After 24 h, cells were harvested. PKCα mRNA and DENV viral copy numbers were quantified by quantitative PCR. Left; bars represent viral copy numbers in the host cells treated with siRNA indicated. Right; bars represent means expressions of PKCα mRNA from 3 independent experiments. Error bars represent S.D., \*; p-value ≤ 0.05. b Expressions of PKCα, DENV NS3, and NS5 were examined by immunoblots using indicated antibodies. GAPDH immunoblot was used as loading control. c Average DENV viral copy numbers in culture mediums from PKCα-depleted HepG2 cells (siPKCα), compared to control cells (siNeg). Bars represent means of 3 independent experiments. Error bars represent S.D. The viral copy numbers were determined by RT-qPCR. d Depletion of PKCα decreased the viability of DENV-infected cells. HepG2 cells were treated as indicated. The 24 h post transfection, cells were infected with DENV. Cell viabilities were examined using MTT assay. Graphs showed average of 3 independent experiments. Error bars represent S.D. \*; p-value ≤ 0.05, \*\*; p-value ≤ 0.01. e Inhibition of PKC by Bisl decreased viability of DENV-infected cells. HepG2 cells were treated with 1 μM Bisl for 30 min, prior to a 2-h infection by DENV strain 16681. Cell viabilities were determined by tryptan blue staining at indicated time points. Bars represent means of 3 independent experiments. Error bars represent S.D., \*; p-value ≤ 0.05

This is because many kinases do not have a clear consensus site. Thus, we incorporated results from all of the tools, hoping to identify the most possible phosphosites on the DENV proteins. From our *in silico* analyses, we found that despites NS5, capsid was also predicted

as a potential substrate for PKC (Fig. 1a). However, in a subsequent experiment, capsid was shown to be a poor PKC substrate in the *in vitro* kinase assay. This implicated that a verification of the *in silico* prediction is indispensable.

Flaviviral NS5 was shown to be a phosphoprotein and is regulated by human kinases [11, 17]. Phosphorylation by host factors in many cases are required for normal function of NS5 proteins, for example phosphorylation of NS5 was shown to involve with NS3-NS5 complex formation [12]. PKG-NS5 interaction is required for viral replication [17, 21]. This interaction was shown to be involved with the NS5 methyltransferase domain. CK I was also shown to phosphorylate the same domain on NS5 and regulate methyltransferase function, hence the production of virus in the host cells [10].

On the other hand, some NS5 phosphorylations have been shown to inhibit the function of NS5. Previous report has shown that the NS5 methyltransferase function of Yellow fever virus (YFV) was suppressed by phosphorylation [24].

In addition, the RdRp domain on NS5 was predicted to be phosphorylated by CK II on residues distinct from those phosphorylated by PKC. The CK II phosphorylation site was located in the 37-amino-acid linker interdomain of NS5 (residues 369 to 405), which contains the nuclear localization signal (NLS). Phosphorylation at this site has been shown to inhibit of NS5 nuclear targeting, resulting in retention of the RdRp in the cytoplasm [11].

Here, we showed that phosphorylation in the NS5 by PKC is inhibitory and is physiologically relevant. Inhibition of this phosphorylation reaction resulted in a significant increase of viral number and reduction of host cell viability. Conversely, activation of PKC by PMA suppressed intracellular DENV production. Thus, it is possible that PKC might represent an intracellular restricting mechanism that prevents viral outburst in the host cells. In accordance with our result, a recent report showed that a siRNA screening identified PIKC1, an protein kinase  $C\alpha$ -interacting protein as a host factor that restricting DENV virus [25].

In this study, we have shown by in vitro kinase assay that the RdRp domain within NS5 was a substrate for PKC. This domain contains three PCK phosphorylation sites (Thr302, Ser796, and Ser885). We hypothesized that some of the PKC phosphorylation sites might be regulatory site for RdRp's function. For example, Ser796, is located near the active site of the RNA polymerase (GDD site) (Fig. 1c) [26]. Thus, hyperphosphorylation of these sites by PCK may interfere with the RNA polymerase function of NS5 RdRp, leading to suppression of DENV replication (Fig. 6). However, further experiments are required to validate the model. Of note, PKC has been shown to be involved with cellular apoptosis. In most contexts, such as in melanoma cell lines [27], bladder carcinoma cell lines [28], glioma cells [29], and salivary gland epithelial cells [30], PKC especially PKCα appeared to inhibit apoptosis (except, in the LNCaP prostrate cells in which expression of PKCα promotes

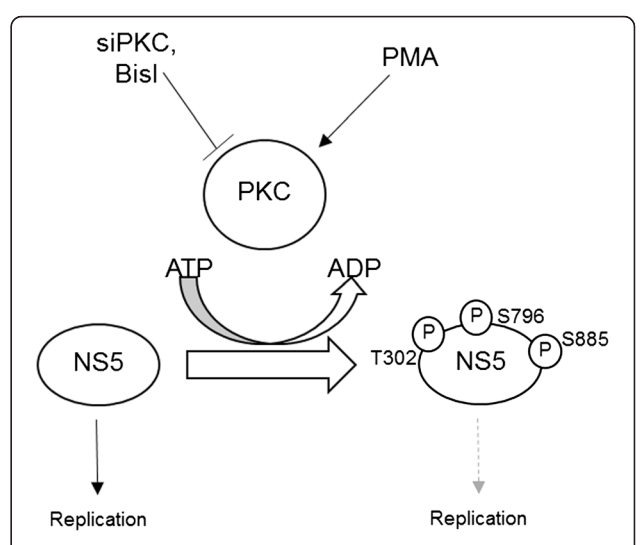


**Fig. 6** Inhibition of NS5 phosphorylation by PKC promotes viral replication. PKC is a host factor, which restricts intracellular DENV2 number by phosphorylating viral NS5. Inhibition of PKC by PKC inhibitor (Bisl) or PKC-specific siRNA (siPKC) results in increased viral copy number

apoptosis) [31]. Loss of PKC $\alpha$  activity either induces death, or sensitizes cells to death signals. Although, our experiments in hepatocellular carcinoma cells found that the inhibitions of PKC activity did not cause any notable cell death under the conditions, it is possible that PKC may also contribute to suppress host cell loss by specifically inhibiting apoptosis signal triggered by DENV infection.

#### **Conclusions**

PKC may act as a restricting mechanism that modulates the DENV replication and represses the viral outburst in the host cells.

#### **Methods**

## In vitro kinase assay

The His-tagged NS5 RdRp protein was purified from bacteria expression following Kamkaew et al. [32]. Dengue Capsid, prM, E, NS1, NS2B, NS3 and NS4B coding DNA were amplified by PCR from pD2-IC plasmid containing DENV2 genome [33]. The PCR products were inserted into pGEX-5X-3 plasmid (GE Healthcare Bio-Sciences). E.coli BL21 (DE3) was used to express dengue proteins according to standard protocol recommended by the manufacturer. The assay use 1 µg DENV proteins as substrate in a reaction with 75 ng of purified human PKC (Sigma). Cdk4/cyclinD1, PKA, CK I kinases were purchased from Calbiochem, Sigma and Promega, respectively. The kinase buffers and the reactions were prepared and performed as recommended by the manufacturer's protocols. After the kinase reactions, the substrates were run on a 12 % SDS-PAGE

gel. Expected bands of substrates were visualized by Coomassie blue staining and were excised from the gel to measure the  $^{\gamma-32}P$  incorporation. The  $^{\gamma-32}P$  was detected by scintillation counter (Perkin Elmer).

#### Cell lines and culture conditions

The human liver hepatocellular carcinoma cell line HepG2 was a kind gift from Dr. Limjindaporn T, Faculty of Medicine, Siriraj Hospital, Mahidol University. The Baby hamster kidney cell line (BHK-21) was a kind gift from Dr. Leardkamolkarn V, Faculty of Sciences, Mahidol University. They were cultured in Dulbecco's Modified Eagle Medium (DMEM) supplemented with 10 % heatinactivated fetal bovine serum (FBS), 100 U/ml penicillin G and 100  $\mu$ g/ml streptomycin (Invitrogen). Cells were grown at 37 °C with 5 % CO<sub>2</sub> in a humidified incubator.

#### Recombinant epitope-tagged DENV2

Construction of the recombinant DENV harboring the His-FLAG-tagged NS5 DENV (etDENV) was described previously [34]. Briefly, the cDNA from DENV serotype 2 strain 16681 in the pD2-IC plasmid [33] was used as the template for the insertion of the epitope tag. The TAP tag comprised of an octahistidine (His8) tag, a triglycine spacer, and FLAG sequence (DYKDDDDK) was inserted into the NS5 gene in pD2-IC via a standard QuikChange procedure. The positive clone containing the tag was verified by DNA sequencing. Wild-type and tagged DENV RNAs were synthesized according to a previous report [33]. Assay for viral kinetics was performed as follows: BHK-21 cells were infected with the viruses, viral titers from day 1 to day 6 post infection were determined using foci formation assay (FFA). We found that the recombinant DENV etDENV produced a comparable kinetic to that of wild type DENV 16681 (Additional file 1: Figure S1) up to 6 days. Once prepared, the viral titration was performed as follows. Supernatant of transfected infected cells was collected for FFA at 7 days post transfection. For FFA, the supernatant was incubated with BHK-21 cells in 96 well plates for 2 h, and subsequently 200 µl of 1.5 % carboxymethylcellulose (CMC) and 2 % FBS in DMEM was added to cover the cells, and the cells were incubated at 37 °C for 3 days. The infected BHK-21 cells were then washed with PBS 3 times and fixed with 3.7 % formaldehyde for 10 min at room temperature. The cells were permeabilized by 1 % Triton X-100 in PBS for 10 min and washed with PBS 5 times. The cells then were incubated with 1:1,000 in PBS anti-DENV E protein (EMD Milipore). Thereafter, the cells were washed with PBS 5 times before incubation with goat anti-mouse conjugated horseradish peroxidase (HRP) antibody at a 1:1,000 dilution for 45 min at 37 °C. The foci were visualized through SigmaFAST<sup>™</sup> DAP (Sigma) and counted under microscopy to determine viral titter.

#### Viral infection

In ever experiment, wild type DENV2 strain 16681 [35] or His-FLAG-tagged DENV was added into host cells at a multiplicity of infection (MOI) of 1, with an exception of the experiment with PMA treatment, in which virus with MOI of 5 was used. Cells were incubated at 37 °C for 90 min to allow incorporation of virus in to cells before being washed twice with PBS to remove excess virus. After that, DMEM medium supplemented with 2 % heat-inactivated FBS was added into the cells. Cells were further incubated at 37 °C for for time points indicated in the figures.

# Computational prediction of phosphorylation sites in Dengue NS5 protein

Bioinformatics tools used for screening of the possible PKC sites, Scansite<sup>™</sup> 2 [18], NetPhosK 2.0 [19], and KinasePhos 2.0 [20], were used for predicting phosphorylation sites in Dengue NS5 protein. A high stringency level was set for Scansite<sup>™</sup>, whereas a 0.9 threshold (high) was used for NetphosK, and a 100 % specificity was used for KinasePhos.

#### Sequence and structure analysis

To identify the conservation among flaviviruses, DENV1 (P27909), DENV2 (AHG23127), DENV3 (P27915), DENV4(P09816), West Nile virus (P06935), Japanese Encephalitis virus (P27395), yellow fever virus (AAC35930), St. Louis encephalitis virus (P09732), Omsk hemorrhagic fever virus (AAR98531), Zika virus (W8R1T1), Gadgets Gully virus (A0EKU2), Kama virus (W5VRZ2) and tickborne encephalitis virus (Q01299) NS5 sequences were compared by BioEdit 7.2.5. The phospho-conservative site was shown in crystal structure of NS5 (PDB ID: 4V0R).

#### Cell viability assay

To assess cytotoxicity of Bisindolylmaleimide I (BisI) Hydrochloride (Cell signaling) to HepG2 cells, the cells were seeded in 96-well plates at a density of  $10^4$  cells/well in DMEM medium supplemented with 10 % heatinactivated FBS for 24 h before BisI treatment. BisI at concentrations of 0.001  $\mu$ M, 0.01  $\mu$ M, 0.1  $\mu$ M, and 1  $\mu$ M in DMEM medium supplemented with 10 % heatinactivated FBS were added onto the cells. DMSO at a final concentration of 0.5 % served as a vehicle control. At 24, 48, and 72 h post-treatment, cell viabilities were assessed by a MTT assay, following the manufacturer protocol. To assess cytotoxicity of siRNA to HepG2 cells, the cells were seeded in a 96-well plate at a density of  $10^4$  cells/well in DMEM medium supplemented with 10 % heat-inactivated FBS for 24 h before being

transfected with PKC $\alpha$  siRNA at 24, 48, and 72 h post-transfection, MTT was added as described above.

#### Viral replication assay in Bisl-treated cells

HepG2 cells (5.5 X  $10^5$  cells) were seeded into culture dishes for 24 h before being treated with various concentrations of BisI, i.e. 0.001  $\mu$ M, 0.01  $\mu$ M, 0.1  $\mu$ M, and 1  $\mu$ M. BisI was added into the cells 30 min before viral infection. BisI was kept constant in the medium during infection with DENV2 at MOI of 1. This was followed by an incubation for 90 min to allow internalization of virus into cells. After the excess virus was removed, and the cells were washed twice by PBS, BisI in DMEM supplemented with 2 % FBS was added into cells and further incubated for the desired times, before the cells were harvested for detection of intracellular viral RNA by RT-qPCR.

#### Viral replication assay in PKCα-knockdown cells

PKCα siRNA (Santa Cruz biotechnologies, SC-29449) or Silencer<sup>®</sup> Negative control siRNA (Thermo, AM4611) were transfected into HepG2 cells using Lipofectamine® RNAiMAX reagent (Invitrogen) following the manufacturer's protocol. HepG2 cells  $(5.5 \times 10^5 \text{ cells})$  were seeded for 24 h before siRNA complexes were added. Twenty nM of siRNA were effective for suppressing PKCα expression. At 24 h post-transfection, DENV2 at MOI of 1 was added into the HepG2 cells and the culture was further incubated for 90 min to allow internalization of virus into the cells. Then, the excess virus was removed, and the cells were washed twice with PBS. Finally, DMEM supplement with 2 % FBS was added into the cells, and the cells were further incubated for another 24 h. Cells were collected for detection of intracellular viral RNA by RT-qPCR and viral proteins by immunoblots.

#### Intracellular viral RNA quantification by RT-qPCR

Total RNA was extracted from DENV-infected cells by Trizol reagent (Invitrogen), according to manufacturer's protocol. The reverse transcriptase reaction was set up using iScriptTM select cDNA synthesis kit (Bio-Rad) for first-strand cDNA synthesis. One microgram of total RNA was used as a template for all RT reaction. The reactions were performed with random primers. qPCR reactions were carried out using 2X KAPPA SYBR Green (KAPPA Biosystem). Amplification and detection were performed using an Applied Biosystems 7500 Real-time PCR system (ABI, California). qPCR conditions were 95 °C for 3 min, followed by 40 cycles of 95 °C for 3 s and 60 °C for 1 min.

Primers are:

NS5-Forward primer 5'-TCCATACATGCTAAACATG A-3'

NS5-Reverse primer 5'-GGGATTTCCTCCCATGATT CC-3'

β-actin-Forward prime 5'-TCTTCCAGCCTTCCTTC

β-actin-Reverse primer 5'-AGCACTGTGTTGGCGTA CAG-3'

#### Western blot analysis

HepG2 cell lysates were suspended in RIPA buffer solution containing 50 mM Tris-base pH 7.4, 150 mM NaCl, 1 % triton X-100, 0.1 % SDS, 1 % sodium deoxycholate, 1 mM EDTA, 1 mM Na<sub>3</sub>VO<sub>4</sub>, 1 mM NaF, 1 mM βglycerophosphate, 0.5 % NP40, 1 mM PMSF and 7× protease inhibitor cocktail. Protein samples were mixed with 6× protein loading dye, boiled and separated using SDS-PAGE. Gel was run for 2 h at 120 V before the proteins were transferred onto PVDF membrane by semi-dry blotting for 30 min at 10 V. After the transfer, nonspecific binding was blocked using 5 % skim milk for 1 h at room temperature. To determine inhibitory activity of PKC by BisI, after 24 post-infection, primary and secondary antibodies were rabbit antibodies against p-PEA15, PEA15, and goat anti rabbit antibody conjugated with horseradish-peroxidase (HRP) (Thermo scientific), respectively. To test whether PKCa siRNA can knock down PKCα after 24 and 48 h post-transfection, expressions of PKCα were detected by using mouse antibody specific to PKCα, and goat antibody specific to GAPDH (loading control) (both were from Santa cruz biotechnologies) as primary antibodies and goat anti-mouse (Novagen) and mouse anti-goat antibodies conjugated with HRP (Santa cruz biotechnologies) as secondary antibodies. To verify expression of NS5, rabbit antibody against NS5 (Thermo scientific) was used, followed by goat anti-rabbit antibody conjugated with HRP as secondary antibodies. The antigen-antibody complexes were detected by using chemiluminesence detection (ECL, Amersham Pharmacia Biotech).

#### Determination of in vivo phosphorylation of NS5 by PKC

In this test, we performed infection of the recombinant virus on BHK-21 cells, due to the relatively high expression level of viral proteins obtained from this cell line. BHK-21 cells were treated with 1  $\mu M$  BisI before, at the time of, and after DENV infection as described above. At 24 h post-infection, cells were washed with cold PBS before extraction of total protein using CLB buffer (50 mM Tris HCl PH 7.4, 250 mM NaCl, 5 mM EDTA, 1 mM Na $_3$ VO $_4$ , 1 mM NaF, 1 mM  $\beta$ -glycerophosphate, 0.5 % NP40, 1 mM PMSF and 7X protease inhibitor cocktail). Three mg of cell lysate were used for FLAG-NS5 immunoprecipitation (IP) with 20  $\mu$ l of anti-FLAG M2 affinity gel (Sigma) in 1 ml reaction according to the manufacturer's instruction. IP products were separated by SDS-PAGE and

transferred onto a PVDF membrane. The membrane was probed with rabbit anti-NS5 (Thermo scientific), mouse anti-phospho-Serine or anti-phospho-Threonine (Sigma) followed by incubation with goat anti-rabbit or goat anti-mouse IgG conjugated with HRP. The antigen-antibody complexes were detected by using chemiluminesence detection (ECL, Amersham Pharmacia Biotech).

#### Statistical analysis

All experiments were performed in triplicate and data are presented as the mean  $\pm$  standard deviation (SD). Statistical comparisons were performed using *Student's t* test. *p*-value  $\leq$ 0.05 was considered to indicate a statistically significant difference.

#### **Additional file**

**Additional file 1:** Viral kinetics of wild type DENV 16681, and the recombinant DENV etDENV. (PDF 63 kb)

#### Competing interests

The authors declare that they have no competing interests.

#### Authors' contribution

WN and TP performed experiments and assisted manuscript preparation. AS, SJ, and RT planned project. SC and TJ planned and performed experiments. SJ and RT drafted and prepared manuscript. All authors read and approved the final manuscript.

#### Acknowledgements

SJ is supported by "Chalermphrakiat" Grant, Faculty of Medicine Siriraj Hospital, Mahidol University, The Thailand Research Fund (RSA5880038), and the Advanced Research on Pharmacology Fund, Siriraj Foundation D003421. TP is supported by a scholarship from Science Achievement Scholarship of Thailand (SAST). SC is supported by Grants-in-Aids for scientific research from Mahidol University (Thailand), and by the Mid-Career Grant (RSA5680054) from Thailand Research Fund (TRF). This project was supported by National Research University of Thailand (NRU) and the DENFREE project (the European Union Seventh Framework Programme (FP7/2007/2011) under Grant Agreement n°282 378).

#### **Author details**

<sup>1</sup>Department of Biochemistry, Faculty of Sciences, Mahidol University, Bangkok, Thailand. <sup>2</sup>Department of Microbiology, Faculty of Sciences, Mahidol University, Bangkok, Thailand. <sup>3</sup>Department of Microbiology and Immunology, Faculty of Tropical Medicine, Thailand Functional Genetics of Infectious Diseases Unit, Institute, Mahidol University, Bangkok, Thailand. <sup>4</sup>Institute Pasteur, Functional Genetics of Infectious Diseases Unit, Paris, France. <sup>5</sup>Centre National de la Recherche Scientifique (CNRS), URA3012, F-75015 Paris, France. <sup>6</sup>Institute of Molecular Biosciences, Mahidol University, Salaya, Nakhon Pathom, Thailand. <sup>7</sup>Systems Biology of Diseases Research Unit, Faculty of Science, Mahidol University, Bangkok, Thailand. <sup>8</sup>Laboratory for Systems Pharmacology, Department of Pharmacology, Faculty of Medicine Siriraj Hospital, Bangkok, Thailand.

# Received: 7 October 2015 Accepted: 23 February 2016 Published online: 01 March 2016

#### References

- Balinsky CA, Schmeisser H, Ganesan S, Singh K, Pierson TC, Zoon KC. Nucleolin interacts with the dengue virus capsid protein and plays a role in formation of infectious virus particles. J Virol. 2013;87(24):13094–106. doi:10.1128/JVI.00704-13.
- 2. Brunetti JE, Scolaro LA, Castilla V. The heterogeneous nuclear ribonucleoprotein K (hnRNP K) is a host factor required for dengue virus

- and Junin virus multiplication. Virus Res. 2015;203:84–91. doi:10.1016/j. virusres.2015.04.001.
- Cervantes-Salazar M, Angel-Ambrocio AH, Soto-Acosta R, Bautista-Carbajal P, Hurtado-Monzon AM, Alcaraz-Estrada SL, et al. Dengue virus NS1 protein interacts with the ribosomal protein RPL18: this interaction is required for viral translation and replication in Huh-7 cells. Virology. 2015;484:113–26. doi:10.1016/j.virol.2015.05.017.
- Reid CR, Airo AM, Hobman TC. The virus-host interplay: biogenesis of + RNA replication complexes. Viruses. 2015;7(8):4385–413. doi:10.3390/v7082825.
- Mairiang D, Zhang H, Sodja A, Murali T, Suriyaphol P, Malasit P, et al. Identification of new protein interactions between dengue fever virus and its hosts, human and mosquito. PLoS ONE. 2013;8(1), e53535. doi:10.1371/ journal.pone.0053535.
- Silva EM, Conde JN, Allonso D, Nogueira ML, Mohana-Borges R. Mapping the interactions of dengue virus NS1 protein with human liver proteins using a yeast two-hybrid system: identification of C1q as an interacting partner. PLoS ONE. 2013;8(3):e57514. doi:10.1371/journal.pone.0057514.
- Le Breton M, Meyniel-Schicklin L, Deloire A, Coutard B, Canard B, de Lamballerie X, et al. Flavivirus NS3 and NS5 proteins interaction network: a high-throughput yeast two-hybrid screen. BMC Microbiol. 2011;11:234. doi:10.1186/1471-2180-11-234.
- Carpp LN, Rogers RS, Moritz RL, Aitchison JD. Quantitative proteomic analysis of host-virus interactions reveals a role for Golgi brefeldin A resistance factor 1 (GBF1) in dengue infection. Mol Cell Proteomics. 2014; 13(11):2836–54. doi:10.1074/mcp.M114.038984.
- Teo CS, Chu JJ. Cellular vimentin regulates construction of dengue virus replication complexes through interaction with NSAA protein. J Virol. 2014; 88(4):1897–913. doi:10.1128/JVI.01249-13.
- Bhattacharya D, Ansari IH, Striker R. The flaviviral methyltransferase is a substrate of Casein Kinase 1. Virus Res. 2009;141(1):101–4. doi:10.1016/j. virusres.2009.01.002.
- Forwood JK, Brooks A, Briggs LJ, Xiao CY, Jans DA, Vasudevan SG. The 37amino-acid interdomain of dengue virus NS5 protein contains a functional NLS and inhibitory CK2 site. Biochem Biophys Res Commun. 1999;257(3): 731–7. doi:10.1006/bbrc.1999.0370.
- 12. Kapoor M, Zhang L, Ramachandra M, Kusukawa J, Ebner KE, Padmanabhan R. Association between NS3 and NS5 proteins of dengue virus type 2 in the putative RNA replicase is linked to differential phosphorylation of NS5. J Biol Chem. 1995;270(32):19100–6.
- Laurent-Rolle M, Boer EF, Lubick KJ, Wolfinbarger JB, Carmody AB, Rockx B, et al. The NS5 protein of the virulent West Nile virus NY99 strain is a potent antagonist of type I interferon-mediated JAK-STAT signaling. J Virol. 2010; 84(7):3503–15. doi:10.1128/JVI.01161-09.
- Reed KE, Gorbalenya AE, Rice CM. The NS5A/NS5 proteins of viruses from three genera of the family flaviviridae are phosphorylated by associated serine/threonine kinases. J Virol. 1998;72(7):6199–206.
- Zhou Y, Ray D, Zhao Y, Dong H, Ren S, Li Z, et al. Structure and function of flavivirus NS5 methyltransferase. J Virol. 2007;81(8):3891–903. doi:10.1128/JVI. 02704-06.
- Malet H, Masse N, Selisko B, Romette JL, Alvarez K, Guillemot JC, et al. The flavivirus polymerase as a target for drug discovery. Antivir Res. 2008;80(1): 23–35. doi:10.1016/j.antiviral.2008.06.007.
- Bhattacharya D, Mayuri, Best SM, Perera R, Kuhn RJ, Striker R. Protein kinase G phosphorylates mosquito-borne flavivirus NS5. J Virol. 2009;83(18):9195– 205. doi:10.1128/JVI.00271-09.
- Obenauer JC, Cantley LC, Yaffe MB. Scansite 2.0: proteome-wide prediction of cell signaling interactions using short sequence motifs. Nucleic Acids Res. 2003;31(13):3635–41.
- Blom N, Gammeltoft S, Brunak S. Sequence and structure-based prediction of eukaryotic protein phosphorylation sites. J Mol Biol. 1999;294(5):1351–62. doi:10.1006/jmbi.1999.3310.
- Wong YH, Lee TY, Liang HK, Huang CM, Wang TY, Yang YH, et al. KinasePhos 2.0: a web server for identifying protein kinase-specific phosphorylation sites based on sequences and coupling patterns. Nucleic Acids Res. 2007;35(Web Server issue):W588–94. doi:10.1093/nar/gkm322.
- Keating JA, Bhattacharya D, Lim PY, Falk S, Weisblum B, Bernard KA, et al. West Nile virus methyltransferase domain interacts with protein kinase G. Virol J. 2013;10:242. doi:10.1186/1743-422X-10-242.
- Edgil D, Diamond MS, Holden KL, Paranjape SM, Harris E. Translation efficiency determines differences in cellular infection among dengue virus type 2 strains. Virology. 2003;317(2):275–90.

- Neveu G, Cassonnet P, Vidalain PO, Rolloy C, Mendoza J, Jones L, et al. Comparative analysis of virus-host interactomes with a mammalian high-throughput protein complementation assay based on Gaussia princeps luciferase. Methods. 2012;58(4):349–59. doi:10.1016/j.ymeth. 2012.07.029.
- Bhattacharya D, Hoover S, Falk SP, Weisblum B, Vestling M, Striker R. Phosphorylation of yellow fever virus NS5 alters methyltransferase activity. Virology. 2008;380(2):276–84. doi:10.1016/j.virol.2008.07.013.
- Kwon YJ, Heo J, Wong HE, Cruz DJ, Velumani S, da Silva CT, et al. Kinome siRNA screen identifies novel cell-type specific dengue host target genes. Antivir Res. 2014;110:20–30. doi:10.1016/j.antiviral.2014.07.006.
- Kao CC, Singh P, Ecker DJ. De novo initiation of viral RNA-dependent RNA synthesis. Virology. 2001;287(2):251–60. doi:10.1006/viro.2001.1039.
- Jorgensen K, Skrede M, Cruciani V, Mikalsen SO, Slipicevic A, Florenes VA. Phorbol ester phorbol-12-myristate-13-acetate promotes anchorage-independent growth and survival of melanomas through MEK-independent activation of ERK1/2. Biochem Biophys Res Commun. 2005;329(1):266–74. doi:10.1016/j.bbrc.2005.01.143.
- 28. Whelan RD, Parker PJ. Loss of protein kinase C function induces an apoptotic response. Oncogene. 1998;16(15):1939–44. doi:10.1038/sj.onc.1201725.
- Mandil R, Ashkenazi E, Blass M, Kronfeld I, Kazimirsky G, Rosenthal G, et al. Protein kinase Calpha and protein kinase Cdelta play opposite roles in the proliferation and apoptosis of glioma cells. Cancer Res. 2001;61(11):4612–9.
- Matassa AA, Kalkofen RL, Carpenter L, Biden TJ, Reyland ME. Inhibition of PKCalpha induces a PKCdelta-dependent apoptotic program in salivary epithelial cells. Cell Death Differ. 2003;10(3):269–77. doi:10.1038/sj.cdd.4401149.
- Garcia-Bermejo ML, Leskow FC, Fujii T, Wang Q, Blumberg PM, Ohba M, et al. Diacylglycerol (DAG)-lactones, a new class of protein kinase C (PKC) agonists, induce apoptosis in LNCaP prostate cancer cells by selective activation of PKCalpha. J Biol Chem. 2002;277(1):645–55. doi:10.1074/jbc. M107639200.
- Kamkaew M, Chimnaronk S. Characterization of soluble RNA-dependent RNA polymerase from dengue virus serotype 2: The polyhistidine tag compromises the polymerase activity. Protein Expr Purif. 2015;112:43–9. doi: 10.1016/j.pep.2015.04.008.
- Kinney RM, Butrapet S, Chang GJ, Tsuchiya KR, Roehrig JT, Bhamarapravati N, et al. Construction of infectious cDNA clones for dengue 2 virus: strain 16681 and its attenuated vaccine derivative, strain PDK-53. Virology. 1997; 230(2):300–8. doi:10.1006/viro.1997.8500.
- 34. Poyomtip T, Hodge K, Matangkasombut P, Sakuntabhai A, Pisitkun T, Jirawanotai S, Chimnaronk S. Development of viable TAP-tagged dengue virus for inverstigation of host-virus interaction in viral replication. J Gen Virol. 2015 Dec (In press)
- Halstead SB, Udomsakdi S, Simasthien P, Singharaj P, Sukhavachana P, Nisalak A. Observations related to pathogenesis of dengue hemorrhagic fever. I. Experience with classification of dengue viruses. Yale J Biol Med. 1970;42(5):261–75.

# Submit your next manuscript to BioMed Central and we will help you at every step:

- We accept pre-submission inquiries
- Our selector tool helps you to find the most relevant journal
- We provide round the clock customer support
- Convenient online submission
- Thorough peer review
- Inclusion in PubMed and all major indexing services
- Maximum visibility for your research

Submit your manuscript at www.biomedcentral.com/submit



THE JOURNAL OF BIOLOGICAL CHEMISTRY VOL. 291, NO. ??, pp. 1–xxx, ???? ??, 2016 © 2016 by The American Society for Biochemistry and Molecular Biology, Inc. Published in the U.S.A.

# Identification of a Conserved RNA-dependent RNA Polymerase (RdRp)-RNA Interface Required for Flaviviral Replication\*

Received for publication, February 25, 2016, and in revised form, June 10, 2016 Published, JBC Papers in Press, June 22, 2016, DOI 10.1074/jbc.M116.724013

Kenneth Hodge<sup>‡1</sup>, Chairat Tunghirun<sup>‡1</sup>, Maliwan Kamkaew<sup>‡</sup>, Thawornchai Limjindaporn<sup>§</sup>, Pa-thai Yenchitsomanus<sup>¶</sup>, and Sarin Chimnaronk<sup>‡2</sup>

From the <sup>‡</sup>Laboratory of RNA Biology, Institute of Molecular Biosciences, Mahidol University, Salaya Campus, Nakhon Pathom 73170 and the <sup>§</sup>Department of Anatomy and <sup>¶</sup>Division of Molecular Medicine, Department of Research and Development, Faculty of Medicine, Siriraj Hospital, Mahidol University, Bangkok 10700, Thailand

Dengue virus, an ~10.7-kb positive-sense RNA virus, is the most common arthropod-communicated pathogen in the world. Despite dengue's clear epidemiological importance, mechanisms for its replication remain elusive. Here, we probed the entire dengue genome for interactions with viral RNA-dependent RNA polymerase (RdRp), and we identified the dominant interaction as a loop-forming ACAG motif in the 3' positive-stranded terminus, complicating the prevailing model of replication. A subset of interactions coincides with known flaviviral recombination sites inside the viral protein-coding region. Specific recognition of the RNA element occurs via an arginine patch in the C-terminal thumb domain of RdRp. We also show that the highly conserved nature of the consensus RNA motif may relate to its tolerance to various mutations in the interacting region of RdRp. Disruption of the interaction resulted in loss of viral replication ability in cells. This unique RdRp-RNA interface is found throughout flaviviruses, implying possibilities for broad disease interventions.

Positive-sense single-stranded RNA viruses initiate replication by the generation of a complementary negative (-)-RNA strand via the action of viral RNA-dependent RNA polymerases (RdRps).<sup>3</sup> In the cases of brome mosaic virus (family Bromoviridae), turnip crinkle virus (Tombusviridae), hepatitis C virus (Flaviviridae), and encephalomyocarditis virus (Picornaviridae), RNA structures in the 3'-untranslated region (UTR) of the positive strand have been characterized as RdRp promoters (1–4). In the case of dengue virus (DENV), a flavivirus with a 5'-type I cap and the absence of a polyadenylated tail, however,

the current model for replication asserts that the 5'-UTR acts as a promoter for (—)-strand synthesis. This position is supported by several lines of *in vitro* evidence. In particular, atomic force microscopy demonstrated cyclization of the (+)-strand genomic RNA, resulting in placement of the 5'-UTR in proximity to the 3' terminus, whereas EMSA and footprinting assays apparently documented RdRp interactions with the first hairpin element in the DENV 5'-UTR, designated stem-loop A (SLA) (5). In addition, an RNA fragment of the DENV 5'-UTR could also stimulate *in vitro* synthesis of a complementary product of the 3'-UTR (5, 6).

To date, investigations of RdRp actions on the flaviviral RNA genome have been limited to in vitro assays on less than 5% of the whole genome with a bias toward UTR regions; therefore, the entire interaction landscape of RdRp has not yet been revealed. It is also unclear whether flaviviral RdRps require a specific RNA promoter for *de novo* initiation of RNA synthesis. To gain insight into accurate mechanisms for synthesis of the viral genome in the cell, here we explored all possible interactions between RdRp and the complete RNA genome in an unbiased in vivo context using a refined yeast three-hybrid (Y3H) scan. Combining bioinformatic evidence with in vitro binding and viral replicon assays, we pinpoint amino acids and nucleotides contributing to previously undocumented RdRp-viral RNA interfaces and suggest a novel means that contributes to strong conservation of this promoter motif throughout flaviviruses, and possibly beyond.

#### Results

Isolation of Viral RNA Elements That Interact with RdRp via Y3H—We devised a Y3H genetic screen to explore the global interaction between viral RdRp and its own entire genomic RNA in a eukaryotic cellular environment (Fig. 1A). Y3H has been exploited to extensively identify protein-RNA interactions and has been shown to generally correlate well with other in vitro assays such as EMSA (7, 8). Because RNA inserts in the Y3H vector should generally not exceed 200 nt, as reporter signals weaken with increasing length, and at least 40 nt are required to provide sufficient length for RNA to fold into functional structures such as hairpins and pseudoknots (9), full-length cDNA from the dengue virus serotype 2 (DENV-2) was randomly digested into fragments of ~100 bp in size via an endonuclease-V-based procedure (10), prior to non-directional

<sup>\*</sup> This work was supported by grants-in-aid for scientific research from Mahidol University, Thailand (to S. C. and P. Y.), a senior research scholar grant from the Thailand Research Fund (to P. Y.), and Mid-Career Grant RSA5680054 from Thailand Research Fund (to S. C.). The authors declare that they have no conflicts of interest with the contents of this article.

<sup>&</sup>lt;sup>1</sup> Both authors contributed equally to this work.

<sup>&</sup>lt;sup>2</sup> To whom correspondence should be addressed: Laboratory of RNA Biology, Institute of Molecular Biosciences, Mahidol University, Salaya Campus, Phutthamonthon, Nakhon Pathom 73170, Thailand. Tel.: 66-2-441-9003 (Ext. 1468); E-mail: sarin.chi@mahidol.ac.th.

<sup>&</sup>lt;sup>3</sup> The abbreviations used are: RdRp, RNA-dependent RNA polymerase; DENV, dengue virus; SLA, stem-loop A; Y3H, yeast three-hybrid; nt, nucleotide; DI, defective interfering; HCV, hepatitis C virus; SL, stem-loop; TL, top loop; 3-AT, 3-aminotriazole; ONPG, o-nitrophenyl  $\beta$ -D-galactopyranoside; cy, cyclized; cir, circular; lin, linear; CS, cyclization sequence; WNV, West Nile virus; JEV, Japanese encephalitis virus; YFV, yellow fever virus.

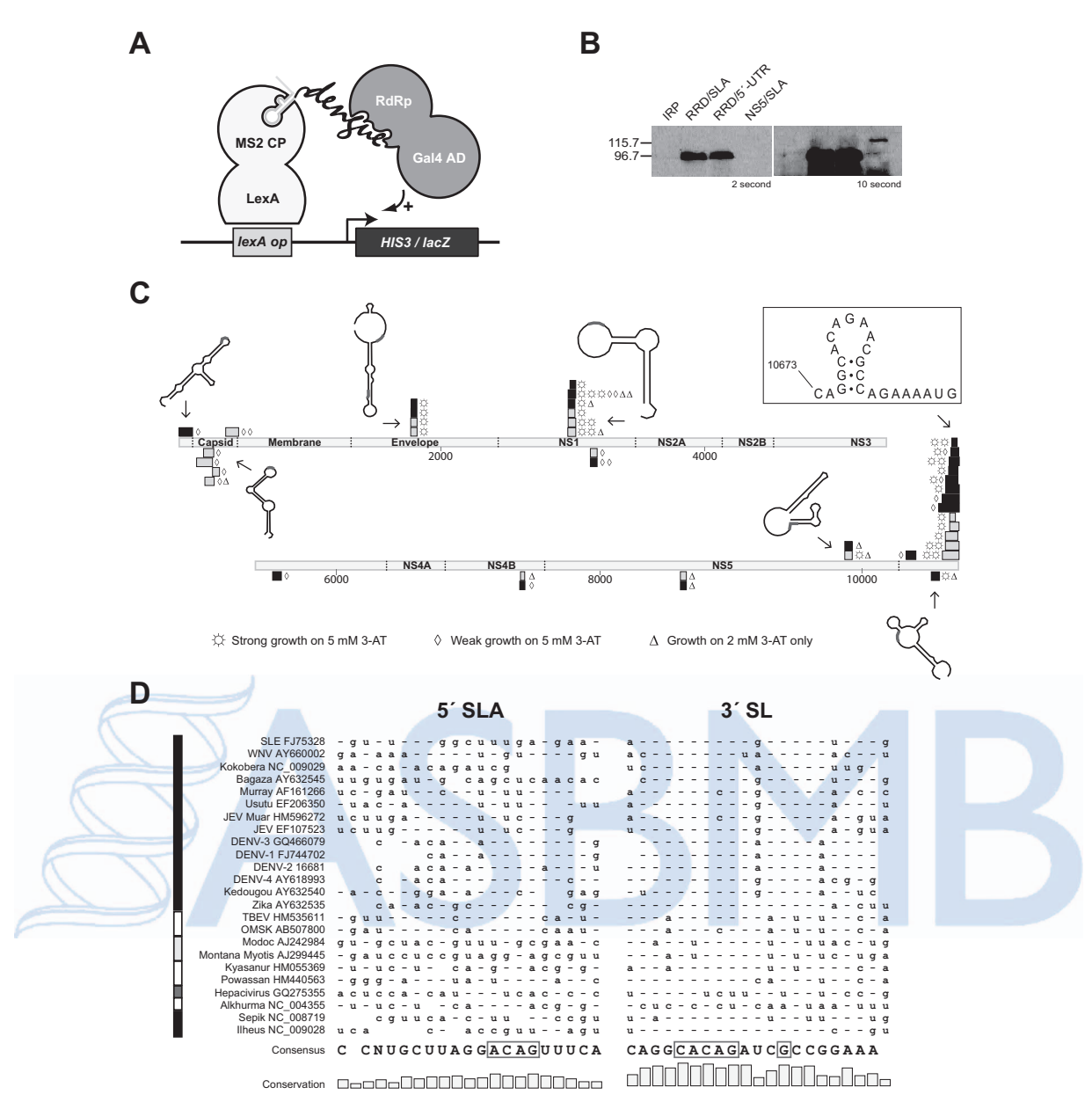


FIGURE 1. Interaction landscape of DENV RdRp with the entire RNA genome. A, schematic diagram of Y3H in this study. B, Western blotting with polyclonal AQ: A anti-NS5 antibodies (Gentex 103350) confirmed the expression of DENV-2 NS5 (120.9 kDa) and its RdRp (90.1 kDa) in Y3H with two representative RNAs, SLA and the full-length 5'-UTR. The protein IRP in pACT2 was used as a negative control. C, DENV genome is depicted as light gray rectangles and is numbered. The coding regions for viral proteins are labeled. Positive strand RNA fragments of the genome that bind the full-length NS5 and RdRp are shown above the genome as black and gray rectangles, respectively, whereas negative fragments are below. Levels of yeast growth in the presence of 3-AT are indicated by three symbols. Representative Mfold structures of RNA fragments are drawn with the CACAG motif in red. D, conservation of the ACAG loop motif is compared between the top loop regions of the 5'-SLA and the 3'-SL. Sequences are ordered according to a phylogenetic tree based on the terminal 120 nucleotides of Flaviviridae. The left vertical bar indicates the type of Flaviviridae as follows: black indicates mosquito-borne viruses; white indicates tick-borne viruses; light gray indicates viruses of no known vector; and dark gray indicates a single hepacivirus example. Consensus nucleotides are indicated once at the bottom of the figure; elsewhere, they are indicated by hyphens, with variations from the consensus indicated by the appropriate letter.

ligation into a modified Y3H RNA expression vector pIIIA MS2-2 with high efficiency through a Gateway recombination protocol (see under "Experimental Procedures" for details).

Sequencing of 100 clones verified suitable Y3H insert sizes and coverage of the entire (+)/(-)-DENV genome (details under "Experimental Procedures"). Protein-RNA interactions were monitored in YBZ-1 yeast coexpressing the RNA library with either the full-length DENV-2 NS5 protein composed of N-terminal methyltransferase and C-terminal RdRp domains or the RdRp subdomain (hereafter referred to as "RdRp") alone.

Expression levels of these two proteins were confirmed via Western blotting, with the smaller RdRp being found at concentrations roughly 10-fold higher than NS5 (Fig. 1B). To cover all possible structural elements in both strands of DENV RNA, a total of  $\sim 10^5$  cotransformants (estimated via plating on nonselective Leu-/Ura media) were subjected to selection with histidine deprivation. A total of 60 sequences, averaging 67 bases, mapping onto the DENV-2 genome were retrieved from yeast growing under three increasingly selective concentrations of 3-AT, a histidine metabolism inhibitor. Sampling ceased

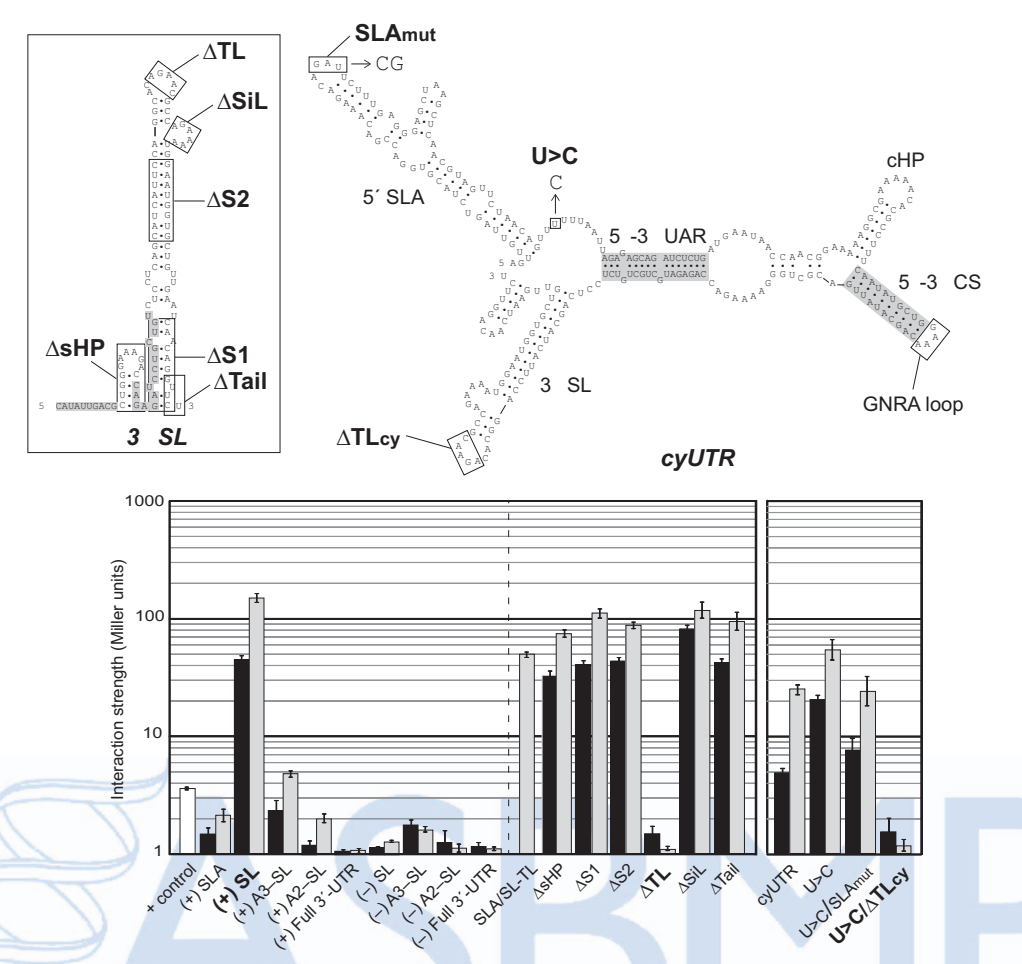


FIGURE 2. DENV RdRp recognizes the top loop of 3'-SL. Linear 3'-SL and a series of its deletion mutants are indicated in the secondary structure with rectangles (upper left panel), whereas the model of the cyclized Y3H RNA construct containing DENV 5'- and 3'-terminal regions (cyUTR) used in this study is in the upper right panel. The long viral open reading frame was replaced by a GNRA loop that linked 5'- and 3'-UTR together in the cyUTR construct. SL mutant  $\Delta$ sHP completely removed the boxed hairpin;  $\Delta$ S1 removed the lower SL stem;  $\Delta$ S2 removed the upper SL stem;  $\Delta$ TL removed the indicated top loop nucleotides;  $\Delta SiL$  removed the side loop; and  $\Delta Tail$  replaced the final 5' nucleotides with CAAAA. In cyUTR, SLAmut replaced the wild-type GAU with CG, and U > C refers to the substitution of a U with a single C. Structural RNA elements are labeled.  $\beta$ -Galactosidase expression assays showing the interaction strengths with the full-length NS5 (black-filled bar) or RdRp (gray) are measured in Miller units. The lower left panel shows RdRp interactions with a variety of linear DENV RNAs with native sequences (left half) and mutations (right half). Results with a cyclized form of UTR are separated into the lower right panel. Error bars indicate

when it became apparent that four clusters of overlapping sequences dominated the mapping. Of all the sequences, the known NS5 interactor, the 5'-SLA, was identified once, growing only at the lowest levels of 3-AT (Fig. 1C). In contrast, a sequence associated with a particularly strong interaction at the last long stem-loop (SL) element in the 3'-UTR was observed on 19 occasions. In one case, a mere 23-nt fragment, consisting of the top stem-loop region of 3'-SL, was associated with robust protein-RNA interaction (Fig. 1C). Other 3'-SL-containing sequences ranged from 40 to 138 nt. Interestingly, the loop contained a highly conserved CACAG pentanucleotide sequence (Fig. 1D) that had been identified as critical for viral growth in a previous study (11). SLA also contains ACAG in a loop structure (Figs. 1D and 2), but the initial A is predicted to participate in the upper base pair of the stem, whereas that of 3'-SL is unpaired, preceded by a C that pairs with a G 8 bases downstream to clamp the loop.

An RNA complementary to a dumbbell structure upstream of 3'-SL, designated A3 (the secondary structure is illustrated in Fig. 7), interacted with NS5 and RdRp at a strength comparable with that of 5' stem-loop A ((-)-A3-SL in Fig. 2), in which a highly conserved ACAG among flaviviruses is present in a predicted loop. The positive complement to this loop likely forms a loop, designated TL2 in previous work (12), which showed that mutations of TL2 resulted in significant replication impairment. Other clusters of interactors were also identified, with two clusters in coding regions being particularly obvious. Several map features are of note. First, an ACAG sequence, predicted to reside at least partially in a loop structure (13), was found in 51 of the 60 sequences in a predicted loop structure (Fig. 1C). Numerous sequences containing ACAG were found during validation of the RNA library, but these sequences were not later identified as RdRp interactors, indicating that a 4-nt sequence alone is indispensable but not sufficient for RdRp binding. Second, the majority of interactors (75%) resided on the positive strand. Because negative strand flaviviral RNA is thought to exist primarily in duplex form in infected cells, RdRp interactions with this strand might not predominate. No preference for RNA binding was observed between NS5 versus RdRp because in every case where the same interacting

sequence was seen at least twice, both NS5 and RdRp were identified as interaction partners. In other words, the methylase domain likely had negligible RNA specificity. Finally, the genomic interaction sequences revealed significant correlation (p < 5E-11, see "Experimental Procedures") with recombination regions documented in DENV-1 (14) and JEV (15) studies and also contained sites at which 5'- and 3'-DENV regions joined together to form defective interfering (DI) particles (16). It is noted that these DI-joining points are enriched in ACA and ACAG (p = 0.0029 and 0.0015, respectively, see "Experimental Procedures"). These facts would imply a possible mechanism of RNA template switching where RdRp encounters these sequences and structures.

RdRp Specifically Recognizes the SL Top Loop in Both Genomic Forms-To validate our Y3H screen with an RNA library, various portions of the DENV 5'- and 3'-(+)/(-)-UTR RNAs were constructed, and protein-RNA interactions were quantified via the ONPG-based assay for the  $\beta$ -galactosidase reporter gene. The results revealed that the binding affinity of RdRp to 3'-SL in Y3H exceeded that of SLA by greater than 2 orders of magnitude (Fig. 2). Previous EMSA and filter binding assays established an *in vitro K*<sub>d</sub> for 5'-UTR RNA-RdRp binding at 8 – 16 nm (5), and surface plasmon resonance rendered a  $K_d$  of 53 nm (17), although a linear extrapolation of SL-binding strength should not be expected. It was noted that SL-binding signals diminished as the length of the RNA inserts increased from 3'-SL alone (95 nt), to SL and the A3 dumbbell structure (A3-SL, 203 nt), to SL and two dumbbell A2-A3 structures (A2-SL, 289 nt), and finally the full 3'-UTR (458 nt) (Fig. 2). This is typical Y3H behavior, one of the variables precluding usage of Y3H as a direct  $K_d$  measurement system (18). Deletions of six features of the 3'-SL showed that this robust interaction is defined entirely by the ACAG top loop (TL) motif ( $\Delta$ TL in Fig. 2). In another experiment, merely replacing the SLA-TL by that of 3'-SL resulted in a 47-fold increase in binding strength in the Y3H context (SLA/SL-TL in Fig. 2). Given that the ACAG sequence in SLA is variable among flaviviruses (Fig. 1D), these results confound the current replication model.

Our Y3H assays were further corroborated by in vitro gel shift assay (EMSA) with highly purified components, including non-tagged DENV RdRp (17) and three RNA transcripts derived from DENV-2 3'-UTRs. We stained both protein and RNA to avoid misinterpretation of RNA EMSA because RNA could form multiple configurations, including multimers in solution, and RNA-binding proteins could have more or less non-sequence-specific binding potential due to their extensive positively charged surfaces. The results showed that RdRp comigrated, i.e. formed stable complexes, with both linSL and cirSL, which corresponded to the 3'-SL configuration as it is found in the linear (lin) and cyclized forms, respectively, of the complete genome (Fig. 3). Deletion of the 3'-SL top loop markedly impaired RdRp complex formation (ΔTL in Fig. 3). RdRp thus specifically recognizes the 3'-SL-TL because the control tRNA showed only a background level of interaction (Fig. 3). Our EMSA results strongly corroborated the Y3H assay and were in clear contrast to previous reports that failed to detect 3'-SL-binding ability (5). Next, to quantify the binding affinity of RdRp with 3'-SL, we exploited an Alpha assay with 5'-bioti-

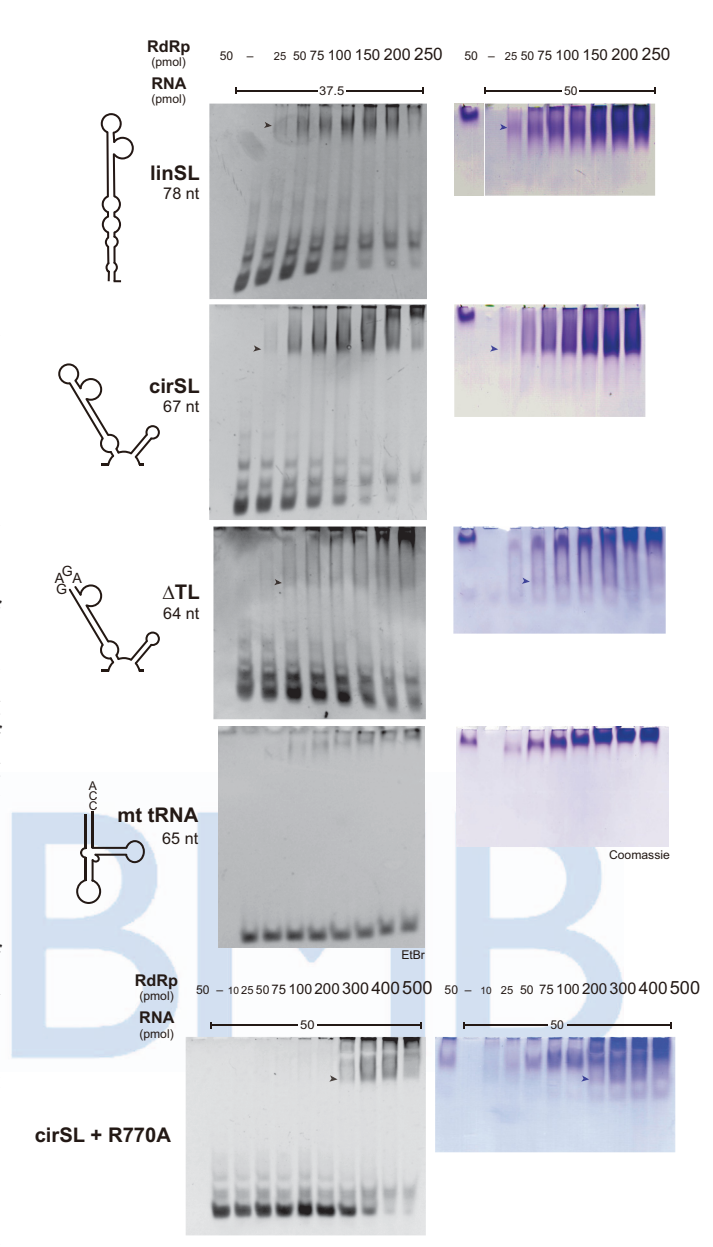


FIGURE 3. *In vitro* EMSA. Mfold secondary structures of RNAs are depicted in the *left row. Arrows* highlight protein-RNA complexes that were evident via both EtBr (*middle row*) and Coomassie (*right row*) staining. The constant amount of RNA in the reaction was increased from 37.5 to 50 pmol in the case of protein staining.

nylated RNA substrates and N-terminally His-tagged RdRp. The Alpha technology has recently been used to determine interactions of RNA-binding proteins in solution (19). We employed truncated forms of 5′-SLA and 3′-SL RNAs in the binding assay to narrow down the interaction site (Fig. 4A). SL binds to RdRp with a  $K_d$  of  $\sim$ 3.2 nM, whereas the deletion of the top loop completely abolished the binding signal. We also performed competition assays between biotinylated SL and unlabeled RNAs (Fig. 4B). SLA RNA failed to compete with SL binding in our assay (data not shown), whereas simple substitution of the top loop of SLA by that of SL (SLA/SL-TL) obviously showed binding inhibition. Altogether, our Y3H, EMSA, and Alpha assays provided indisputable proof of specific RdRp/SL-TL interaction.

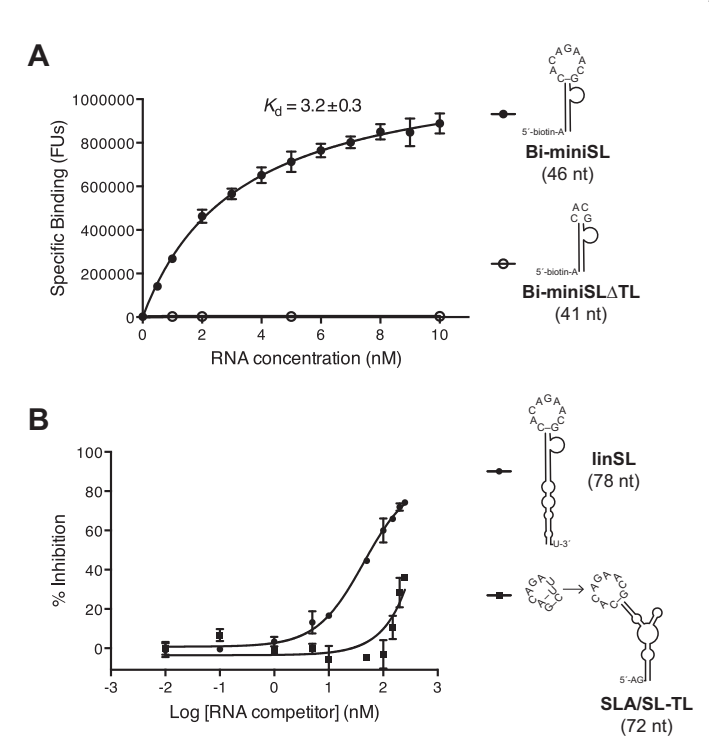


FIGURE 4. In vitro Alpha binding assay. A, saturation binding experiment of RdRp with truncated 3'-SL. The Alpha-binding signal is shown in fluorescence units (FU). B, competition assay with unlabeled RNA. RdRp and Bi-miniSL concentrations were kept constant at 200 and 10 nm, respectively. Mean and standard deviation values are derived from three independent experiments. We note that SLA did not show a binding signal in both saturation binding and competition assay.

To faithfully model NS5 interactions with genomic RNA in its cyclized form, a 254-nt RNA construct (cyUTR) containing, in order, the 5'-UTR, 5'-CS, a GNRA loop-forming sequence, the 3'-CS that binds with the 5'-CS, and the 3'-terminal SL structure was engineered (Fig. 2, right panels). In this form, the initial 1445'-nucleotides are predicted to be placed in the vicinity of the last 106 nt of the 3'-UTR via complementary interactions mimicking the cyclized form of DENV UTRs (20). As expected, a deletion mutant disrupting the ACAG motif in 3'-SL ( $\Delta$ TLcy) caused a 50-fold loss of binding affinity, which paralleled the differing affinities between the 5'-SLA and 3'-SL linear constructs. However, it could not be ruled out that SLA may be involved in a structural rearrangement of UTRs in the cyclized form because mutation of the SLA-TL decreased the potent wild-type signal by half. Nonetheless, these results emphasized the 3'-SL-TL as the predominant RdRp-binding site in both genomic forms. Moreover, a deletion mutant of the 3'-SL-TL ( $\Delta$ TL) in our DENV-2 replicon (see "Experimental Procedures" for details) completely abolished viral RNA replication in BHK-21 cells, similar to the GAA mutation that inactivated the polymerase activity of NS5 (Fig. 5D). Taken together, our results suggested the ACAG motif in the 3'-SL-TL serving as a *cis*-element for (-)-strand viral RNA synthesis in cells.

RdRp Thumb Domain Recognizes the ACAG Motif—Because the underlying molecular basis for RNA specificity of RdRp remains obscure, we undertook a global search for the RNAbinding surface on DENV RdRp. To this end, a library of mutant RdRps in the Y3H protein expression vector was created by

Mutazyme polymerase. The final optimized library contained an estimated 10<sup>5</sup> unique RdRp sequences with a 0.5% mutation rate. Following transformation into yeast expressing the 3'-SL RNA, 84 mutant RdRp sequences were retrieved from strongly growing yeast (the positive selection). Therefore, these mutants were not likely associated with RNA binding, and by deduction (see "Experimental Procedures"), RdRp regions that appeared intolerant to mutations could be discerned (Fig. 5A). Our approach minimized the false-negative binding selection that could stem from nonsense mutations and mutations that changed the local protein structure. Our analysis immediately highlighted two specific regions, including 10 residues surrounding Tyr-766 and Ile-850 residing in the C-terminal "thumb" domain of RdRp. Despite their distance in primary sequence, these two groups of residues are mapped onto the same region in the crystal structure of DENV RdRp (Fig. 5B) (21, 22). A third region encompassing Val-310 in the N terminus also appeared to be sensitive to mutations. The region is part of an interdomain linker joining fingers with thumb domains and was shown to be implicated in binding of the viral helicase NS3, as well as importin- $\beta$ , a nuclear import factor (23). We further analyzed 2446 DENV RdRp sequences from the NCBI database, combined with Y3H random mutagenesis, and mapped all variable residues onto the DENV RdRp structure (Fig. 5B, left panel). Strikingly, there was only a single invariant region on the molecular surface, and its area was capable of 3'-SL-TL accommodation. The putative 3'-SL-binding region possesses strong positively charged electrostatic surfaces (Fig. 5B, middle panel), and it is located at the rim of the helical bundle in the thumb domain separated from the active site in the palm domain by  $\sim$ 30 Å. There are no earlier reports of the RNA binding ability of the thumb domain nor structural similarities to any known RNA-binding modules via the DALI algorithm (24).

To pinpoint residues responsible for the RNA recognition, site-directed mutagenesis was conducted, yielding steep declines in 3'-SL-binding affinity in several cases; most strikingly, R770A, R773A, and R856A substitutions completely abrogated the interaction. Y838A and K841A mutations also had severely deleterious effects (Fig. 5C, left panel). The protein expression levels of these mutants were comparable with that of the wild type in yeast (Fig. 5C, right panel). These critical residues are strongly conserved in flaviviruses, with Arg-773 retained into Flaviviridae (Fig. 6C). Site-directed mutagenesis of RNA-binding residues in our DENV-2 replicon abolished viral replication at 4 days after transfections into BHK-21 cells, whereas mutations of irrelevant neighboring Trp-833 and Asp-881 residues showed few effects (Fig. 5D). EMSA studies with the recombinant R770A mutant corroborated these results, as binding to input RNAs was obviously weakened (Fig. 3), whereas the protein folding and polymerase activity of the mutant were retained (data not shown). These critical mutants also eliminated interactions with 5'-SLA in Y3H (data not shown), making it unlikely that more than one RNA-binding site exists in RdRp for simultaneous binding with two or more ACAG motifs. Our results emphasized an advantage of a combined Y3H random mutagenesis approach in discovering an RNA-binding motif without possible biases associated with

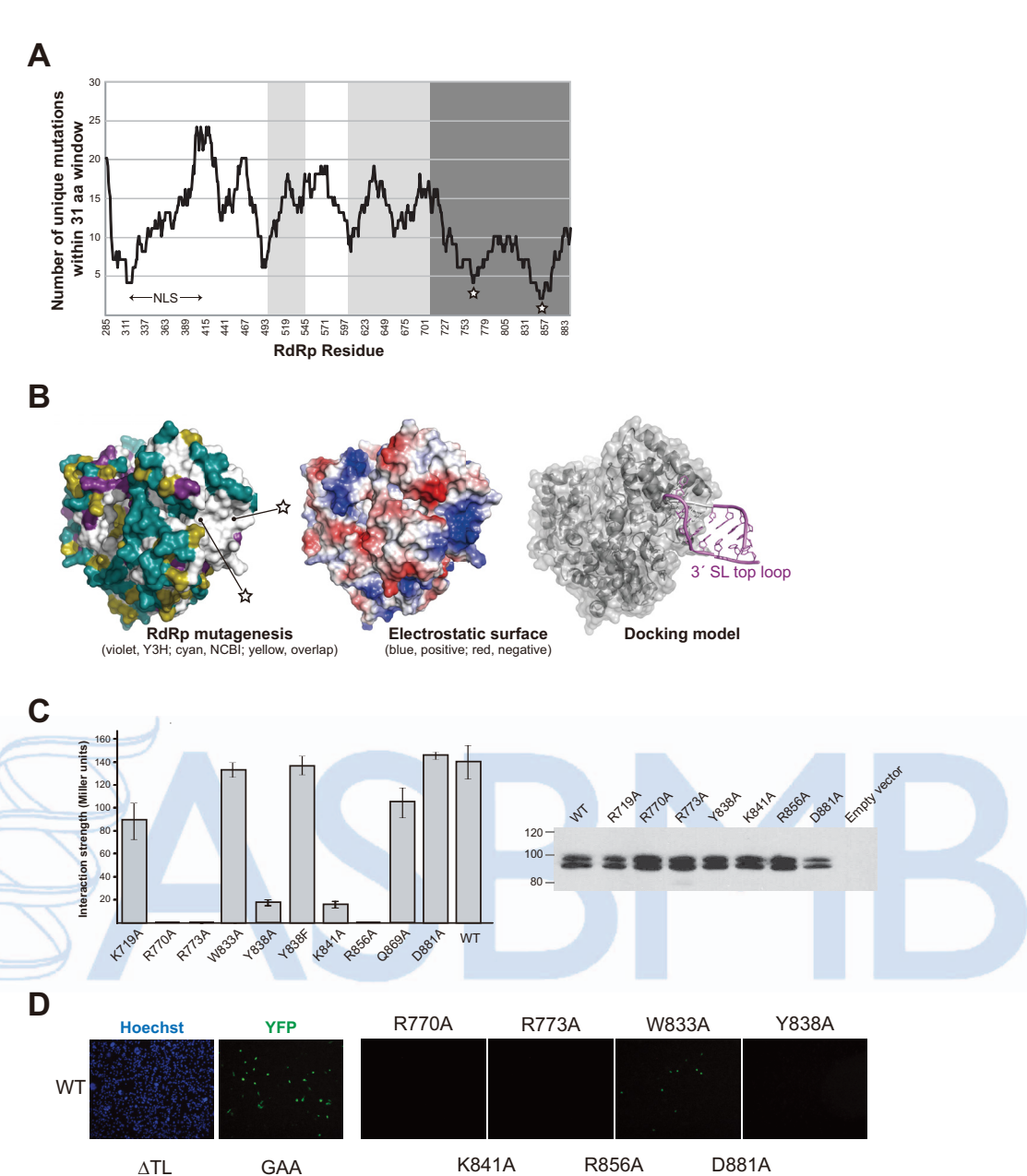


FIGURE 5. Exploration of 3'-SL-binding sites in RdRp using Y3H random mutagenesis. A, random RdRp mutants retaining SL-binding capacity were sequenced and analyzed as under "Experimental Procedures." Results show two specific regions of interest in the thumb domain (dark gray), which were highly susceptible to mutations (stars). White areas indicate the finger domain and light gray shows the palm domain. B, mutations allowing RdRp binding in Y3H are mapped onto the crystal structure (Protein Data Bank code 2J7W) in the left panel (violet), together with naturally occurring variations found in 2,446 DENV sequences from the NCBI database (cyan). Residues overlapping between the two data sets are shown in yellow. In the middle panel, the protein solvent-accessible surfaces were generated with the program APBS handled in PyMOL and are colored according to their electrostatic potential from red to blue. Our results prompted us to manually create an RNA-docking model using YFV SL structures (Protein Data Bank code 2KPC) (right panel). RdRP and SL-TL were manually docked on PyMOL to minimize steric clashes and to reproduce mutational studies. C, Miller assays for SL interactions with specific RdRp mutants are shown (left panel), together with their expression in yeast (right panel). We have no clear explanation for the double banding pattern that was occasionally observed. D, DENV replicon assay with RdRp mutants in BHK-21 cells. Viral replication was investigated via YFP signals 4 days after transfection to monitor RNA synthesis. YFP signals are shown for each mutant.  $\Delta$ TL refers to mutations that altered the 3'-SL top loop to the extent that RdRp binding was abrogated in Y3H (Fig. 2). GAA refers to an inactive RdRp by mutation of its catalytic triad, GDD.

mutagenesis strategies that are heavily reliant on conservation data or the assumption that particular amino acids (e.g. arginine and lysine) would be crucial in RNA interactions.

Our results allowed manual construction of an RNA-docking model based on available DENV-3 RdRp and YFV SL structures

(2J7W and 2KPC, respectively), without apparent severe clashes (Fig. 5B, right panel). Arg-773 lies inside the binding cleft and forms an in-line stack with three essential residues, Arg-770, Tyr-838, and Lys-841, likely creating a TL RNA-accommodating platform (Fig. 6D). A Y838F mutation did not

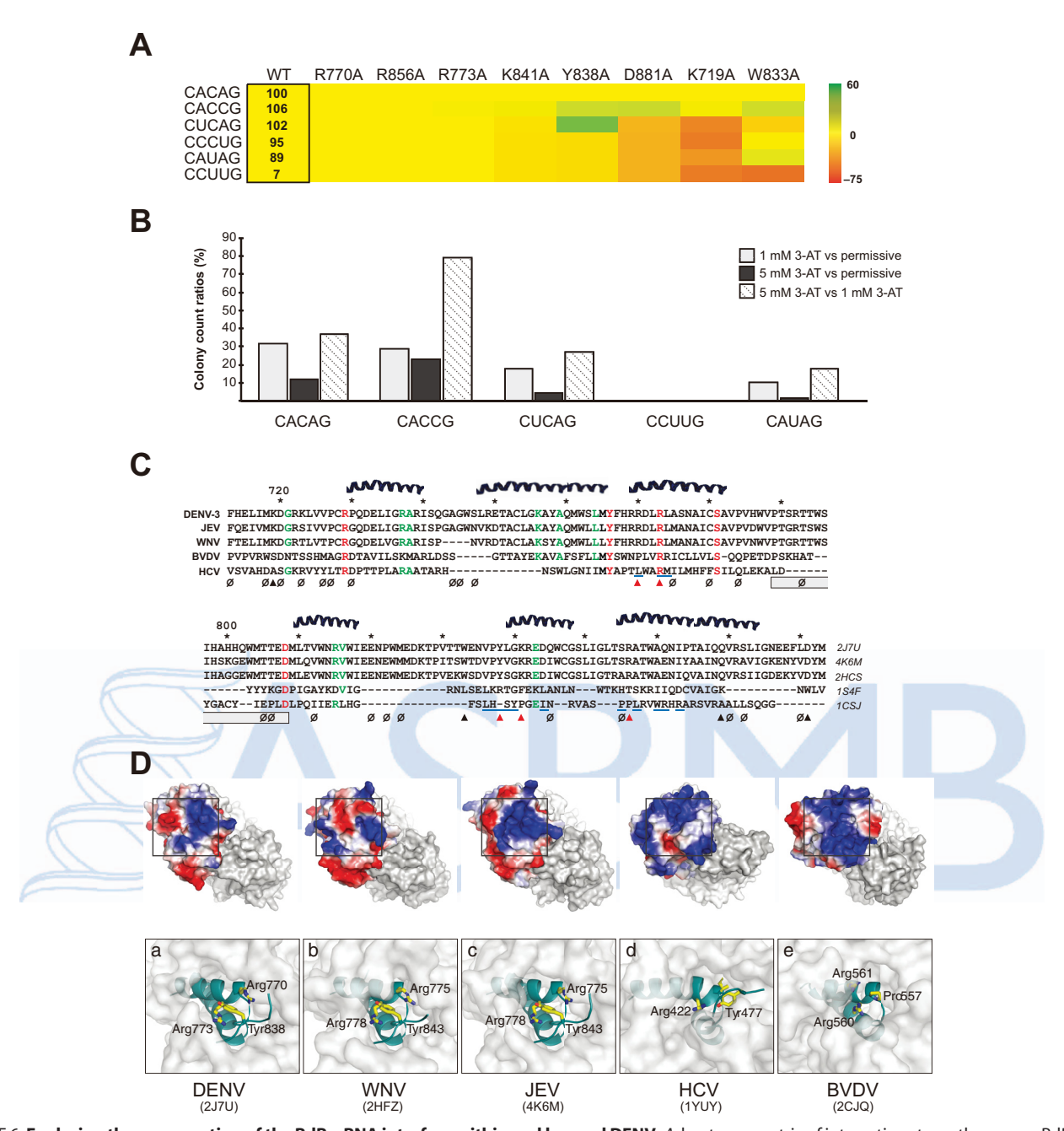


FIGURE 6. Exploring the conservation of the RdRp-RNA interface within and beyond DENV. A, heat map matrix of interaction strengths among RdRp and 3'-SL variants. Relative interaction strengths of 3'-SL variants with the DENV RdRp are shown in a box as a percentage of the wild-type (WT) RdRp-CACAG pair.  $Colors, indicating \ a\ 3'-SL-TL\ variant's\ sensitivity\ to\ protein\ alterations, were\ arrived\ at\ as\ follows:\ \%\ changes\ in\ interaction\ strengths\ between\ mutant\ RdRp\ and\ sensitivity\ to\ protein\ alterations, were\ arrived\ at\ as\ follows:\ \%\ changes\ in\ interaction\ strengths\ between\ mutant\ RdRp\ and\ sensitivity\ to\ protein\ alterations, were\ arrived\ at\ as\ follows:\ \%\ changes\ in\ interaction\ strengths\ between\ mutant\ RdRp\ and\ sensitivity\ to\ protein\ alteration\ strengths\ between\ mutant\ RdRp\ and\ sensitivity\ to\ protein\ alteration\ strengths\ between\ mutant\ RdRp\ and\ sensitivity\ to\ protein\ alteration\ strengths\ between\ mutant\ RdRp\ and\ sensitivity\ to\ protein\ alteration\ strengths\ between\ mutant\ RdRp\ and\ sensitivity\ to\ protein\ alteration\ strengths\ between\ mutant\ RdRp\ and\ sensitivity\ to\ protein\ alteration\ strengths\ between\ mutant\ RdRp\ and\ sensitivity\ to\ protein\ sensitivity\ sensitivity\ to\ protein\ sensitivity\ to\ protein\ sensitivity\ to\ protein\ sensitivity\ sensitivity\ to\ protein\ sensitivity\ sensitivity\$ 3'-SL variant combinations versus those of WT RdRp and 3'-SL variants are calculated. These percentage changes are then compared (via simple subtraction) to the relevant RdRp-CACAG interaction strengths. Numerous RNA variants, including some residing on the 5'-SLA, are not included on the table, as their interactions with RdRp were particularly weak. B, analysis of 3'-SL-TL's tolerance for mutations in Arg-773. A library of Arg-773 RdRp mutants (R773X) was examined via Y3H with five 3′-SL-TL variants under one permissive and two selective conditions. C, DALI structural alignments of the thumb domains from five available Flaviviridae RdRp structures. Residues with perfect conservation are colored in red, and ones that align in four sequences are green. The null symbols ( $\wp$ ) indicate mutations that had no effect in 3'-SL-binding in our Y3H random mutagenesis. Filled triangles point to residues that were chosen for site-directed mutagenesis, and red triangles indicate crucial residues in 3'-SL-TL-binding. HCV residues making contacts with thumb 2 inhibitors in previous studies are highlighted by blue lines. The gray rectangle shows the region that was deleted in an HCV structural study (45). D, superposition of five Flaviviridae RdRp structures reveals similarity in the SL-binding site of DENV RdRp comprising an Arg-770 – Tyr-838 – Arg-773 stacking platform. In all cases, two non-contiguous helices combine to form a positively charged pocket (blue) centering on a perfectly conserved Arg-773 in DENV.

affect SL binding activity, suggesting a key role of side-chain stacking in RNA recognition (Fig. 5C). The RNA-binding site is located adjacent to a bound zinc ion (~12 Å) in the thumb domain. According to our model, the last base of the ACAG motif is  $\sim$ 50 Å distant from the first base of the RNA template in the catalytic site of RdRp. Therefore, the distance formed by

the 42 bases downstream of the ACAG motif to the 3' end should be indispensable for enabling initiation of RNA synthesis in cis. Interestingly, the complex of RdRp with cirSL was more compact than that of linSL, i.e. sharp bands migrated faster in EMSA, implying that the 3' single-stranded region might make extensive contacts near the active site of RdRp (Fig. 3).

Conservation of the ACAG Motif Relates to Tolerance for RdRp Mutants-Next, we randomly mutated the ACAG sequence in the 3'-SL-TL and challenged it against RdRp in Y3H. Although 256 variants were generated, strong yeast growth on selective media was associated only with yeast containing either ACAG or ACCG sequences. We also generated several specific SL mutants that mimic some of the more common TL variants in Flaviviridae, e.g. the AUAG that is often found in pestiviruses. A number of these mutants interacted with RdRp at wild-type levels, raising the following question: if strong interactions are retained in several TL variants, what accounts for the strong conservation of ACAG in flaviviruses? Data gathered in experiments where TL variants were cotransformed with mutant RdRps offer the possible explanation that ACAG and ACCG are especially tolerant of mutations in the RNA-binding site of RdRp (Fig. 6A). For instance, although an R719A mutation minimally reduced affinity for wild-type 3'-SL, the same mutation nearly abrogated the interaction when TL was replaced by a UCAG sequence. Our "mutation tolerance" hypothesis is further corroborated by a cotransformation of a random library of Arg-773 mutants (R773X) with specific 3'-SL variants. Transformed yeasts were then grown under one permissive and two selective conditions. Colonies were counted on the various plates, and ratios between growth on selective versus less-selective conditions were calculated (Fig. 6B). In particular, the wild-type 3'-SL (CACAG) and R773X pair gave colony counts on 1 mm 3-AT media as 32% of the counts on permissive media and on strongly selective media as 12% of those on permissive media, whereas cotransformants of 3'-SL with AUAG in TL showed only 2% of permissive media counts, suggesting that ACAG tolerates a wider spectrum of Arg-773 mutations than AUAG. It is also noted that about 80% of the CACCG colonies that grew under 1 mm 3-AT were able to grow under 5 mm 3-AT conditions.

#### Discussion

We used an unbiased Y3H scan to probe the entire DENV genome for interactions with its polymerase, RdRp. Despite thousands of varying sequences in our Y3H RNA library, 12% of which included double-ligated products with an average size of 122 nt representing possible long range RNA-RNA contacts, the 3'-terminal stem-loop motif emerged as the dominant interactor. Although quite compact, the 3'-SL combination of RNA sequence and structure is certainly sufficient to eliminate most of the host RNAs from candidacy for polymerization. Indeed, the vast majority of catalogued RNA-binding proteins recognize short sequences (25) and, to a lesser extent, small structures (26).

Clues for importance of the 3'-SL-TL for RdRp interaction have been reported in previous works. Observations regarding the conserved nature and predicted structure of the 3'-SL CACAG pentanucleotide date back to 1986 (27). Of particular interest, Harris and co-workers (28) were able to reduce viral replication in BHK-21 cells by 1,000-fold upon silencing 3'-SL-TL with a 20-nt morpholino oligomer. Targeting of SLA also impeded viral replication, but the oligomer was complementary to the SLA lower stem, as opposed to the TL with which RdRp has been shown to interact using RNA footprinting

(6). At least two mutational studies on the 3'-SL-TL have been conducted in the case of WNV replicons, both of which revealed that various mutations severely limited viral replication, and one showed that replication, not translation, was affected (11, 29). Yet another WNV study showed complete abrogation of replicon replication when the CACAG pentanucleotide was replaced with UCUAG, implying that the CACAG bound the replicase (30). Other in vitro assays also showed RdRp interactions with the 3'-UTR in closely related viruses such as JEV (31). Contrary to earlier EMSA studies, we show that DENV RdRp formed a complex with 3'-SL in both genomic forms using in vitro EMSA and in vivo Y3H, consistent with a model in which RdRp remains bound to 3'-SL-TL in either genomic form. Although our results certainly did not exclude a role for 5'-SLA, multiple evidence from our results made it clear that 3'-SL must be included in the replication picture. Our results prompt scrutiny of the evidence supporting a role of genome cyclization in positioning the 3' terminus in proximity of the 5' promoter for initiation of replication (5). It should be noted that a balance between cyclized and linear forms has been suggested for numerous purposes, such as regulation of RNA synthesis versus translation to ensure generation of full-length RNA strands, and control of the ratio of positive to negative strands, and the timing of encapsidation (32-35). It was predicted that genome cyclization stimulates shortening of the 3'-SL lower stem, releasing the 3' terminus as a short single-stranded form (20). The location of the 3'-SL-TLbinding interface with respect to both the catalytic region and the 3' terminus thus should allow a higher level of replication after the particular viral event of cyclization by providing access of the free 3' end of viral genome to the active site (Fig. 7). DENV and HCV studies also support our idea, showing that subtle alterations in length and strandedness (single versus double) of the 3' templates could drastically stimulate *in vitro* RdRp activities (36, 37).

Sequence alignments of the SL-TL among flaviviruses show that the CACAG pentanucleotide is particularly conserved, with occasional substitutions at the 4th nucleotide (e.g. JEV: Muar HM596272, A-C, Fig. 1D). The motif is even found in tick-borne encephalitis flavivirus. Moreover, a CACAG or CAUAG sequence is often observed in the 3'-SL-TL in bovine viral diarrhea virus, a pestivirus. A perfectly conserved CACAG also resides in a stem-loop in hepacivirus; interestingly, the sequence exists in an RdRp-coding region that has been implicated in interactions with RdRp protein (38) and is fundamental for viral replication possibly via both RNA-RNA and RdRp-RNA interactions (39). The pattern may even extend beyond Flaviviridae, as an ACAG sequence has been identified in a brome mosaic virus subgenomic promoter, with point mutations to the 5'-A, -C, and -G greatly diminishing RdRp activity; however, the recognition mechanism appears to be purely sequence-dependent (40). In our work, a number of CACAG variants (e.g. CAUAG) bound to DENV RdRp with comparable affinity. We would not confine the motif's sole function to RdRp binding as, for instance, the CACAG motif in HCV is assumed to pair with a complementary sequence in the 3'-UTR to form a kissing loop (39). However, an unrecognized mechanism for RNA sequence conservation emerged when we paired SL and

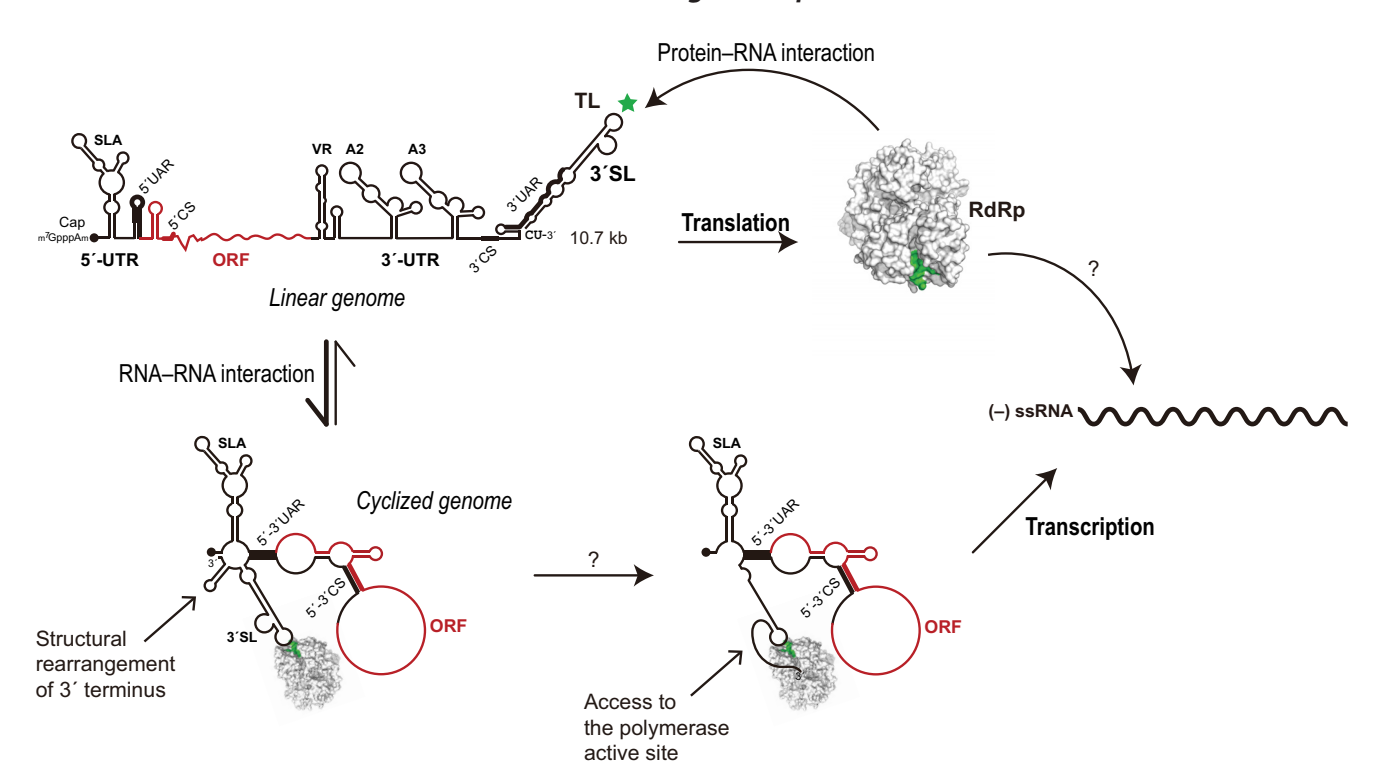


FIGURE 7. Schematic model of DENV replication based on our results coupling with earlier studies. We propose that the structural rearrangements in both polymerase and the 3' end region of genomic RNA upon binding of RdRp to the 3'-SL-TL and genomic cyclization play key roles in regulation of viral replication cycle. Accurate mechanisms for recruitment of the 3' end into the active site of RdRp as well as recognition of the negative stranded genome by RdRp still remain elusive.

RdRp mutants in a Y3H context and found that multiple 3'-SL-TL variants were intolerant to RdRp mutations, although the 3'-SL-TL with ACAG appeared able to withstand some of these alterations. Consistently, ACAG is more resistant to RdRp harboring randomly mutated Arg-773 than AUAG. In other words, ACAG confers the most optimal chance for viral RdRp to specifically interact with RNA under mutational pressure. However, considerably more work involving extensive mutagenesis of both RdRp and the SL-TL would be required to firmly establish such a mutational tolerance hypothesis.

To date, RdRp structures from five Flaviviridae, DENV, WNV, JEV, bovine viral diarrhea virus, and HCV, have been determined (21, 41-44). In all cases, a strongly positively charged RNA-binding cleft encompassing Arg-773 in DENV is obvious. Moreover, analogous stacking arrangements with adjacent arginine and tyrosine residues are also present (Fig. 6, C and D). Intriguingly, the DENV SL-TL-binding site entirely coincides with the binding sites of "thumb 2" inhibitors against HCV RdRp, and numerous direct protein-inhibitor contacts were made with residues corresponding to critical DENV residues identified in this study (Fig. 6C). This coincidence is indicative of the inhibitory action in which RNA binding is impeded, resulting in defects in viral RNA synthesis. In at least one case, an HCV inhibitor that binds to homologous SL-binding region causes a shift from a closed to open RdRp conformation (43). The recent achievement in solving an HCV RdRp complexed with double-stranded RNA revealed that the elimination of a  $\beta$ -hairpin loop spanning residues 442–454 (Fig. 6C), corresponding approximately to residues Pro-789-Met-804 in DENV, induces significant conformational changes to an open

form with a 20° rotation of the thumb domain, allowing primertemplate RNA duplex access to the catalytic core (45). Taken together, it is tempting to speculate that SL binding stimulates structural rearrangement of the thumb domain, thereby providing template RNA access to the active site and initiating de novo RNA synthesis in vivo (Fig. 7). Although RdRp has been demonstrated to promiscuously utilize numerous short templates in optimized in vitro environments, this lack of fidelity could likely prove disastrous in the complex RNA-saturated world of the cell, where the presence of random dsRNA initiates an antiviral response (46), necessitating the strong discriminatory mechanism that the promoter provides in the absence of a primer.

Our finding of strong conservation of the promoter interface in flaviviruses suggests that it could serve broadly as a drug target, although its specificity and the apparent lack of eukaryotic homologs should minimize off-target effects. In addition, interception of the interactive interfaces should reduce chances of mutational resistance because viral adaptation has to synchronously occur in both protein and RNA molecules. Conceivably, once DENV RdRp's spatial and temporal relation with its RNA targets is more fully delineated, principles of viral replication that extend well beyond Flaviviridae may be unveiled.

#### **Experimental Procedures**

Molecular Cloning—Viral RNA was isolated from DENV-2 strain 16681 and used to generate full-length cDNA according to the SuperScript III procedure (Life Technologies, Inc.). The 5' and 3' halves of the DENV genome were amplified using TaKaRa Ex Taq polymerase and inserted into the pSC-A vector

between SacI and XbaI sites with the StrataClone PCR cloning kit (Stratagene). Clones were blue-white screened and validated by DNA sequencing.

Plasmids containing the 5' half of the DENV-2 genome (bases 1-5428) or 3' half (5429-10723) were used as PCR template in the presence of dUTP prior to random fragmentation with endonuclease-V to ~100 bp according to Dyson's protocol (10). In brief, no more than 5  $\mu$ g of PCR products were treated in 2× fragmentation buffer (20 mm HEPES-KOH, pH 7.4, 100 mm NaCl, 1 mm MnCl<sub>2</sub>) and 6 units of endonuclease-V (New England Biolabs) for 15 h at 37 °C. The fragmented DNA pool was excised from 1.5% agarose gel and then blunted with 2 units of T4 DNA polymerase (New England Biolabs) at 12 °C for 30 min, followed by heat inactivation at 75 °C for 20 min.

Ligation of fragments directly into a Smal-digested and dephosphorylated pIIIA MS2 vector (9.1 kb) was found to be very inefficient. To overcome this difficulty, a Gateway-based protocol (Invitrogen) was devised to generate the desired final vectors for Y3H studies. To this end, a 3.7-kbp compact entry vector was created by inserting the MS2-2 region (925 bp) of the standard Y3H pIIIA MS2-2 plasmid, necessary for RNA expression, into the pCR8/GW/TOPO vector (Invitrogen). Subsequently, DENV-2 DNA fragments were blunt-end cloned into this entry vector at its SmaI site. A second SmaI digestion of the ligated products prior to the transformation effectively eliminated all empty vectors, giving rise to nearly 100% cloning efficiency. This step was enabled by the fact that the pCR8/MS2-2 vector's sole SmaI site is eliminated in the ligation reaction and by the fact that DENV-2 DNA contains only one Smal site. Concurrently, a destination vector containing the remainder of the pIIIA MS2-2 backbone was constructed with the Gateway Vector Conversion System (Invitrogen). Gateway recombination finally generated Y3H pIIIAMS2-2 vectors with genomic fragment inserts.

Y3H protein expression vectors containing the full DENV-2 NS5 protein or its RdRp subunit alone (beginning from Pro272) were constructed into the pACT2 vector between BamHI and XhoI restriction sites downstream of the gal4 activation domain. Several linear forms of DENV UTR RNAs were amplified from the cDNA, and blunt-end cloned into the pIIIA MS2-2 vector at the Smal site. The cyclized form of DENV UTR RNA was constructed via a two-step PCR procedure, by which the full 5'-UTR and the 3'-SL and CS regions were individually amplified and joined together via PCR ligation. Mutations were introduced into SL and the cyclized UTR through the QuikChange protocol (Stratagene). Earlier Y3H studies have shown that long poly-U stretches diminish Y3H signals, as RNA polymerase III is known to terminate at these repeats, eliminating key Y3H features that are required for retention of the transcript in the yeast nucleus (47). To avoid premature termination by the presence of a tandem U sequence in the SLB stem of the 5'-UTR of our cyclization-mimic, we introduced a single cytosine within the middle of the poly-U tract (U>C in Fig. 2), resulting in a 3-fold increase in NS5 and RdRp apparent affinity.

Validation of DENV RNA Library—Following DNA sequencing of 100 clones, the RNA library was found to possess an average insert length of 95 nt. 49% of the sequences were of positive orientation. None of the sequences were identical, giving a 50% probability that at least 7,200 sequences were present in the library based on the "reverse birthday problem" (i.e. if, on another planet, none of the 100 students in a room have the same birthday, what is the minimum likely length of a year?). The solution is approximated as shown in Equation 1,

$$Pr(n, m) \approx 1 - e^{-m^2/2n}$$
 (Eq. 1)

where the desired probability is Pr; m corresponds to the number of non-identical sequences identified, and *n* is the number of sequences expected in the library at the input probability.

Coverage of the genome could be checked by two means. First, a Monte-Carlo-based algorithm was employed to simulate random placement of these sequences on the genome (21.4) kb when the minus strand is considered). Predicted random sequence coverage could then be compared with actual sequence coverage; our library showed greater coverage than 19% of computer-generated outcomes. Second, the single most strongly binding RNA motif was found in 15 non-identical sequences following probing of the library with RdRp, suggesting a high level of coverage. Therefore, the efficient generation of a quality RNA library of DENV covering both 10.7-kb (+)and (-)-strands was demonstrated for the first time.

Random Mutagenesis of RdRp-PCR-based random mutagenesis was conducted to generate mutant RdRp products with the GeneMorph II EZCLone domain mutagenesis kit (Stratagene). In brief, specific primers upstream and downstream of the RdRp insert, 5'-AAACCTAGATATAATTGGG-AAAAGAATAG-3' and 5'-CCACAGAACTCCTGCTTCT-CCC-3', were used to introduce random mutations into the 1.9-kb PCR product via Mutazyme DNA polymerase. Varying the initial amount of DNA template from 361 to 0.95 ng was necessary to obtain the appropriate mutational rate. Products of error-prone PCR serving as megaprimers were then incorporated into the Gateway entry vector by swapping the existing wild-type with the mutants to create a random library. Initial sequencing verified an even distribution of mutations along RdRp. It was found that frameshifts caused by deletions and substitutions were common at high mutation rates, and therefore, a 0.5% nucleotide mutation rate was settled on. In vitro recombination between Gateway entry vectors carrying the mutant library and the destination vector carrying the pACT2 backbone was catalyzed through the Gateway LR Clonase II enzyme mix kit (Invitrogen), yielding a mutant RdRp library in a Y3H-suitable expression vector. Yeasts containing the Y3H DENV SL RNA expression vector were then transformed with the protein mutant library onto selective plates, and colony PCR was performed on strongly growing yeast to isolate the mutant sequences.

Y3H Screen—Yeast transformations were carried out with YBZ1 strain using the standard lithium acetate method. Single step co-transformation with 2–3  $\mu$ g of each plasmid per 200  $\mu$ l of yeast suspension was preferred over two single transformation steps, reducing background, and minimizing opportunities for genome or plasmid mutations. Yeast growth was initially screened on weakly selective Leu<sup>-</sup>/His<sup>-</sup> plates. Subsequently, interaction candidates were subjected to more selective conditions of Leu-/Ura-/His with increasing concentrations of

3-AT, a histidine metabolism inhibitor, as high as 25 mm. Plasmid pAD-IRP (pACT2 with a rabbit IRP domain insert) was used as a positive control in conjunction with the RNA expression plasmid pIIIA-IRE, containing the rat ferritin light chain IRE. Numerous negative controls were used to ensure that RNA-independent or protein-independent activation of reporter expression did not occur (e.g. single transformants, pACT2-RdRp co-transformed with pIIIA-IRE). In the case of the Y3H library, colony PCR was employed to obtain sequences of interactors. Colony counts were performed with ImageJ software.

The 2-nitrophenyl  $\beta$ -D-galactopyranoside (ONPG)-based Miller assay was used to quantify interaction strengths of protein-RNA pairs and to confirm that screening results based on expression of HIS3 reporter gene were not spurious. The assays were performed at least in triplicate as earlier described (48) with slight modifications. In brief, 1-ml yeast cultures grown to  $0.5-1.0~A_{600}$  were harvested and permeabilized in 220  $\mu$ l of solution containing  $\sim$ 23% chloroform, 0.03% 2-mercaptoethanol, and 0.01% SDS. 700  $\mu$ l of 1 mg/ml ONPG was added to the lysate, and the reactions were quenched with 500  $\mu$ l of 1 M  $Na_2CO_3$  prior to measurement of  $A_{420}$ . The Miller assay formula is  $(1000 \times A_{420})/(A_{600} \times V \times \text{time})$ , where V is the reaction volume and time is in minutes.

In Vitro EMSA-Non-tagged and N-terminally hexahistidine-tagged DENV-2 RdRp (NS5 residues 277-900) was prepared as described earlier in our report (17). Five RdRp mutations that severely impaired SL binding in Y3H were also generated via the QuikChange procedure, but only R770A showed comparable protein expression and solubility levels to the wild type. To avoid misinterpretation that might be caused by a structural alteration in protein, in *in vitro* assays only the recombinant R770A mutant was pursued. The folding of purified R770A was further assessed by circular dichroism (CD). Purified RdRp was stored in 10% glycerol-containing buffer at −80 °C until use. DENV-2 RNAs, including 5'-UTR (nucleotides 1-159), SLA (nucleotide 1-69), cirSL (nucleotides 10,657–10,723), and linSL (nucleotides 10,646–10,723), were generated by in vitro transcription using T7 RNA polymerase. In the case of biotin labeling, the transcription reaction consisted of 1 part biotinylated UTP (Thermo Scientific catalog no. AM8450, carrying an 11-carbon linker) to 3 parts UTP, which should give a mean of 4 biotin moieties per transcript. Transcripts were purified via gel excision and refolded while in 0.3 M NaOAc, pH 6.0, 0.5 mm EDTA, 5 mm Mg(OAc)<sub>2</sub>, and 0.1% SDS overnight at 4 °C.

The RdRp-RNA interaction was determined by EMSA. The binding reaction (10  $\mu$ l) was performed by mixing 37.5 or 50 pmol of RNAs with increasing concentrations of the RdRp protein in a binding buffer consisting of 50 mm Tris-HCl, pH 8.8, 10 mm Mg(OAc)<sub>2</sub>, 65 mm NH<sub>4</sub>OAc, 1 mm EDTA, 1 unit of RNase inhibitor, and 5% glycerol at room temperature for 20 min. RdRp-RNA complexes were resolved on native 5% polyacrylamide gels supplemented with 5% glycerol at 4 °C. Gels were stained by ethidium bromide and Coomassie Blue to visualize RNA and protein, respectively. It was noted that the DENV-2 RdRp protein alone scarcely migrated into the native gel due to its relatively large size (73.2 kDa) and high pI (> 8.0).

*In Vitro Alpha Assay*—Alpha Screen histidine (nickel chelate) detection kit (PerkinElmer Life Sciences) was exploited in this study. 5'-Biotinylated RNAs were purchased from Integrated DNA Technologies (Coralville, IA), including truncated SL (Bi-miniSL, 5'-biotin-ACAGCAUCAUUCCAGGCACAGAA-CGCCAGAAAAUGGAAUGGUGCUG), truncated SL with deletion in the top loop (Bi-miniSLΔTL, 5'-biotin-ACAGCA-UCAUUCCAGGCACGCCAGAAAAUGGAAUGGUGCUG), and truncated SLA (Bi-miniSLA, 5'-biotin-ACUACGUGGAC-CGACAAAGACAGAUUCUUUGAGGGAGCUAAGCUCA-ACGUAG). All RNAs were pre-heated at 70 °C for 3 min, and then slowly cooled to room temperature in a folding buffer (20 mм HEPES, pH 7.4, 50 mм NaCl, 2 mм EDTA) before use. All assays were performed in 384-well white-gray Alpha Plates (PerkinElmer Life Sciences; catalog no. 6005350) in 25-μl reactions at room temperature. Initially, assay conditions were extensively optimized by cross-titration between protein and RNA concentrations to yield the maximum Alpha signal and to determine the "hooking zone," where quenching of the signal is observed due to an excess of the binding partner. 200 nm RdRp and RNA (total 12  $\mu$ l) were incubated in the reaction mixture containing 25 mm HEPES, pH 7.4, 100 mm NaCl, 2 mm MgCl<sub>2</sub>, and 0.1% BSA for 30 min. Then the nickel-chelated acceptor beads (30 µg/ml final concentration) were added and incubated in the dark for 30 min, following by addition of the streptavidin donor beads (20 µg/ml final concentration) and a 30-min incubation in the dark before the assay was conducted on an EnSpire<sup>TM</sup> 2300 Multilabel Plate Reader (PerkinElmer Life Sciences). Equilibrium dissociation constants  $(K_d)$  between SL and RdRp were quantified from the saturation binding experiments. The data were then fitted on a nonlinear regression curve by using the one-site binding mode in GraphPad Prism software (San Diego).

The Alpha competition assay was performed in a 25-µl reaction with non-biotinylated RNAs as competitor. 200 nm Histagged RdRp was allowed to react with RNA competitors in various concentrations ranging from 0.01 to 250 nm at room temperature for 20 min. Bi-miniSL RNA was then added to 10 nm and reacted for 30 min. The signal was developed as mentioned above with 30  $\mu$ g/ml acceptor and 20  $\mu$ g/ml donor beads.

Replicon Construction—Full-length DENV-2 16,681 cDNA (10,723 bp) in the pUC19 vector was used for construction of the DENV-2 replicon in this study. The pre-M/E genes were replaced by the YFP gene fused with autoproteolytic FMDV 2A sequence from foot and mouth disease virus, and the natural junction cleavage sites, C/preM and E/NS1, were retained for maintaining the proteolytic processing of polyprotein (49). All DENV replicon mutants in this study were constructed by QuikChange site-directed mutagenesis and confirmed by sequencing.

RNA Transcription, Transfection, and Fluorescence Imaging— DNA templates for the in vitro run-off transcription were generated by PCR with the forward primer, 5'-GAAAT<u>TAAT-</u> ACGACTCACTATTAGTTGTTAGTCTACGTGGACCGAC-3', carrying the T7 promoter sequence (underline), and the reverse primer, 5'-AGAACCTGTTGATTCAACAGCACC-3', and purified using the QIAquick gel extraction kit (Qiagen). DENV replicon RNAs were synthesized using the RiboMAX large scale RNA production system kit (Promega) with the fol-

tapraid4/zbc-bc/zbc-bc/zbc03516/zbc4983-16z

lowing optimized protocol: the 50-µl reaction mixtures containing 7.5 mm each GTP, CTP, and UTP, 2 mm ATP, 3 mm  $m^7$ GpppA cap analog (New England Biolabs), and 5  $\mu$ g of DNA template were incubated for 4 h at 37 °C. DNA templates were eliminated by DNase I treatment, and subsequently, transcripts were purified using RNeasy mini kit (Qiagen). Transcribed RNA quality was analyzed by gel electrophoresis. 500 ng of replicon RNAs were transfected with Lipofectamine 2000 (Invitrogen) according to the manufacturer's instructions into BHK-21 cells plated in a 24-well plate with  $2 \times 10^4$  cells/well. After 4 days, cells were fixed, stained with Hoechst 33258, and imaged. At this late stage, the YFP signal is indicative of the level of viral RNA synthesis inside the cell (12).

Bioinformatics—To calculate the probability that known recombination regions coincide with RdRp interaction sites, we first noted that 43 out of 60 interaction points fell within known recombination points. We asked the following question. What is the probability that 43 (or more) interaction points fall within the known recombination regions (that occupy 30.3% of the genome)? We then used the probability mass function for the calculation. If DI joining points are included in the calculation, the probability diminishes to  $2.6 \times 10^{-15}$ . If we view clusters, instead of individual sequencing results, there are 13 clusters, 6 of which land in recombination regions, p = 0.17. If DI joining points are considered, p = 0.019.

Li et al. (16) have underlined the sequences where 5'-3'joining occurred to form DI particles in a previous study. To account for the possibility that joining may have occurred at the 5' or 3' ends of an ACA sequence, we extended these joining point sequences by 6 nt (3 nt to each side) and calculated the probability that a specific 3-nt sequence could be found in the extended joining points. Under these parameters, there are 152 frames in which ACA could be found. We then applied the probability mass function to determine the probability that ACA occurs 8 (or more) times in 152 possible frames, with a probability of 0.0156 (1/64) in any particular frame (assuming a G/C ratio of 1.0). Similarly, ACAG is seen 4 times in 124 possible frames with a probability of 0.0039 of appearing in any particular frame. These are conservative estimates, as the calculations assume that, for example, two ACA sequences could be found in a 4-nt sequence (which is not possible).

To determine RdRp regions that were insensitive to mutations introduced via random mutagenesis (Fig. 5A), all mutant sequences from strongly growing yeast were aligned, and only unique mutations were counted and tallied in each alignment column. These tallies were summed over all possible 31 column windows (15 to the left + 1 + 15 to the right of the "center" amino acid) and plotted residue-by-residue. This method is actually a simplification of a protocol previously developed in our laboratory (50). Programs relating to Monte Carlo-based determination of RNA library quality and for calculating the sequence-to-sequence volatility of all N-nucleotide motifs in a database were created in-house.

Author Contributions—S. C. designed the study; K. H., C. T., and M. K. performed the experiments and analyzed the data; P. Y. and T. L. provided materials and advice; S. C., K. H., and C. T. wrote the manuscript, which was commented on by all authors.

Acknowledgments—We thank Prof. Marvin Wickens for kindly providing Y3H plasmids and Sasiprapa Khunchai for sharing Y2H methods and experience. We also thank Nunghatai Sawasdee is for managerial assistance.

#### References

- 1. Dreher, T. W., and Hall, T. C. (1988) Mutational analysis of the sequence and structural requirements in brome mosaic virus RNA for minus strand promoter activity. J. Mol. Biol. 201, 31-40
- 2. Song, C., and Simon, A. E. (1995) Requirement of a 3'-terminal stem-loop in in vitro transcription by an RNA-dependent RNA polymerase. J. Mol. Biol. 254, 6-14
- 3. Oh, J. W., Sheu, G. T., and Lai, M. M. (2000) Template requirement and initiation site selection by hepatitis C virus polymerase on a minimal viral RNA template. J. Biol. Chem. 275, 17710-17717
- 4. Cui, T., and Porter, A. G. (1995) Localization of binding site for encephalomyocarditis virus RNA polymerase in the 3'-noncoding region of the viral RNA. Nucleic Acids Res. 23, 377-382
- 5. Filomatori, C. V., Lodeiro, M. F., Alvarez, D. E., Samsa, M. M., Pietrasanta, L., and Gamarnik, A. V. (2006) A 5' RNA element promotes dengue virus RNA synthesis on a circular genome. Genes Dev. 20, 2238-2249
- 6. Filomatori, C. V., Iglesias, N. G., Villordo, S. M., Alvarez, D. E., and Gamarnik, A. V. (2011) RNA sequences and structures required for the recruitment and activity of the dengue virus polymerase. J. Biol. Chem. 286, 6929 - 6939
- 7. Hook, B., Bernstein, D., Zhang, B., and Wickens, M. (2005) RNA-protein interactions in the yeast three-hybrid system: affinity, sensitivity, and enhanced library screening. RNA 11, 227-233
- Wurster, S. E., and Maher, L. J., 3rd. (2010) Selections that optimize RNA display in the yeast three-hybrid system. RNA 16, 253-258
- 9. Sassanfar, M., and Szostak, J. W. (1993) An RNA motif that binds ATP. Nature 364, 550 - 553
- 10. Dyson, M. R., Perera, R. L., Shadbolt, S. P., Biderman, L., Bromek, K., Murzina, N. V., and McCafferty, J. (2008) Identification of soluble protein fragments by gene fragmentation and genetic selection. Nucleic Acids Res.
- 11. Tilgner, M., Deas, T. S., and Shi, P. Y. (2005) The flavivirus-conserved penta-nucleotide in the 3' stem-loop of the West Nile virus genome requires a specific sequence and structure for RNA synthesis, but not for viral translation. Virology 331, 375-386
- 12. Manzano, M., Reichert, E. D., Polo, S., Falgout, B., Kasprzak, W., Shapiro, B. A., and Padmanabhan, R. (2011) Identification of cis-acting elements in the 3'-untranslated region of the dengue virus type 2 RNA that modulate translation and replication. J. Biol. Chem. 286, 22521-22534
- 13. Zuker, M. (2003) Mfold web server for nucleic acid folding and hybridization prediction. Nucleic Acids Res. 31, 3406-3415
- 14. Chen, S. P., Yu, M., Jiang, T., Deng, Y. Q., Qin, C. F., Han, J. F., and Qin, E. D. (2008) Identification of a recombinant dengue virus type 1 with 3 recombination regions in natural populations in Guangdong province, China. Arch. Virol. 153, 1175-1179
- 15. Chuang, C. K., and Chen, W. J. (2009) Experimental evidence that RNA recombination occurs in the Japanese encephalitis virus. Virology 394,
- 16. Li, D., Lott, W. B., Lowry, K., Jones, A., Thu, H. M., and Aaskov, J. (2011) Defective interfering viral particles in acute dengue infections. PloS one 6,
- 17. Kamkaew, M., and Chimnaronk, S. (2015) Characterization of soluble RNA-dependent RNA polymerase from dengue virus serotype 2: the polyhistidine tag compromises the polymerase activity. Protein Expr. Purif. **112,** 43–49
- 18. Bernstein, D. S., Buter, N., Stumpf, C., and Wickens, M. (2002) Analyzing mRNA-protein complexes using a yeast three-hybrid system. Methods 26,
- 19. D'Agostino, V. G., Adami, V., and Provenzani, A. (2013) A novel high throughput biochemical assay to evaluate the HuR protein-RNA complex formation. PLoS One 8, e72426



- 20. Sztuba-Solinska, J., Teramoto, T., Rausch, J. W., Shapiro, B. A., Padmanabhan, R., and Le Grice, S. F. (2013) Structural complexity of Dengue virus untranslated regions: cis-acting RNA motifs and pseudoknot interactions modulating functionality of the viral genome. Nucleic Acids Res. **41,** 5075–5089
- 21. Yap, T. L., Xu, T., Chen, Y. L., Malet, H., Egloff, M. P., Canard, B., Vasudevan, S. G., and Lescar, J. (2007) Crystal structure of the dengue virus RNA-dependent RNA polymerase catalytic domain at 1.85-angstrom resolution. J. Virol. 81, 4753-4765
- 22. Noble, C. G., Lim, S. P., Chen, Y. L., Liew, C. W., Yap, L., Lescar, J., and Shi, P. Y. (2013) Conformational flexibility of the Dengue virus RNA-dependent RNA polymerase revealed by a complex with an inhibitor. J. Virol. 87, 5291-5295
- 23. Brooks, A. J., Johansson, M., John, A. V., Xu, Y., Jans, D. A., and Vasudevan, S. G. (2002) The interdomain region of dengue NS5 protein that binds to the viral helicase NS3 contains independently functional importin  $\beta$ 1 and importin  $\alpha/\beta$ -recognized nuclear localization signals. J. Biol. Chem. 277, 36399 - 36407
- 24. Holm, L., and Rosenström, P. (2010) Dali server: conservation mapping in 3D. Nucleic Acids Res. 38, W545-W549
- 25. Cook, K. B., Kazan, H., Zuberi, K., Morris, Q., and Hughes, T. R. (2011) RBPDB: a database of RNA-binding specificities. Nucleic Acids Res. 39, D301-D308
- 26. Auweter, S. D., Oberstrass, F. C., and Allain, F. H. (2006) Sequence-specific binding of single-stranded RNA: is there a code for recognition? Nucleic Acids Res. 34, 4943-4959
- 27. Brinton, M. A., Fernandez, A. V., and Dispoto, J. H. (1986) The 3'-nucleotides of flavivirus genomic RNA form a conserved secondary structure. Virology 153, 113-121
- 28. Holden, K. L., Stein, D. A., Pierson, T. C., Ahmed, A. A., Clyde, K., Iversen, P. L., and Harris, E. (2006) Inhibition of dengue virus translation and RNA synthesis by a morpholino oligomer targeted to the top of the terminal 3' stem-loop structure. Virology 344, 439 – 452
- 29. Elghonemy, S., Davis, W. G., and Brinton, M. A. (2005) The majority of the nucleotides in the top loop of the genomic 3' terminal stem loop structure are cis-acting in a West Nile virus infectious clone. Virology 331, 238 – 246
- 30. Khromykh, A. A., Kondratieva, N., Sgro, J. Y., Palmenberg, A., and Westaway, E. G. (2003) Significance in replication of the terminal nucleotides of the flavivirus genome. J. Virol. 77, 10623-10629
- 31. Chen, C. J., Kuo, M. D., Chien, L. J., Hsu, S. L., Wang, Y. M., and Lin, J. H. (1997) RNA-protein interactions: involvement of NS3, NS5, and 3' noncoding regions of Japanese encephalitis virus genomic RNA. J. Virol. 71, 3466 - 3473
- 32. Khromykh, A. A., Meka, H., Guyatt, K. J., and Westaway, E. G. (2001) Essential role of cyclization sequences in flavivirus RNA replication. J. Virol. 75, 6719 - 6728
- 33. Villordo, S. M., Alvarez, D. E., and Gamarnik, A. V. (2010) A balance between circular and linear forms of the dengue virus genome is crucial for viral replication. RNA 16, 2325-2335
- 34. Hahn, C. S., Hahn, Y. S., Rice, C. M., Lee, E., Dalgarno, L., Strauss, E. G., and Strauss, J. H. (1987) Conserved elements in the 3' untranslated region of flavivirus RNAs and potential cyclization sequences. J. Mol. Biol. 198,
- 35. Proutski, V., Gould, E. A., and Holmes, E. C. (1997) Secondary structure of

- the 3' untranslated region of flaviviruses: similarities and differences. Nucleic Acids Res. 25, 1194-1202
- 36. You, S., and Padmanabhan, R. (1999) A novel in vitro replication system for Dengue virus. Initiation of RNA synthesis at the 3'-end of exogenous viral RNA templates requires 5'- and 3'-terminal complementary sequence motifs of the viral RNA. J. Biol. Chem. 274, 33714-33722
- 37. Kao, C. C., Yang, X., Kline, A., Wang, Q. M., Barket, D., and Heinz, B. A. (2000) Template requirements for RNA synthesis by a recombinant hepatitis C virus RNA-dependent RNA polymerase. J. Virol. 74, 11121-11128
- 38. Cheng, J. C., Chang, M. F., and Chang, S. C. (1999) Specific interaction between the hepatitis C virus NS5B RNA polymerase and the 3' end of the viral RNA. J. Virol. 73, 7044-7049
- 39. Friebe, P., Boudet, J., Simorre, J. P., and Bartenschlager, R. (2005) Kissingloop interaction in the 3' end of the hepatitis C virus genome essential for RNA replication. J. Virol. 79, 380-392
- 40. Siegel, R. W., Adkins, S., and Kao, C. C. (1997) Sequence-specific recognition of a subgenomic RNA promoter by a viral RNA polymerase. Proc. Natl. Acad. Sci. U.S.A. 94, 11238-11243
- 41. Malet, H., Egloff, M. P., Selisko, B., Butcher, R. E., Wright, P. J., Roberts, M., Gruez, A., Sulzenbacher, G., Vonrhein, C., Bricogne, G., Mackenzie, J. M., Khromykh, A. A., Davidson, A. D., and Canard, B. (2007) Crystal structure of the RNA polymerase domain of the West Nile virus non-structural protein 5. J. Biol. Chem. 282, 10678-10689
- 42. Lu, G., and Gong, P. (2013) Crystal structure of the full-length Japanese encephalitis virus NS5 reveals a conserved methyltransferase-polymerase interface. PLoS Pathog. 9, e1003549
- Biswal, B. K., Cherney, M. M., Wang, M., Chan, L., Yannopoulos, C. G., Bilimoria, D., Nicolas, O., Bedard, J., and James, M. N. (2005) Crystal structures of the RNA-dependent RNA polymerase genotype 2a of hepatitis C virus reveal two conformations and suggest mechanisms of inhibition by non-nucleoside inhibitors. J. Biol. Chem. 280, 18202-18210
- 44. Choi, K. H., Gallei, A., Becher, P., and Rossmann, M. G. (2006) The structure of bovine viral diarrhea virus RNA-dependent RNA polymerase and its amino-terminal domain. Structure 14, 1107–1113
- 45. Mosley, R. T., Edwards, T. E., Murakami, E., Lam, A. M., Grice, R. L., Du, J., Sofia, M. J., Furman, P. A., and Otto, M. J. (2012) Structure of hepatitis C virus polymerase in complex with primer-template RNA. J. Virol. 86, 6503-6511
- Karpala, A. J., Doran, T. J., and Bean, A. G. (2005) Immune responses to dsRNA: implications for gene silencing technologies. Immunol. Cell Biol. 83, 211-216
- 47. SenGupta, D. J., Zhang, B., Kraemer, B., Pochart, P., Fields, S., and Wickens, M. (1996) A three-hybrid system to detect RNA-protein interactions in vivo. Proc. Natl. Acad. Sci. U.S.A 93, 8496 - 8501
- 48. Dolan, J. W., and Fields, S. (1990) Overproduction of the yeast STE12 protein leads to constitutive transcriptional induction. Genes Dev. 4, 492 - 502
- 49. Alvarez, D. E., De Lella Ezcurra, A. L., Fucito, S., and Gamarnik, A. V. (2005) Role of RNA structures present at the 3'UTR of dengue virus on translation, RNA synthesis, and viral replication. Virology 339, 200-212
- 50. Choksupmanee, O., Hodge, K., Katzenmeier, G., and Chimnaronk, S. (2012) Structural platform for the autolytic activity of an intact NS2B-NS3 protease complex from dengue virus. Biochemistry 51, 2840-2851

